


Fall 12-20-2019

The Role of Histone Chaperone FACT Complex in Base Excision Repair Pathway and Its Therapeutic Potential in Colon Cancer and Medulloblastoma

Heyu Song
University of Nebraska Medical Center

Follow this and additional works at: <https://digitalcommons.unmc.edu/etd>

 Part of the [Cancer Biology Commons](#), [Genetics Commons](#), [Neoplasms Commons](#), and the [Translational Medical Research Commons](#)

Recommended Citation

Song, Heyu, "The Role of Histone Chaperone FACT Complex in Base Excision Repair Pathway and Its Therapeutic Potential in Colon Cancer and Medulloblastoma" (2019). *Theses & Dissertations*. 400.
<https://digitalcommons.unmc.edu/etd/400>

This Dissertation is brought to you for free and open access by the Graduate Studies at DigitalCommons@UNMC. It has been accepted for inclusion in Theses & Dissertations by an authorized administrator of DigitalCommons@UNMC. For more information, please contact digitalcommons@unmc.edu.

**THE ROLE OF HISTONE CHAPERONE FACT COMPLEX IN BASE
EXCISION REPAIR PATHWAY AND ITS THERAPEUTIC
POTENTIAL IN COLON CANCER AND MEDULLOBLASTOMA**

by

Heyu Song

A DISSERTATION

Presented to the Faculty of
the University of Nebraska Graduate College
in Partial Fulfillment of the Requirements
for the Degree of Doctor of Philosophy

Medical Sciences Interdepartmental Area
Graduate Program
(Genetics, Cell Biology & Anatomy)

Under the Supervision of Dr. Kishor K. Bhakat

University of Nebraska Medical Center
Omaha, Nebraska

September, 2019

Supervisory Committee:

Kishor K. Bhakat, Ph.D.

Laura D. Bilek, Ph.D.

Karen A. Gould, Ph.D.

Tadayoshi Bessho, Ph.D.

ACKNOWLEDGEMENTS

I would like to extend my gratitude to many people who have generously contributed to my time during graduate school.

First, I would like to express my deepest appreciation to my mentor, Dr. Bhakat, who has been incredibly patient and supportive since the first day I joined the lab. Your logical and critical thinking has guided me through the graduate study and made such a comprehensive research project feasible. Thank you for your profound belief in my abilities and allowing me to grow. Your brilliant suggestions on both academic and personal levels have benefited me tremendously.

I would also like to extend my sincere thanks to my committee members, Drs. Laura Bilek, Karen Gould and Tadayoshi Bessho, for their great support, constructive criticism and invaluable advice. I also wish to thank Dr. Gould and Dr. Bilek for their encouragement and patience throughout the duration of my graduate study. I very much appreciate Dr. Vimla Band for the unwavering support. Special thanks to Dr. Jenny Wang and her lab members for the great amount of assistance. I'd like to extend my gratitude for Dr. Sutapa Ray for the invaluable support and advice on the MB project. I'd also like to recognize the effort that I received from Dr. Shaoyan Xi from Sun Yat-sen University Cancer Center for our collaborative project. Many thanks to Dr. Kai Fu for his tremendous amount of help and support during this time. Thanks should also go to Dr. Hollingsworth for his critical reading and valuable comments for my manuscripts.

I had great pleasure of working with my lab members, Somsubhra, Dan, Shrabasti, Pranjal, Suravi, Hannah and Mason. I'd like to acknowledge the assistance from Lynne, Bryan and Bhopal. I'd also like to recognize the help that I received from Jiang Jiang and Lijun at Tissue Science Facility, Salma Elhag at Tissue Bank, Grace and Kris from

Comparative Medicine. Thanks are also due to the UNMC Graduate Studies Research Fellowships for the financial support that I otherwise would not have been able to develop my scientific discoveries.

Finally, but by no means least, thanks go to mum, dad and my husband Jiping for almost unbelievable support. They are the most important people in my world and I dedicate this thesis to them.

THE ROLE OF HISTONE CHAPERONE FACT COMPLEX IN BASE EXCISION REPAIR PATHWAY AND ITS THERAPEUTIC POTENTIAL IN COLON CANCER AND MEDULLOBLASTOMA

Heyu Song

Supervisor: Kishor K. Bhakat, Ph.D.

University of Nebraska Medical Center, 2019

Base excision repair (BER) pathway is required for the removal of damaged bases caused by alkylation, oxidation and ring-saturation. Human apurinic/apyrimidinic endonuclease 1 (APE1) plays a central role in BER pathway. Although repair of damaged bases by recombinant APE1 has been well investigated in vitro, how APE1 gains access to damaged bases in the context of chromatin is largely unknown. A prominent member of the histone chaperone family, FACT (Facilitates Chromatin Transcription) is thought to reorganize nucleosomes through the destabilization of multiple intra-nucleosome contacts. FACT complex is composed of two polypeptides identified as SPT16 (Suppressor of Ty 16) and SSRP1 (structure-specific recognition protein 1) that are both essential for nucleosome reorganization. Previous reports demonstrate that SPT16 is essential for transcription-coupled nucleotide excision repair (TC-NER) and homologous recombination repair (HRR). However, whether FACT complex interacts with APE1 and is involved in BER pathway remains unknown.

Here, we identified both subunits (SPT16 & SSRP1) of FACT complex as the prominent interacting partners of APE1. We show that the interaction of APE1 with FACT complex enhances upon induction of DNA damages. We demonstrate that FACT complex not only promotes the binding and subsequent acetylation of APE1 (AcAPE1), but also

regulates the mobility and binding dynamics of APE1 to damage sites in chromatin. Furthermore, we found that FACT complex was required for efficient repair of DNA damages in BER pathway.

Given the prognostic significance of APE1 overexpression in various cancers, we test the translational potential of targeting FACT complex to interfere BER function in two tumor models, colon cancer and medulloblastoma, a most common brain tumor in children. We show that both APE1 and FACT levels are elevated in primary tumor tissue of colon cancer and medulloblastoma patients. A group of small molecules currently in phase II clinical trial, curaxins, is found to cause chromatin trapping effect of FACT complex. We demonstrate that curaxins inhibit FACT function and exhibits synergistic effect of tumor killing when combined with chemotherapeutic agent both in vitro and in vivo using xenograft models. Colon cancer and medulloblastoma were used as our primary tumor models.

TABLE OF CONTENTS

ACKNOWLEDGEMENTS	I
TABLE OF CONTENTS.....	V
LIST OF FIGURES.....	VII
LIST OF ABBREVIATIONS	XIII
INTRODUCTION.....	1
BASE EXCISION REPAIR PATHWAY	1
APE1 AND ITS BIOCHEMICAL ACTIVITIES	5
POSTTRANSLATIONAL MODIFICATION OF APE1	8
ROLE OF APE1 IN TUMORS	9
APE1 INHIBITORS	10
FACILITATES CHROMATIN TRANSCRIPTION (FACT) COMPLEX	12
CURAXINS	14
HYPOTHESIS	14
CHAPTER 1. TARGETING HISTONE CHAPERONE FACT COMPLEX OVERCOMES	
5-FU RESISTANCE IN COLON CANCER	17
INTRODUCTION	17
MATERIALS AND METHODS	19
RESULTS.....	26
DISCUSSION	82

CHAPTER 2. TARGETING FACT COMPLEX INTERFERES DNA DAMAGE REPAIR AND TRANSCRIPTION AND SENSITIZES MEDULLOBLASTOMA TO CHEMOTHERAPY AND RADIATION.....	88
INTRODUCTION	88
MATERIALS AND METHODS:	90
RESULTS.....	95
DISCUSSION	138
DISCUSSION	142
BIBLIOGRAPHY	148

LIST OF FIGURES

Figure 1. Steps of BER pathway.....	4
Figure 2. Domain structure, amino acid sequence and posttranslational modifications of APE1.....	7
Figure 3. Schematic depiction of our hypothesis.....	16
Figure 4. APE1 shRNA significantly enhances 5-FU cytotoxicity in HCT116 cells.	26
Figure 5. APE1 siRNA significantly enhances 5-FU cytotoxicity in HCT116 and DLD1 cells.....	27
Figure 6. IC ₅₀ of 5-FU drops markedly after APE1 knockdown in HCT116 and DLD-1 cells.....	28
Figure 7. IP of endogenous AcAPE1 reveals both subunits of FACT complex as interacting partner.....	30
Figure 8. Co-IP of AcAPE1 in nuclear and chromatin extracts confirms the interaction of AcAPE1 with FACT complex.	31
Figure 9. Confocal microscope demonstrates the colocalization of AcAPE1 and FACT complex.....	31
Figure 10. APE1 forms complex with FACT in chromatin, and acetylation is not essential for this interaction.	32
Figure 11. Colocalization of AcAPE1 and FACT complex increases upon induced DNA damages.	34
Figure 12. Colocalization of APE1 and FACT complex remains unchanged upon MMS treatment.....	35
Figure 13. Pearson correlation coefficient of AcAPE1 and FACT complex increases upon induction of DNA damages.....	38

Figure 14. MMS treatment increases the expression of FACT complex and AcAPE1 in chromatin fraction.....	38
Figure 15. Interaction of AcAPE1 and FACT complex increases upon induction of DNA damages.	39
Figure 16. Occupancy of AcAPE1 and SPT16 to p21 and DTL promoter regions significantly increases upon MMS treatment.....	40
Figure 17. FACT KD decreases the level of AcAPE1 but has no effect on total APE1 level.....	42
Figure 18. AcAPE1 level decreases upon knockdown of FACT complex.....	43
Figure 19. APE1 expression remains unchanged upon FACT KD.	44
Figure 20. FACT KD prevents the increase of occupancy of AcAPE1 to p21 and DTL promoter regions upon MMS treatment.	45
Figure 21. FACT KD prevents the increase of occupancy of APE1 to p21 and DTL promoter regions upon MMS treatment.	46
Figure 22. APE1 dynamics decreases after FACT KD.....	47
Figure 23. MMS treatment increases AP sites, and FACT KD cells retains significantly more AP sites after recovery.	49
Figure 24. FACT KD impairs BER activity after MMS treatment as demonstrated by alkaline comet assay.	50
Figure 25. Downregulation of FACT sensitizes HCT116 and RKO cell lines to 5-FU.	51
Figure 26. Chemical structures of QC and CBL0137.	53
Figure 27. QC causes chromatin trapping effect on FACT complex.....	53
Figure 28. CBL0137 causes chromatin trapping effect on FACT complex and decreases AcAPE1 level.....	54
Figure 29. CBL0137 decreases the expression level of AcAPE1 in a dose-dependent manner.....	55

Figure 30. CBL0137 has no effect on the expression of total APE1.....	56
Figure 31. CBL0137 inhibits BER function on 5-FU induced DNA damage repair.....	57
Figure 32. CBL0137 inhibits BER function on MMS induced DNA damage repair.	58
Figure 33. CBL0137 alone does not induce DNA damage.....	59
Figure 34. QC or CBL0137 alone has minimal effect on cell viability.	60
Figure 35. Combination of 5-FU plus curaxins demonstrated synergistic effect on inhibition of cell viability.	60
Figure 36. Combination of 5-FU plus QC significantly inhibits HCT116 xenograft growth with synergistic effect when compared to monotherapy of 5-FU or QC.....	62
Figure 37. Combination of 5-FU plus CBL0137 significantly inhibits HCT116 xenograft growth with synergistic effect when compared to monotherapy of 5-FU or CBL0137.....	64
Figure 38. Combination of 5-FU plus QC significantly inhibits DLD-1 xenograft growth with synergistic effect when compared to monotherapy of 5-FU or QC.....	65
Figure 39. Combination of 5-FU plus CBL0137 significantly inhibits DLD-1 xenograft growth with synergistic effect when compared to monotherapy of 5-FU or CBL0137.....	66
Figure 40. Representative xenograft mice picture demonstrates no gross weight change noted at the completion of study.....	67
Figure 41. No major organ toxicity is noted on H&E staining after treatment.....	68
Figure 42. Combining 5-FU with QC significantly decreases percentage of positive Ki-67 staining in xenograft.	69
Figure 43. Combination therapy induces apoptosis in xenograft tumor.	70
Figure 44. QC causes chromatin trapping effect of SSRP1.	71
Figure 45. Expression of FACT complex and AcAPE1 is elevated in colon cancer tissues.	72
Figure 46. Expression of FACT complex and AcAPE1 is elevated in multiple colon cancer cell lines.....	73

Figure 47. AcAPE1 and SSRP1 expression increases in tumors of higher T stage.	75
Figure 48. Percentage of AcAPE1 and SSRP1 positive staining cells increases as tumor progresses in terms of invasion depth.	76
Figure 49. Tumors of higher stage demonstrate higher portion of cells with high intensity.	77
Figure 50. The AcAPE1 and SSRP1 expression is correlated in colon cancer.....	78
Figure 51. Minimal or none responders have significantly higher percentage of AcAPE1 and SSRP1 staining.	79
Figure 52. Minimal or none responders have significantly higher percentage of AcAPE1 and SSRP1 staining.	80
Figure 53. Illustration of MMR deficient patient in our cohort and their staining of AcAPE1 and SSRP1.	81
Figure 54. Overexpression of AcAPE1 and SSRP1 is observed in MB.	96
Figure 55. MB tissues have higher percentage of AcAPE1 and SSRP1 positive staining as compared to normal tissues.	98
Figure 56. The expression of AcAPE1 and SSRP1 is correlated in MB.	99
Figure 57. Survival analysis based on AcAPE1 and SSRP1 expression.....	100
Figure 58. Survival analysis using R2 genomics demonstrates that high expression levels of AcAPE1 and SSRP1 is correlated with poor overall survival.....	101
Figure 59. Elevated expression of AcAPE1 and FACT complex is observed in various MB cell lines.	103
Figure 60. AcAPE1 is associated with FACT complex.	104
Figure 61. Confocal microscopy demonstrates the colocalization of AcAPE1 and FACT complex.....	105
Figure 62. Increased association of AcAPE1 and FACT complex upon irradiation is observed.	106

Figure 63. Confocal microscopy demonstrates increased colocalization of AcAPE1 and FACT complex upon irradiation treatment.	107
Figure 64. FACT KD decreases the expression of AcAPE1 but not total APE1.	109
Figure 65. FACT KD abrogates the enhanced occupancy of AcAPE1 to p21 and DTL promoter regions upon irradiation.	110
Figure 66. SIM demonstrates that the enhanced colocalization of SSRP1 and AcAPE1 upon cisplatin treatment is abrogated by FACT KD.	112
Figure 67. FACT KD significantly impairs BER repair on irradiation induced damage. .	113
Figure 68. CBL0137 decreases the expression of AcAPE1 and FACT complex in whole cell extracts of MB cells.	115
Figure 69. CBL0137 causes chromatin trapping effect on FACT complex and decreases the expression of AcAPE1 in HD-MD03 cells.....	116
Figure 70. CBL0137 causes chromatin trapping effect on FACT complex and decreases the expression of AcAPE1 in ONS-76 cells.	117
Figure 71. CX decreases the expression of AcAPE1 and its colocalization with FACT complex.	118
Figure 72. CX impaired DNA damage repair after irradiation.	119
Figure 73. CX-treated cells fail to repair irradiation induced damages after 36-hour release.	120
Figure 74. CX alone has minimal effect on cell viability.	122
Figure 75. CX alone has minimal inhibitory effect on colony formation assay.	123
Figure 76. CX sensitizes HD-MB03 and ONS-76 cells to cisplatin.	124
Figure 77. CX significantly decreases cell viability in radiation treatment.....	125
Figure 78. Combination therapy with cisplatin plus CX results in significant inhibition on colony formation in MB cells.	126

Figure 79. Combination therapy with radiation plus CX results in significant inhibition on colony formation in MB cells.	128
Figure 80. Combination of cisplatin plus CX inhibits HD-MB03 xenograft growth with synergistic effect.....	130
Figure 81. No significant weight change of mice was observed throughout treatment period.	132
Figure 82. H & E staining demonstrates no major toxicity in major organs after treatment.	133
Figure 83. IHC staining of xenograft tumor demonstrates anti-proliferative and pro-apoptotic effect of combination therapy.	134
Figure 84. Combination therapy exhibits anti-proliferative and pro-apoptotic effects on MB xenograft tumors.	135
Figure 85. Combination therapy decreases the expression of AcAPE1 and SSRP1 in MB xenograft tumors.	136

LIST OF ABBREVIATIONS

AcAPE1	acetylated APE1
ANOVA	analysis of variance
AP	apurinic/aprimidinic
APE1	apurinic/aprimidinic endonuclease-1
BBB	blood brain barrier
BER	base excision repair
ChIP	chromatin immunoprecipitation
CID	C-terminal intrinsically disordered domain
CRC	colorectal cancer
CX	curaxin
dRP	deoxyribose phosphate
dMMR	defective mismatch repair
DSB	double-strand break
FACT	facilitates chromatin transcription
5-FU	5-fluorouracil
HRR	homologous recombination repair
IHC	immunohistochemistry
IP	immunoprecipitation
IV	intravenously

MANOVA	multivariate analysis of variance
MB	medulloblastoma
MMS	methyl methanesulfonate
MTS	mitochondrial targeting sequence
MX	methoxyamine
nCaREs	negative Ca ²⁺ responsive elements
NER	nucleotide excision repair
NES	nuclear export signal
NIR	nucleotide incision repair
NLS	nuclear localization signal
NSCLC	non-small-cell lung carcinoma
PCC	Pearson correlation coefficient
Pol β	polymerase β
PTH	parathyroid hormone
PTM	post-translational modification
QC	quinacrine
Ref-1	redox factor-1
SHH	Sonic Hedgehog
SIM	Structured Illumination Microscopy
SP-BER	short-patch BER
SPT16	Suppressor of Ty 16

SSBs	single strand breaks
SSRP1	Structure Specific Recognition Protein 1
TC-NER	transcription-coupled nucleotide excision repair
TMZ	temozolomide
TNM	T=primary tumor, N=lymph node, M=metastasis
TS	thymidylate synthase
WNT	Wingless

INTRODUCTION

Base excision repair pathway

Human genome is continuously exposed to genotoxic stress. The maintenance of genome stability is critical for cell survival. Various forms of endogenous DNA damage are generated spontaneously everyday. With one exception, all the DNA repair pathways follow five steps: Recognition of damage by repair proteins, Removal, Reconstruction, and Reinstatement (3). Direct reversal, being the only exception, is the only single-step DNA repair process that removes an alkyl group from certain oxygen positions of damaged guanine and thymine bases without excising bases or distorting DNA's phosphodiester backbone. Base modification is the most common lesion in DNA. Base excision repair (BER) pathway is responsible for repairing most of the endogenous DNA damage including alkylation, oxidation, deamination and depurination, as well as single-strand breaks (SSBs) (4). These small lesions do not distort the DNA helix structure, however, can change the base-pairing property of the genetic materials and thus are mutagenic and potentially carcinogenic if left unrepaired. Mismatch repair (MMR) corrects single-base mismatches (A:G, T:C) and misaligned short nucleotide repeats to ensure replication fidelity. Helix-distorting, bulky lesions and large adducts when only one of the two DNA strands is affected are repaired by Nucleotide excision repair (NER). On the other hand, double strand breaks (DSBs) are very toxic and hard to repair. Two main pathways are involved: nonhomologous end joining (NHEJ) and homologous recombination repair (HRR).

BER is a highly coordinated pathway with the following five fundamental steps (**Figure 1**):

- i) Removal of DNA lesions by DNA glycosylase. The initial step of BER is excision of substrate base from duplex DNA by a DNA glycosylase. There are 11 human glycosylases that recognizes non-functional bases and remove the damaged base by cleaving the N-glycosyl bond between the base and the sugar. This will result in either abasic sites or 3'- α β unsaturated aldehyde and a 5'- phosphate.
- ii) Cleavage of abasic sites by apurinic/apyrimidinic (AP) endonuclease (APE). APE incises the DNA backbone immediately 5' to the abasic site to generate a strand break with a priming 3'-OH group and a non-conventional 5'-deoxyribose phosphate (dRP). APE1 exhibits 3'-phosphodiesterase, 3'-5'-exonuclease, and 3'-phosphatase activities. The major AP endonuclease in mammals is APE1, which accounts for more than 95% of the total cellular AP site incision activity (5). The APE1 is essential for survival as previous study has shown that homozygous mutant mice lacking APEX gene die during embryonic development (6,7).
- iii) Removal of sugar remnant. The DNA strand breaks generated in the above process contain terminal blocking groups, such as 5'-dRP, 5'-OH, 3'-PO₄, 3'-phosphoglycolate (3'-PG), and 3'-PUA. These groups will block the downstream repair and must be removed. Various proteins are involved. For example, DNA polymerase β (Pol β) possesses a polymerase activity and a dRP lyase activity that is able to remove 5'-dRP (8). APE1 has 3'-phosphodiesterase activity that can remove 3'-PG residues (9).
- iv) Single nucleotide gap filling by DNA polymerase. Pol β is the main human DNA polymerase that operates on short nucleotide gaps, such as those that arise during short-patch BER (SP-BER). It contains a 31-kDa polymerase domain and an amino-terminal 8-kDa lyase domain (10). A "knockout" of the pol β gene

in mice results in embryonic lethality, indicating its essential role during fetal development (11).

- v) Nick sealing by DNA ligase. In BER, this step is completed predominantly by DNA ligase I. Alternatively, DNA ligase III in complex with XRCC1 protein ligates the ends of the DNA strand. Both ligases are ATP-dependent and generate a covalent phosphodiester bond between the 3'-OH end of the upstream nucleotide and the 5'-PO₄ end of the downstream nucleotide to seal the nick (12).

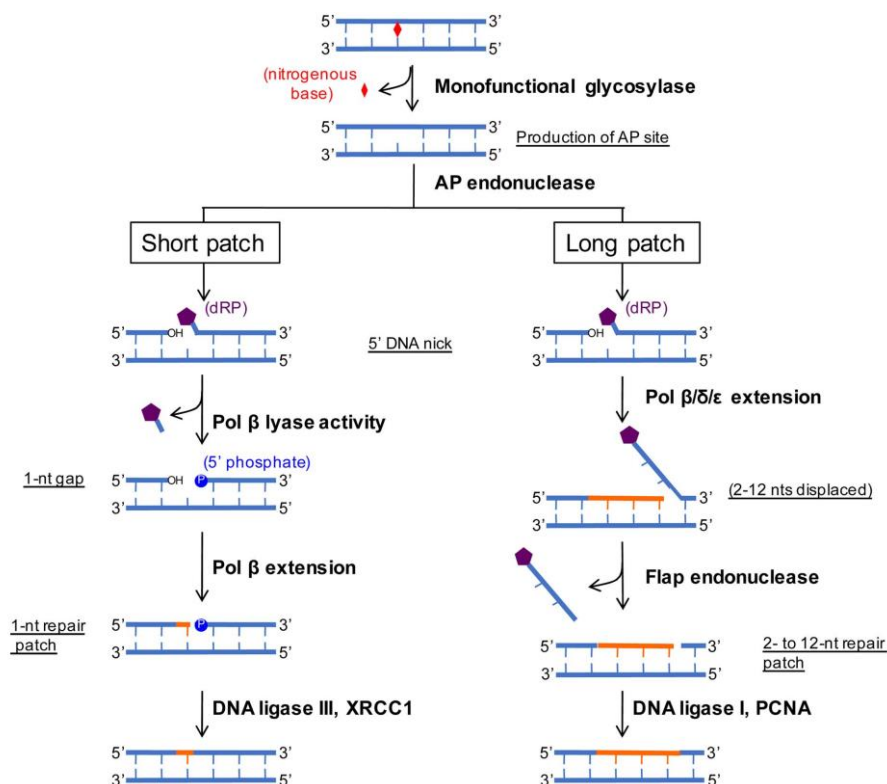


Figure 1. Steps of BER pathway.

Modified from Meas et al. (1). BER takes place by short-patch repair or long-patch repair that largely use different proteins downstream of the base excision. The repair process initiates with recognition and removal of damaged or inappropriate bases by DNA glycosylases, forming an AP site. These sites are cleaved by AP endonucleases, resulting in single-stranded breaks (SSBs). SSBs are processed by either “short-patch” (single nucleotide) or “long-patch” (2–10 new nucleotides) repair. Polβ is the main polymerase that catalyzes “short-patch” base excision repair. The final step is nick sealing by DNA ligase.

APE1 and its biochemical activities

In 1990s, the transcript encoding the human AP endonuclease (at the time, termed APE, HAP1, and APEX, since named apurinic/aprimidinic endonuclease 1 [APE1]/APEX1) was cloned by the Demple, Hickson, and Seki groups (13-15). Around the same time, APE1 was independently identified (and the gene subsequently cloned) by Curran and colleagues as the major nuclear protein (termed REF-1) to stimulate the DNA-binding activity of the AP-1 (Fos/Jun) transcription factor complex (16). Since then, APE1 has been described as a multifunctional protein that contains several domains and participates in several biological processes (**Figure 2**).

APE1 is a 36.5 kilodalton (kDa) protein encoded by a 3 kilobase (kb) gene, which is located on chromosome 14. It is expressed ubiquitously in humans, and depending on the cell types its concentration varies, average concentration of approximately 0.35 to 7×10^6 molecules per cell. The biochemical activities of APE1 are summarized as follows.

AP endonuclease activity. There are two types of AP endonuclease in human, including APE1 and APE2. With its robust activity, APE1 accounts for >95% of endonuclease function in cells (17). It plays a central role in BER by incising the DNA 5' to AP sites to generate accessible 3'-OH termini prior to repair synthesis. APE1 uses a rigid, pre-formed, positively charged surface to kink the DNA helix and engulf the AP-DNA strand. APE1 inserts loops into both the DNA major and minor grooves and binds a flipped-out AP site in a pocket that excludes DNA bases and racemized β -anomer AP sites (18).

3'-repair diesterase. Early research shows that APE1 has not only a powerful class II AP site incision activity, but also the ability to excise 3'-end blocking groups. These 3'-end damages include 3'-phosphates, 3'-phosphoglycolate esters, and 3'-deoxyribose fragments which are believed to prevent primer extension by a DNA polymerase or nick ligation by a DNA ligase (14,19). APE1 is rate limiting for the repair of DNA strand breaks

induced by hydrogen peroxide (presumably 3'-phosphates) and bleomycin (3'-phosphoglycolates) (20).

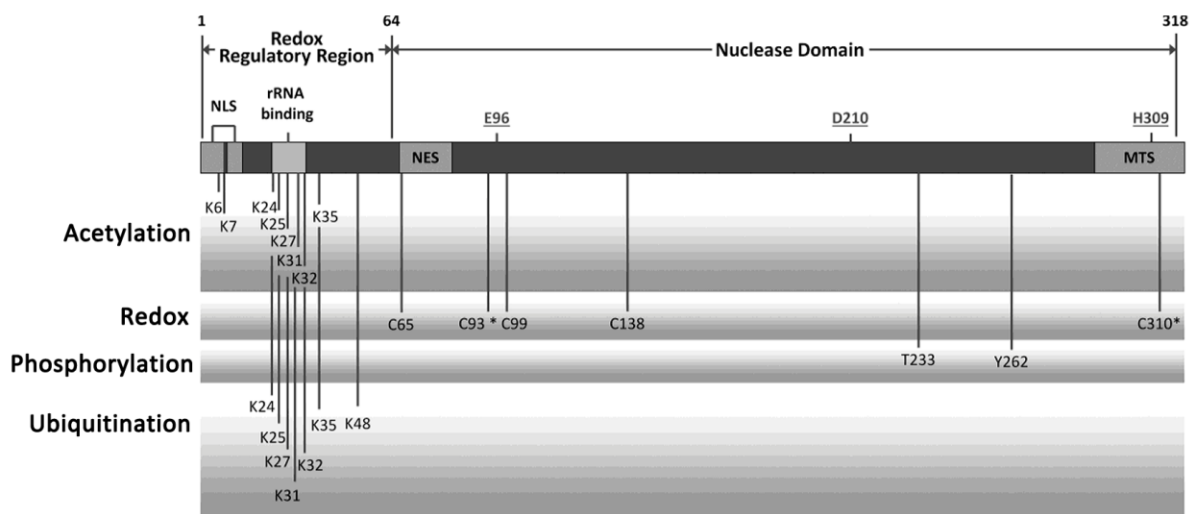
3' to 5' exonuclease. APE1 has 3' to 5' exonuclease activity. However, it is poorly processive and ≥ 100 -fold less efficient than its AP endonuclease activity (15,21).

RNA cleavage. APE1 exhibits RNase H activity. Similar to 3' to 5' exonuclease activity, the biological significance of this activity is unknown. Recently APE1 has been shown to be involved in RNA quality control as it has the ability to cleave AP sites in RNA to prevent error-prone translation (22,23).

Nucleotide incision repair (NIR). In NIR, an endonuclease directly nicks DNA containing free radical-induced base lesions acting as a back-up repair pathway to BER (24). This endonuclease was identified to be APE1 in human (25). APE1 incises DNA containing 5,6-dihydro-2'-deoxyuridine, 5,6-dihydrothymidine, 5-hydroxy-2'-deoxyuridine, alpha-2'-deoxyadenosine and alpha-thymidine adducts, generating 3'-hydroxyl and 5'-phosphate termini (25).

Redox regulation. APE1 has been reported to modulate the redox status of both ubiquitous (e.g., AP-1, Egr-1, NF- κ B, p53, CREB, and HIF-1 α) and tissue-specific transcription factors (e.g., PEBP-2, Pax-5, and -8, TTF-1) with functions in stress responses and other cellular processes (26).

Trans-acting modulation. APE1 is part of the components of negative Ca²⁺ responsive elements (nCaREs) that responds to a rising extracellular calcium level (27). This complex suppresses not only secretion of parathyroid hormone (PTH) but also expression of the PTH gene to ensure constant plasma Ca²⁺ level. APE1 binds to nCaRE PTH sequences in cooperation with the two subunits of the Ku antigen, p70 and p80 (28). The complex formation of APE1 is controlled by lysine (K6 and K7) acetylation (29).



←———— Nuclear localization sequence (NLS) —————→
 MPKRGKKGAV AEDGDEL RTE PEAKKSKTAA KKNDKEAAGE DPALYEDPPD
 QKTSPSGKPA TLKICSWNVD GLRAWIKKKG LDWVKEEAPD ILCLQETKCS
 ENKLP AELQE LPGLSHQYWS APSDKEGYSG VGLLSRQCPL KVSYGIGEEE
 HDQEGRVIVA EFDSFVLVTA YVPNAGRGLV RLEYRQRWDE AFRKFLKGLA
 SRKPLVLCGD LNVAHEEIDL RNPKGNNKNA GFTPQERQGF GELLQAVPLA
 DSRHLYPNT PYAYTFWTYM MNARSKNVGW RLDYFLLSHS LLPALCDSKI
 RSKALGSDHC PITLYLAL

Figure 2. Domain structure, amino acid sequence and posttranslational modifications of APE1.

Adapted from Li M et al. *Antioxid Redox Signal*. 2014 (2). The nuclear localization sequence is localized in the N-terminal, spanning residues 1 to 34. The truncated form of NLS is called NΔ33. The endonuclease domain spans roughly from residues 64 to 318. Post-translational modifications including acetylation, phosphorylation and ubiquitination are depicted. NLS, nuclear localization signal; NES, nuclear export signal; MTS, mitochondrial targeting sequence; PTM, post-translational modification.

Posttranslational modification of APE1

After translation, APE1 undergoes various modifications which in turn affect its endonuclease activity, redox function, transcriptional modulation and subcellular localization. So far four different types of PTMs (**Figure 2**) have been reported (reviewed in (30)).

Phosphorylation. APE1 could be phosphorylated with predicted sites at a.a. residues of 19T, 123S, or 233T by casein kinase II, which was reported to be enhancing its endonuclease activity (31). Later, Fritz et al. reported that phosphorylation enhanced Ref-1 activity but did not affect its nuclease activity (32). The various results reported have not reached conclusion regarding the biological effect of APE1 phosphorylation. Additionally, APE1 phosphorylation activity in cells is very weak and endogenous phosphorylated APE1 has not been confirmed (33).

S-nitrosation. Qu et al. reported that nuclear-cytoplasmic translocation was dependent on S-nitrosation modification of APE1, as simultaneous mutation of S-nitrosation target sites Cys93 and Cys310 completely abrogated the cytoplasmic redistribution. The modification in cells is induced by S-nitrosoglutathione, a nitric oxide donor and also an S-nitrosating agent (34).

Acetylation. Bhakat et al. reported in 2003 that the acetylation of APE1 was carried out by histone acetyl transferase (HAT) p300. The acetyl acceptor Lys residues were also found at K6 and K7 in the APE1 polypeptide (29). Later, the same group developed an antibody specifically directed at acetylated APE1 (AcAPE1), confirming the endogenous presence of AcAPE1 (35). Later, other Lys residues including K24, K25, K27, K31 and K32 were identified in the N-terminal domain (36,37). APE1 acetylation is a key modulation for its gene repressor function and in transcriptional activation of the multi-drug resistance gene MDR1. Recent report demonstrates that APE1 is acetylated (AcAPE1)

after binding to the AP sites in chromatin and that AcAPE1 is exclusively present on chromatin throughout the cell cycle. Acetylation-mediated neutralization of the positive charges of the lysine residues in the N-terminal domain of APE1 induces a conformational change; this in turn enhances the AP endonuclease activity of APE1 (38).

Ubiquitination. APE1 ubiquitination occurred specifically at Lys residues near the N-terminus, and was markedly enhanced by mouse double minute 2 (MDM2), the major intracellular p53 inhibitor. DNA damage agents increased APE1 ubiquitination. Interestingly, unlike the wild-type APE1, ubiquitin-APE1 fusion proteins were predominantly present in the cytoplasm (39). Further study revealed that monoubiquitinated APE1 was present in the nucleus, and analyzing global gene expression profiles with or without induction of a ubiquitin-APE1 fusion gene suggested that monoubiquitination enhanced the gene suppression activity of APE1 (40).

Role of APE1 in tumors

The multifunctional nature of APE1 alludes to its expansive role in various diseases, especially cancers. APE1 is involved in processes such as tumorigenesis, cancer aggressiveness, increased angiogenesis, radiotherapeutic and chemotherapeutic resistance, and overall poor prognosis (reviewed in (41)). For example, APE1 has been studied in prostate cancer, where it demonstrates a higher percentage of cells staining positive for APE1 in the cytoplasm and an increased intensity of APE1 nuclear staining (42). Colon cancer, the second leading cause of cancer related death in the US, exhibits overexpression of APE1 (43). Similarly, APE1 overexpression has been observed in pancreatic cancer, ovarian cancer, breast cancer, non-small cell lung carcinoma, and medulloblastoma (44,45).

APE1 possess two major functions in cells, including the critical role in BER pathway and transcriptional regulatory functions with redox and direct coactivator or corepressor functions. The finding of APE1 upregulation has led to the investigation of the role of APE1 in cancer. In colon cancer cells, using siRNA to knockdown APE1 has resulted in increased sensitivity to radiation therapy. This finding is further tested in xenograft model, where siRNA delivered subcutaneously leads to reduced tumor growth (46). Targeting Ref-1 function of APE1 via APX3330 inhibits the proliferation and adhesion of pancreatic cancer cell lines, arrests cell cycle progression, and decreases the transcriptional activation of major transcription factors (47,48). These findings have suggested that APE1 may be a target for cancer treatment, and has led to the search for APE1 inhibitors, which we will detail below.

APE1 inhibitors

APE1 appears to be a promising target for cancer therapy for the following reasons:

- 1) The expression of APE1 is upregulated or dysregulated in multiple cancers. It has been shown to be elevated in NSCLC, breast cancer, osteosarcoma, melanoma, cervical cancer, bladder cancer, hepatocellular carcinoma, ovarian cancer, and colon cancer (reviewed in (45)).
- 2) Interference or inhibition of APE1 function increases cytotoxicity of common chemotherapeutic agents, including temozolomide (TMZ), cisplatin, and gemcitabine.
- 3) The overexpression of APE1 is correlated with poor prognostic features of cancer patients, such as chemoresistance, poor treatment response, poor survival and recurrence.

APE1 inhibitors have been under development over the past decades. Currently, there are two classes of inhibitors available, including methoxyamine (MX) and E3330. They have distinct mechanism of action and have been investigated extensively in prior literature. MX is an orally available agent that binds to the aldehyde on the AP site covalently and prevents APE1 from binding to damage sites (49). It is considered as indirect inhibitor of APE1, or more appropriately, inhibitor of BER pathway. It has also been used for AP site quantification (50). As a result, it lacks binding specificity and may causes off-target effects. For example, it will bind to any aldehyde group in DNA. Nevertheless, it has been introduced clinically in phase I trial as a component of combination therapy with fludarabine for advanced hematologic malignancies (51). It is used in 20 patients and hematologic toxicity was frequent; most common grade 3–4 toxicities were lymphopenia (70%), neutropenia (60%), leukopenia (50%) and anemia (40%). In another phase I trial, MX is combined with TMZ in patients with solid tumors and lymphomas (52,53). Similarly, hematologic toxicity was noted included neutropenia, anemia, thrombocytopenia, and hemolysis. It is deemed that MX is overall well tolerated in these studies. There are currently three phase II trial with one of them being terminated. In an effort to use MX combined with temozolomide in recurrent glioblastoma, the study was terminated because pre-specified response criteria are not met to proceed to next stage of study (NCT02395692). The other two studies are in active recruiting phase, including NCT02535312 that uses MX with cisplatin and pemetrexed disodium in advanced solid tumors or mesothelioma, and NCT01851369 that uses MX with temozolomide for relapsed solid tumors and lymphomas.

As described previously, the redox domain of APE1 (often referred to as redox factor-1, Ref-1) is involved in the activation of re-dox-sensitive transcription factors. E3330, a novel quinone derivative, was initially found to selectively inhibited NF-kappa B-mediated

gene expression without affecting degradation of I kappa B alpha, translocation of NF-kappa B into the nucleus, or post-translational modification of NF-kappa B (54). Later, Shimizu et al used novel latex beads for rapid identification of drug receptors using affinity purification. E3330 was found to selectively inhibit the redox domain of APE1 (55). E3330 exposure affects a number of critical intracellular pathways involved in endothelial cell differentiation, homeostasis and development, with the effect of inhibiting the in vitro growth of endothelial cell and endothelial progenitor cells (EPCs). The cytotoxicity of the combination of TNF-related apoptosis-inducing ligand, TNF alpha, Fas ligand, and E3330 increased synergistically in a dose-dependent manner compared to either E3330 alone in all HCC cell lines by MTT assay. However, the combination of some chemotherapeutic drugs and E3330 did not decrease the cell viability (56).

To sum up, biochemical, preclinical and clinical studies discussed in the previous section confirm that APE1 is a valid anticancer drug target. Currently there is no ideal inhibitor that inhibits APE1 DNA repair activity and augment cytotoxicity when combined with chemotherapeutic agents.

Facilitates Chromatin Transcription (FACT) Complex

Although repair of damaged bases by recombinant BER proteins has been well investigated in vitro, how repair factors gain access to damaged bases in the context of chromatin is largely unknown. The fundamental unit of the chromatin polymer is the nucleosome, which represents the first order of DNA packaging in the nucleus and as such is the principal structure that determines DNA accessibility. Histone chaperones are a diverse family of histone-binding proteins that shield non-specific interactions between the negatively charged DNA and the positively charged histones, to allow the ordered formation of the nucleosome structure. Other than having the common feature of being

acidic, histone chaperones are a diverse group of proteins with little sequence similarity. Histone chaperones sequester core histones from DNA until a more energetically favorable nucleosomal arrangement becomes available (57).

The human FACT complex was first identified in 1998 as a factor essential for transcriptional elongation through chromatin (58). Later it was further characterized to be composed of two subunits, SSRP1 and SPT16, both of which are essential for its function. FACT complex has been previously shown to reorganize nucleosomes through the disruption of core histone-histone and histone-DNA interactions (59). It is also capable of depositing the H2A-H2B dimer and (H3-H4)₂ tetramer onto DNA (60). Additionally, it has been linked to activation of the tumor suppressor protein p53 and to histone variant (H2AX-H2B) exchange in response to induced DNA damage (61,62). FACT is implicated in various chromatin processes including transcription and DNA replication, recombination, and repair (63), during which it functions by reorganizing nucleosomes through the disruption of core histone-histone and histone-DNA interactions. By promoting accelerated histone exchange, SPT16 is essential in the completion of transcription-coupled nucleotide excision repair (TC-NER), allowing efficient restart of transcription after repair of the blocking lesions (64). In DNA double-strand break repair, SPT16 helps E3 ubiquitin ligase RNF20 with the regulation of chromatin structure through ubiquitylation of histone H2B, so that early homologous recombination repair (HRR) proteins can access the DNA in eukaryotes during repair. Depletion of SPT16 causes pronounced defects in accumulations of repair proteins and, consequently, decreased HRR activity (65).

While its involvement in nucleotide excision repair (NER) and double-strand break (DSB) repair pathway has been well demonstrated, whether FACT complex is involved in BER pathway remains unknown.

Curaxins

Curaxins is a group of small molecules that were identified in a phenotype-based screening for the ability to simultaneously activate p53 and inhibit NF- κ B without causing detectable genotoxicity (66). In search for its mechanism of action, it was discovered that curaxins bind DNA via intercalation of the carbazole body accompanied by the protrusion of two side chains into the major groove and a third side chain into the minor groove of DNA, inducing tight binding of FACT to chromatin that results in functional inhibition (67). Later, Safina et al reports that binding of curaxins leads to uncoiling of nucleosomal DNA, accumulation of negative supercoiling and conversion of multiple regions of genomic DNA into left-handed Z-form. Nucleosome disassembly caused by curaxins opens multiple FACT-binding sites, which are normally hidden inside the nucleosome. The isolated C-terminal intrinsically disordered domain (CID) of SSRP1, but not HMG domain, binds these alternative DNA structures and triggers p53 response (68).

Curaxins have caught increasing attentions since the initiation of clinical trial. The first clinical phase I trial was launched in July 2013 to determine the maximally tolerated dose and recommended phase II dose of CBL0137 when administered intravenously (IV) to patients with metastatic or unresectable advanced solid malignancies (NCT01905228). Since then, two clinical trials with broader application were started for those with hematological malignancies, metastatic extremity melanoma or sarcoma (NCT02931110 and NCT03727789).

Hypothesis

Altered DNA repair processes have been observed in tumorigenesis and chemotherapy resistance, leading to tumor recurrence and eventually death. Alkylating agents remain a mainstay of chemotherapy. Consequently, it is necessary to elucidate the

mechanism underlying resistance to these agents before identifying an appropriate target for increasing chemosensitization. BER pathway is primarily involved in repairing both endogenous and exogenous genome damages induced by alkylating agents. APE1 plays a key role in the BER pathway via repairing AP sites generated spontaneously or after removal of alkylated bases by DNA glycosylases. Although repair of damaged bases by recombinant BER proteins has been well investigated in vitro, how repair factors gain access to damaged bases in the context of chromatin is largely unknown. Previously FACT complex has been shown to be involved in NER and DSB repair pathways. Nevertheless, the role of FACT in BER remains unclear.

Our study shows that FACT is the prominent interacting partner of acetylated APE1 (AcAPE1). Furthermore, we have shown that downregulation of FACT sensitizes tumor cells to alkylating drugs. We hypothesize that FACT is the key factor facilitating APE1 to access damage sites in chromatin and that this interaction is essential for efficient DNA damages repair and inducing chemoresistance in tumor cells (**Figure 3**).

As corollary, we hypothesize that targeting the interaction of APE1 with FACT may serve as an alternative target in enhancing chemosensitivity.

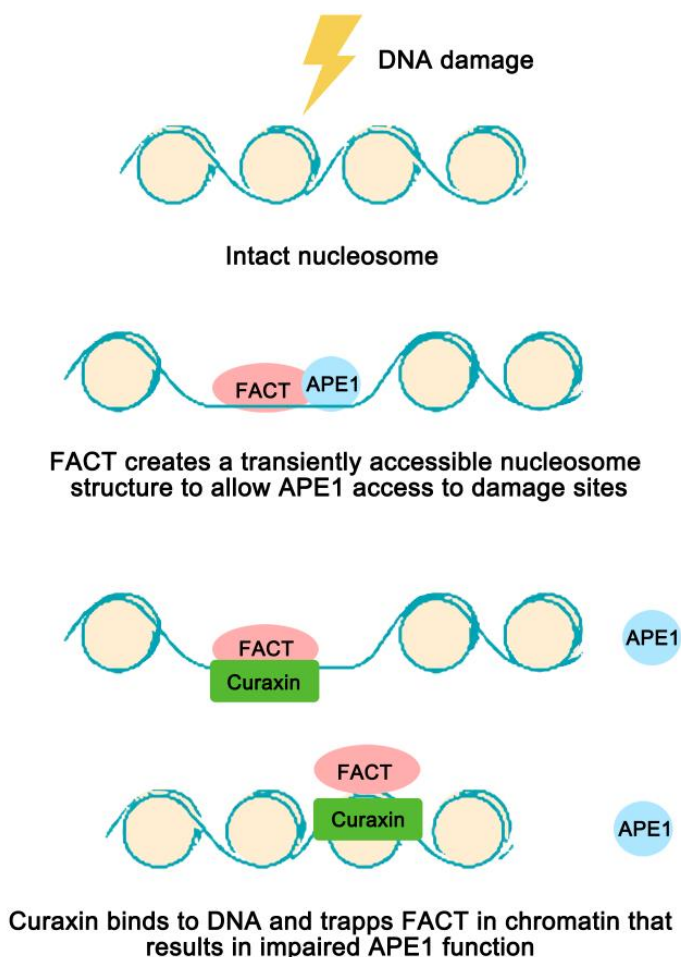


Figure 3. Schematic depiction of our hypothesis.

Eukaryotic genomes are highly condensed in chromatin, which is dominated by arrays of the basic repeating units termed nucleosome. This packaging limits the accessibility of DNA, thus creating a barrier that plays a major role in regulating nuclear processes such as DNA transcription, replication, and repair. In the setting of DNA damage, FACT complex creates a transiently accessible nucleosome structure to allow APE1 access to damage sites. Curaxins is a group of small molecules that causes chromatin trapping effect. We hypothesize that inhibition of FACT complex disrupts the interaction of FACT and APE1 and leads to interference of BER function.

CHAPTER 1. TARGETING HISTONE CHAPERONE FACT COMPLEX OVERCOMES 5-FU RESISTANCE IN COLON CANCER

Introduction

Colorectal cancer (CRC) is the second leading cause of cancer related deaths in the US. According to the American Cancer Society, more than 50% of new cases are diagnosed at advanced stages and require adjuvant chemotherapy. The pyrimidine analog 5-fluorouracil (5-FU) forms the backbone for almost all chemotherapeutic regimens for CRC (69). However, a subset of CRC patients who develop cancer with microsatellite instability or defective mismatch repair (dMMR) show resistance to 5-FU (70,71). Studies have shown that dMMR CRC patients with stage III tumors do not benefit from 5-FU-based adjuvant (FOLFOX) therapy (70,72). In accordance with clinical observations, in vitro studies have shown that dMMR CRC cells are resistant to the cytotoxic effects of 5-FU (73). Therefore, elucidating the mechanisms of 5-FU resistance in dMMR CRC and identifying novel therapeutic targets to increase the efficacy of 5-FU in dMMR CRC represents an unmet need.

Though the mechanism of actions of 5-FU is not completely understood, its cytotoxicity has been ascribed to the inhibition of thymidylate synthase (TS), the key enzyme of de novo pyrimidine biosynthesis (74). However, numerous studies have established that 5-FU metabolites can induce cytotoxicity through incorporation into RNA and genomic DNA (75,76), and that both DNA Mismatch Repair (MMR) and Base Excision Repair (BER) pathways are primarily involved in the repair of the resultant DNA lesions (76,77). In the case of FU incorporation opposite dG, the resulting FU:dG mispair would be efficiently processed by the MMR pathway, resulting in single-stranded breaks (SSBs) (77,78). However, repeated incorporation of FU:dG leads to futile attempts by the MMR

system and persistent SSBs will result in double-strand breaks that in turn induce apoptosis (79). On the other hand, the BER pathway is able to directly remove FU from newly synthesized DNA in the case of FU:dA or FU:dG (76,80), resulting in apurinic/apyrimidinic (AP) sites that are further processed by AP-endonuclease (APE1) (2). APE1 plays a central role in the BER pathway by cleaving the DNA backbone immediately 5' to lesions (35,81). The resulting strand breaks are repaired via the highly coordinated BER pathway (82). We have recently shown that APE1 is acetylated (AcAPE1) at AP sites in chromatin by p300 and that acetylation enhances its AP-endonuclease activity (38,83). We hypothesize that dMMR CRC cells have an increased requirement of BER pathway for efficient repair of 5-FU-induced DNA damages, and that targeting APE1-dependent BER pathway will sensitize dMMR CRC to 5-FU.

In this study, we sought to examine the role of BER pathway in promoting 5-FU resistance in CRC cells with deficient MMR system. We found that downregulation of APE1 sensitizes dMMR CRC cells to 5-FU in vitro. Furthermore, we identified FACT complex as an interacting partner of APE1 in chromatin and characterized the role of FACT complex in BER pathway. Curaxins, a class of small molecules that inhibit FACT complex, were tested extensively in combination with 5-FU using multiple dMMR CRC cell lines in vitro and in vivo as a means of improving 5-FU therapeutic response. To provide further support of potential applicability of this novel therapeutic strategy, we examined the expression of APE1 and FACT in CRC patient specimens and correlated with the treatment response. Together, our study unveils a novel role of FACT complex in promoting 5-FU resistance, and demonstrates that targeting FACT with curaxins is a promising strategy to overcome 5-FU resistance in dMMR CRC patients.

Materials and methods

Cell culture, plasmids, siRNAs, transfection and treatments

HCT116 cells (ATCC# CCL-247) were grown in McCoy's 5A medium (Gibco) supplemented with 10% fetal calf serum (FCS; Sigma) and antibiotic mixture of 100 U/ml penicillin and 100 µg/ml streptomycin (Gibco). HCT116 cell line stably expressing APE1-shRNA was a kind gift from Dr. Sheila Crowe (University of California, San Diego) and was cultured in McCoy's 5A supplemented with 0.01% puromycin (Gibco). HEK-293T cells (ATCC # CRL-3216) were cultured in DMEM-high glucose medium (Gibco) with 10% fetal calf serum (FCS; Sigma) and antibiotic mixture of 100 U/ml penicillin and 100 µg/ml streptomycin (Gibco). RKO cell line was obtained from Dr. Jing Wang (Eppley Institute, UNMC). RKO and DLD-1 cells (ATCC# CCL-221) were grown in EMEM medium (ATCC). All cell lines were authenticated using STR DNA profiling by Genetica DNA laboratories (Burlington, NC) two years ago before being used in this study. These cells were routinely assayed for mycoplasma. Mutation of Lys residue (K6, 7, 27, 31 and 32) to arginine or to glutamine in APE1-FLAG-tagged pCMV5.1 plasmid were generated using a site-directed mutagenesis kit (Agilent-Stratagene, Santa Clara, CA) as described previously (38). Exponentially growing HEK293T cells were transfected with wild type (WT) APE1, K6,7,27,31,32 to arginine (K5R) or to glutamine (K5Q), N-terminal 33 amino acid deleted (NΔ33) mutants expression plasmids. siRNAs targeting SSRP1 (Sigma, EHU015991) and SPT16 (Sigma, EHU039881; Dharmacon, J-009517), as well as control siRNA (Dharmacon, D-001810) were transfected into RKO, HCT116, and HCT116^{APE1shRNA}. APE1 siRNAs were obtained from Sigma-Aldrich (WD04424567) and Dharmacon (J-010237). Cells were transfected using Lipofectamine 2000 (Invitrogen, Carlsbad, CA) and harvested after 48 hrs. Methyl Methanesulfonate (MMS), quinacrine (QC), and 5-FU were

obtained from Sigma-Aldrich. CBL0137 was obtained from Cayman Chemical for in vitro study, and from Incuron, LCC (Buffalo, NY) for in vivo study.

Identification of interacting proteins of AcAPE1

Chromatin extracts were immunoprecipitated (IP) with anti-AcAPE1 and control IgG antibodies (38). The IP samples were boiled for 5 min and resolved in 12.5 % SDS-PAGE gel followed by staining with Coomassie blue (PageBlue™, Thermo Scientific). Identification of protein bands was performed by MALDI-TOF-TOF analysis in the Mass Spectrometry and Proteomics Core Facility (University of Nebraska Medical Center, Omaha, NE, USA).

Western Blot Analysis

Cell fractionation was performed as described previously (81). Whole cell lysates or cell fractions were resolved on 10 to 12.5 % SDS-PAGE gel and transferred to nylon membranes for blotting. Whole cell lysates of HCEC, GEO, LoVo and SW620 were provided by Dr. Jing Wang (UNMC). Primary antibodies were used including SPT16 (Abcam, 204343), SSRP1 (Biolegend, 609702), FLAG (Sigma, F1804), TRF1 (Abcam, 10579), α -HSC70 (B6-Sc7298, Santa Cruz Biotechnology), H2A (Abcam, 26350), APE1 (Novus Biologicals, NB100-116), α -tubulin (Abcam, 52666) and AcAPE1 (35,84). Immunoblot signals were detected using Super Signal West pico chemiluminescent substrate (Thermo Scientific) after treating with HRP-conjugated secondary Ab (GE Healthcare).

MTT assay

Cells were seeded at a density of 5×10^3 in 96-well plates. After 24-hour incubation in the medium to allow for cell attachment, the fresh medium was added and cells were treated with vehicle control (DMSO alone) or indicated doses of 5-FU dissolved in DMSO

for 72 hours. The MTT reagent (Sigma-Aldrich, M5655) was added to a final concentration of 0.5 mg/ml to each well. The assay was performed as per manufacture's protocol. Three independent experiments with six replicates were performed for each group.

Patient tissue samples and analysis

Colon cancer samples were obtained from tissue bank at University of Nebraska Medical Center (UNMC) and University of Texas Medical Branch. Tissues were collected in accordance with institution's review board approval and informed consent was waived. The deparaffinized sections were stained per standard IHC protocol. The antibodies used were: AcAPE1 (1:200), Ki67 (1:500, CST, 9027) and SSRP1 (1:100). Staining intensity and percentage of positive cells were analyzed by Definiens Releases Tissue Studio® 4.3. We used a stain deconvolution algorithm to separate the DAB chromogen stain and the hematoxylin counterstain in all tissue cores. We then measured the brown chromogen intensity across all tissues to obtain the range of pixel density. Based on the range, we divided the staining intensity into 3 categories using one third threshold increment in the range. Tissue lysates were prepared and analyzed by Western Blot as described previously (44).

Treatment response is assessed by clinician using modified Ryan Tumor Regression Grading System (85).

Complete response: no viable cancer cells

Moderate response: small groups of cancer cells

Minimal response: residual cancer outgrown by fibrosis

No response: minimal or no tumor killed; extensive residual cancer

Immunoprecipitation (IP) and FLAG-IP

Nuclear and chromatin extracts of HCT116 or RKO cells were pre-cleared with protein A/G Plus agarose beads and IP was performed with AcAPE1 antibody or control IgG (Santa Cruz, sc-2003). The chromatin extracts of control and MMS-treated cells were immunoprecipitated with the same antibody. FLAG-IP was done with mouse monoclonal α -FLAG M2 antibody-conjugated agarose beads (Sigma-Aldrich, A2220) in nuclear extracts of HEK293T cells transfected with FLAG tagged constructs as described previously (84). The immunoprecipitated proteins were resolved in SDS-PAGE and identified by Western Blot analysis with the indicated antibodies.

Immunofluorescence

Cells grown on coverslips were fixed with 4% formaldehyde (Sigma-Aldrich) and stained with immunofluorescence as described previously (38). Primary antibodies used were mouse monoclonal anti-APE1 (1:100; Novus Biologicals, NB100-116), anti-AcAPE1 (1:50), SSRP1 (1:100; Biolegend, 609702), SPT16 (1:50; Abcam, 204343). Images were acquired by use of a fluorescence microscope with a 63x oil immersion lens (LSM 510; Zeiss), and structured illumination microscopy (SIM) was done with an Elyra PS.1 microscope (Carl Zeiss) by using a 63x objective with a numerical aperture of 1.4. ImageJ software was used to measure Manders colocalization using the JaCoP plug-in.

Chromatin Immunoprecipitation (ChIP) Assay

ChIP assay was performed after double crosslinking of cells with disuccinimidyl glutarate and formaldehyde, with protein A/G Plus agarose beads (Santa Cruz, sc-2003) using with AcAPE1, SPT16 and control IgG (Santa Cruz) following the procedure as described earlier (38,84). The immunoprecipitated purified DNA was used to amplify the p21 and DTL promoter regions using SYBR GREEN-based (Thermo Scientific) Real Time

PCR analysis. The following primers are used: p21 forward 5'-CAGGCTGTGGCTCTGATTGG-3', reverse 5'-TTCAGAGTAACAGGCTAAGG-3'; DTL forward 5'-TCCTGCAAATTTCCCGCAAC-3', reverse 5'-GGCTATGGCGAACAGGAACT-3'. Data were represented as relative enrichment with respect to IgG control based on $2^{-\Delta CT}$ method.

AP site measurement assay

HCT116 cells were transfected with control and siRNA against SSRP1 and SPT16. After 48 hrs, cells were treated with 1 mM MMS for 1 hr and released in fresh media for 6 hrs. Total genomic DNA was isolated by Qiagen DNeasy kit following manufacturer's protocol. AP sites were measured using aldehyde reactive probe (Dojindo Laboratories) as described previously (38).

Fluorescence Recovery after Photobleaching (FRAP)

N-terminal GFP tagged -APE1 (86) was transfected into HCT116 cells. 24 hours after transfection of control and FACT siRNAs, cells were treated with DMSO or MMS. FRAP experiments were performed as described previously (87). All FRAP data were normalized to the average prebleached fluorescence after removal of the background signal. The curve was plotted using GraphPad Prism 7 and each curve represented an average of 10 measurements from different regions of cells.

Xenograft studies

All animal experiments were performed following the approval of Institutional Animal care and use committee (IACUC). The experiments and reports are adhered to the Animal Research: Reporting of In Vivo Experiments (ARRIVE) guidelines. HCT116 and DLD-1 cells (1×10^6 in 100 μ L medium) were injected subcutaneously over the left and right flanks in 6-week old male athymic nude mice (Charles Rivers, Wilmington, MA). The

average weight was 27 ± 3.6 grams. Subcutaneous tumors were allowed to grow for 1-2 weeks before treatments. When tumor volume reaches 100 mm^3 , the mice were randomly divided into four treatment groups (each groups $n=5$ mice) and received treatments every other day for three weeks. The following drugs: 5-FU 20 mg/kg, QC 50 mg/kg, CBL0137 30 mg/kg were injected intraperitoneally. Combination group received both 5-FU and QC or CBL0137 100 μL PBS was given to control group. Body weight and tumor volume were measured and recorded before each treatment. The mice were euthanized in gas canister with gradual fill carbon dioxide after the end of treatment cycles. Xenograft tumor was fixed in formalin and paraffin-embedded tissue sections were used to perform IHC staining Ki67 and TUNEL assay. The percentage of positive staining was quantified with 10 random high-power field images from three different sections using TMARKER (88). Additive or synergistic effect was examined using online tool SynergyFinder (<https://synergyfinder.fimm.fi>) (89).

Statistical analysis

Results are shown as the mean \pm SEM of three independent experiments. Shapiro-Wilk test was used to test for normality distribution. If the Sig. value of the Shapiro-Wilk Test is greater than 0.05, the data is considered normal. For comparison among multiple groups, one-way analysis of variance (ANOVA) followed by Dunnett's post-hoc test or Tukey's HSD test was used depending on the nature of comparison. Student's t test was applied if only two groups were compared. When there were more than one continuous dependent variables, one-way multivariate analysis of variance (one-way MANOVA) was used to determine whether there were any differences between independent groups. If data did not distribute normally, Kruskal-Wallis test followed by Games-Howell post-hoc test was used as a non-parametric counterpart of ANOVA for multiple comparison, and Mann-Whitney U test as counterpart of Student's t test for two group comparison.

Statistical analyses were performed in SPSS v22.0 (IBM SPSS Statistics). A p-value of less than 0.05 is considered statistically significant. * $p < 0.05$, ** $p < 0.01$, *** $p < 0.001$, **** $p < 0.0001$.

Results

Downregulation of APE1 sensitizes dMMR CRC cells to 5-FU in vitro

To examine the role of APE1 in promoting 5-FU resistance in CRC, we used highly 5-FU resistant dMMR colon adenocarcinoma HCT116 (73) and isogenic HCT116 cells expressing APE1-specific shRNA (38). We found that downregulation of APE1 sensitized HCT116 to 5-FU (**Fig. 4**). This phenomenon was confirmed in DLD-1 and HCT116 by siRNA interference (**Fig. 5**), as evidenced by a decrease in the IC₅₀ by approximately 10-fold (**Fig. 6**).

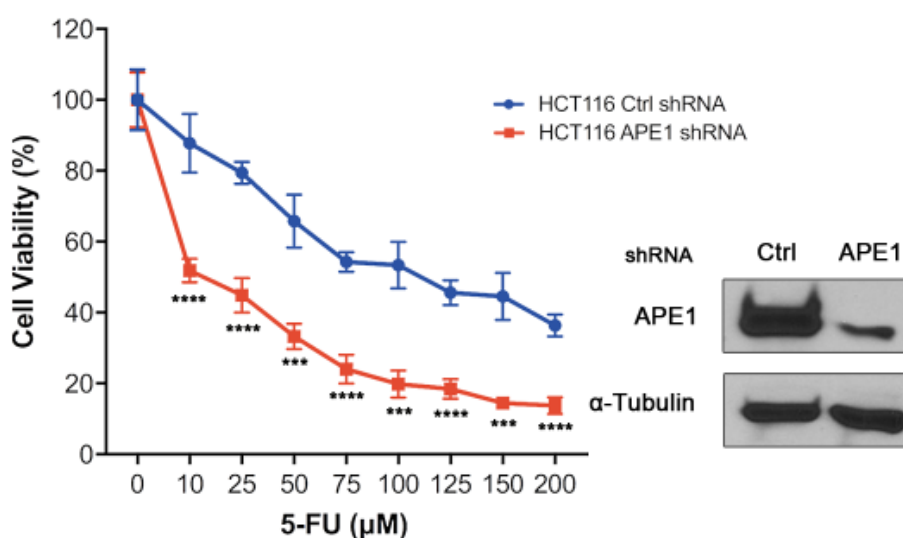


Figure 4. APE1 shRNA significantly enhances 5-FU cytotoxicity in HCT116 cells.

To investigate whether APE1 plays a role in 5-FU resistance in colon cancer, HCT116 cells stably expressing control (ctrl) shRNA or APE1-shRNA were treated with various doses of 5-FU for 72 hours. HCT116 is a mismatch repair deficient cell line and highly resistant to 5-FU. Viable cells were quantitated in six replicates for each dose by MTT assay (Left). To verify the successful knockdown of APE1, the level of APE1 was measured by immunoblot analysis (Right), which demonstrated significant decrease of

APE1 level with shRNA. As shown in MTT assay, cell viability significantly reduced after APE1 knockdown. Results are shown as the mean \pm SEM of three independent experiments. One-way ANOVA with Dunnett's post-hoc test, *** $p < 0.001$, **** $p < 0.0001$.

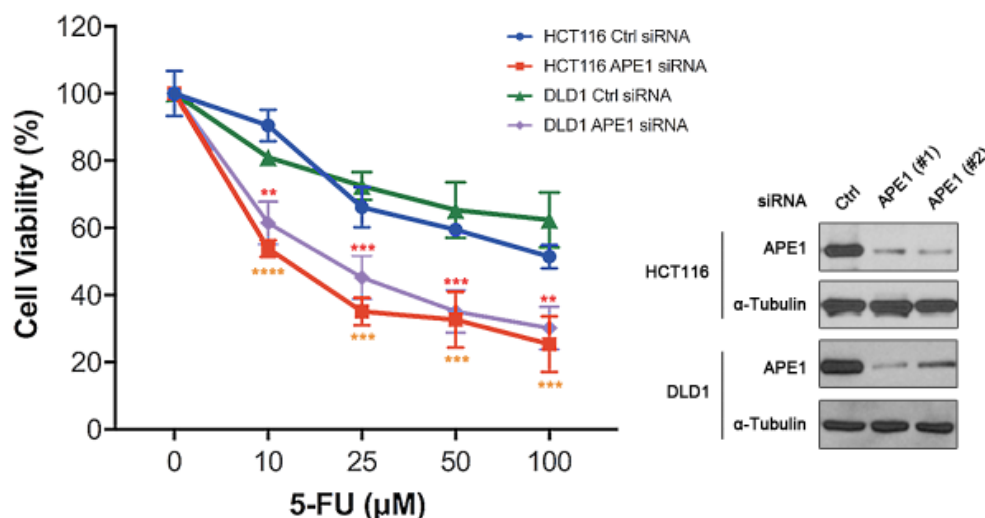


Figure 5. APE1 siRNA significantly enhances 5-FU cytotoxicity in HCT116 and DLD1 cells.

To further confirm our finding from Figure 4, we used siRNA to knockdown APE1 level in HCT116 and DLD-1 cells. Both HCT116 and DLD-1 are mismatch repair deficient cell lines and highly resistant to 5-FU. Cells were exposed to 5-FU for 72 hours and MTT assay was performed. Immunoblot image showing the levels of APE1 after siRNAs transfection has decreased significantly, indicating successful knockdown of APE1 (Right). Note that two different siRNAs of APE1 are used, both of which showed successful knockdown of APE1 in either cell line. Consistent with prior experiment, we noted APE1 knockdown significantly enhanced 5-FU cytotoxicity. Yellow asterisks mark the comparison between HCT116-ctrl siRNA and HCT116-APE1 siRNA. Red asterisks mark the comparison between DLD1-ctrl siRNA and DLD1-APE1 siRNA. Six technical repeats were performed

per sample and three biological replicates for each siRNA were analyzed. Results are shown as the mean \pm SEM. One-way ANOVA with Dunnett's post-hoc test, ** $p < 0.01$, *** $p < 0.001$, **** $p < 0.0001$.

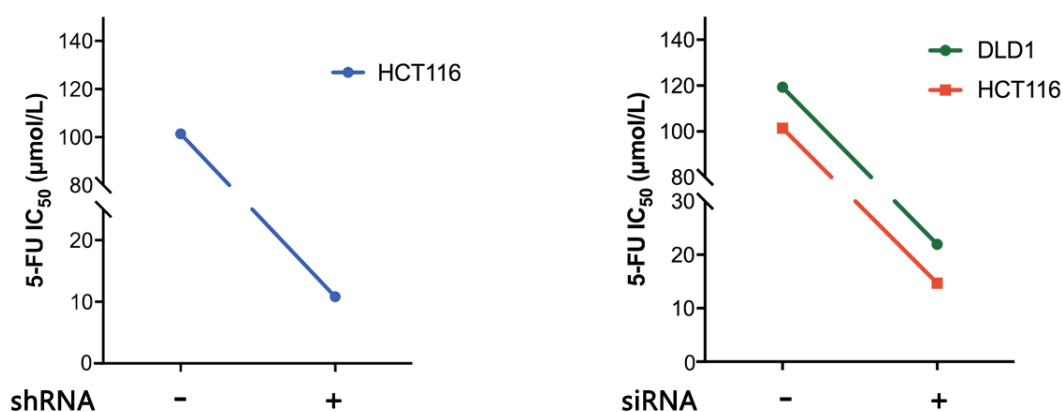


Figure 6. IC₅₀ of 5-FU drops markedly after APE1 knockdown in HCT116 and DLD-1 cells.

We used GraphPad to fit a dose response curve to determine the IC₅₀. Line charts illustrating a ~10-fold drop in IC₅₀ of 5-FU after APE1 knockdown by shRNA or siRNA. Figure 4-6 together demonstrated apparent change of 5-FU efficacy after APE1 knockdown, suggesting that APE1 plays a key role in 5-FU resistance which provides rationale for the following studies.

APE1 interacts with nucleosome remodeling histone chaperone FACT complex in chromatin

In the absence of highly selective and nontoxic small molecule inhibitors of DNA repair function of APE1 (90), we set out to identify targets that regulate APE1 function in cells. To identify the interacting partners of AcAPE1, we immunoprecipitated (IP)

endogenous AcAPE1 from the chromatin fraction using our AcAPE1-specific antibody. After separation in SDS-PAGE followed by identification of protein bands by MALDI-TOF-TOF analysis, we identified a large number of proteins involved in the repair of damaged DNA as the prominent AcAPE1 interacting partners (**Fig. 7**). We found DNA Ligase III, PARP1, both subunits (SPT16 & SSRP1) of FACT complex, nucleolin, chromatin assembly factor 1a (CHAF1a), and all four core nucleosome histones H2A, H2B, H3 and H4 in the AcAPE1 IP complex. We focused on the FACT complex because increasing evidence suggests that FACT complex plays a role at sites of UV damage and single-strand breaks (SSBs) in cells (91,92). FACT complex, a heterodimer of Structure-Specific Recognition Protein1 (SSRP1) and Suppressor of Ty (SPT16), was originally identified as a histone chaperone complex that facilitates the removal and deposition of histone H2A/H2B in nucleosome during transcription initiation and elongation (63,93). We confirmed the interaction of AcAPE1 with FACT complex by immunoprecipitating AcAPE1 from nuclear and chromatin extracts followed by Western blot analysis. We found both subunits of FACT in AcAPE1 IPs, in both chromatin and nuclear fractions (**Fig. 8**). Confocal microscopy revealed colocalization of AcAPE1 with SPT16 and SSRP1 in the nucleus (**Fig. 9**). To examine whether acetylation of APE1 is required for its interaction with FACT complex, we immunoprecipitated FLAG-tagged WT-APE1 and nonacetylatable K5R mutant from nuclear fractions. No significant differences were observed in the amount of SPT16 bound with WT and non-acetylatable K5R APE1 IPs, indicating that acetylation of APE1 is not essential for its interaction with FACT complex (**Fig. 10**). We also used the FLAG-tagged N-terminal 33 amino acids deleted N Δ 33 mutant and K5Q APE1 mutant which cannot enter the nucleus and stably bind to chromatin in cells (38,86). Our data showed that inhibition of either nuclear localization or chromatin binding of APE1 significantly reduced the amount of SPT16 or SSRP1 in APE1 IP (**Fig. 10**). Together,

these data indicate that APE1 forms complex with FACT in chromatin, and acetylation is not essential for this interaction.

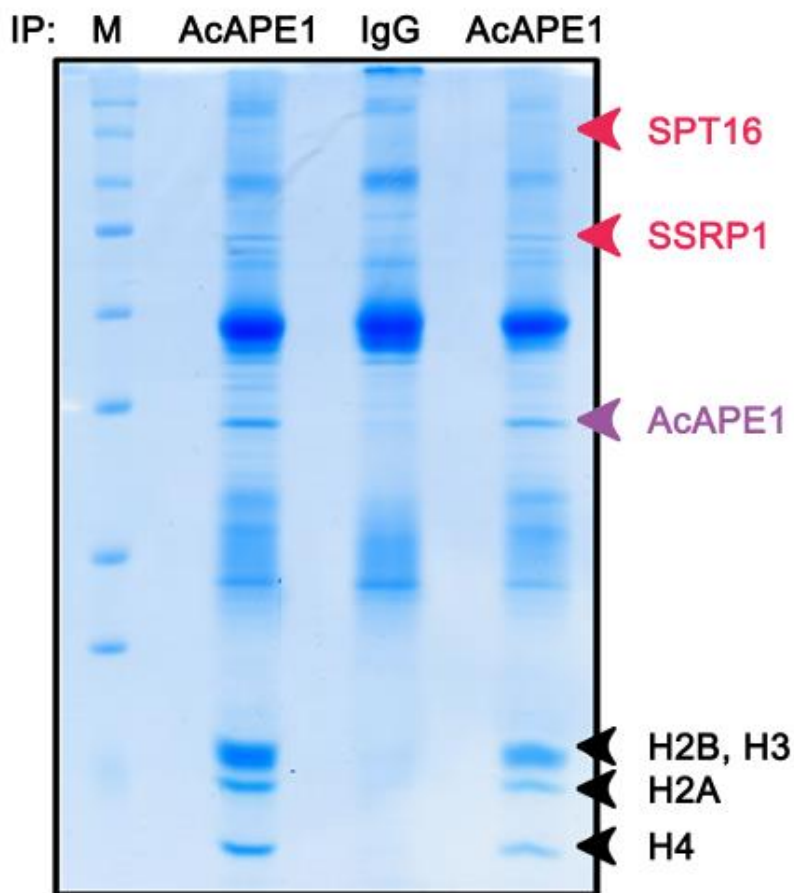


Figure 7. IP of endogenous AcAPE1 reveals both subunits of FACT complex as interacting partner.

To identify the interacting partners of AcAPE1 in chromatin, endogenous AcAPE1 was immunoprecipitated from chromatin extracts and resolved in SDS-PAGE gel followed by MALDI-TOF/TOF analysis. We identified multiple proteins, including H2A, H2B, H3, H4, and both subunits of FACT complex (SSRP1 and SPT16) as shown by arrow.

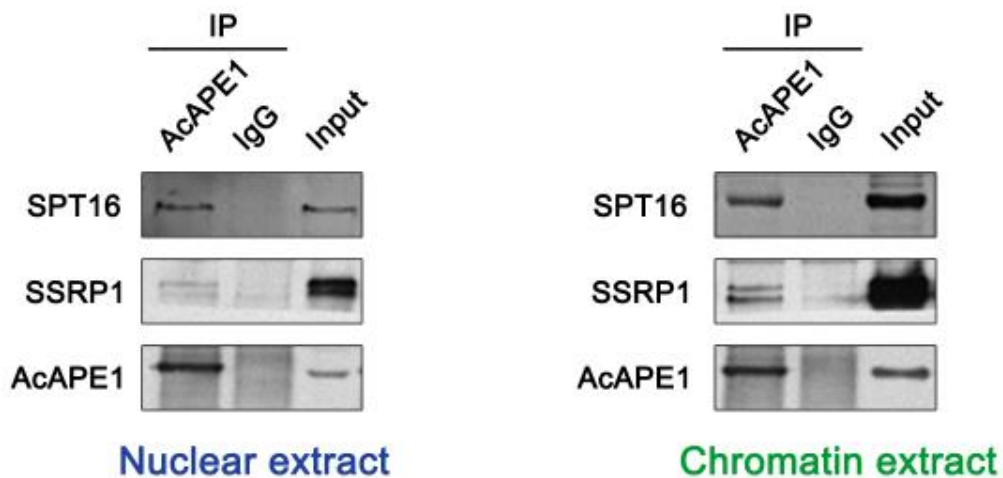


Figure 8. Co-IP of AcAPE1 in nuclear and chromatin extracts confirms the interaction of AcAPE1 with FACT complex.

To confirm our unbiased mass spec. approach of finding of AcAPE1 and FACT interaction, we used co-IP with AcAPE1 antibody followed by Western blot analysis which showed the presence of SSRP1 and SPT16 in AcAPE1 IP complex from nuclear and chromatin extracts.

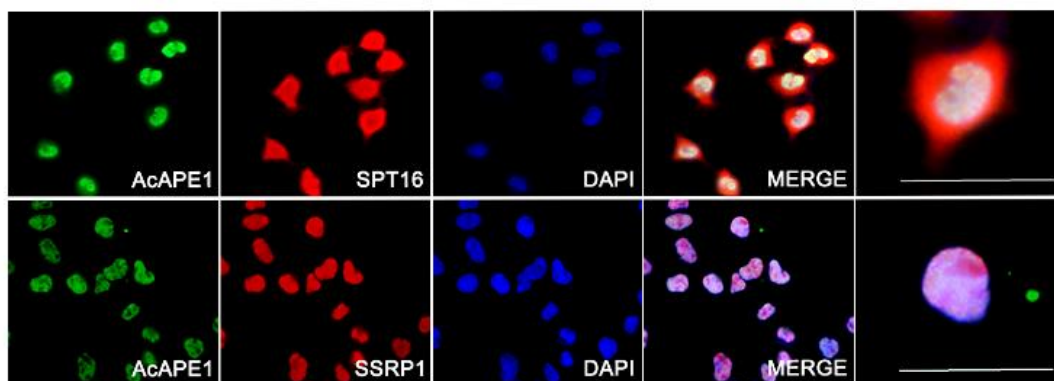


Figure 9. Confocal microscope demonstrates the colocalization of AcAPE1 and FACT complex.

Consistent with co-IP and western blot analysis, we visualized the colocalization of AcAPE1 with SPT16 and SSRP1 using confocal microscope. Note that the colocalization is located in nuclei only. Three biological replicates were analyzed. Representative images were shown. Bar = 50 μ m.

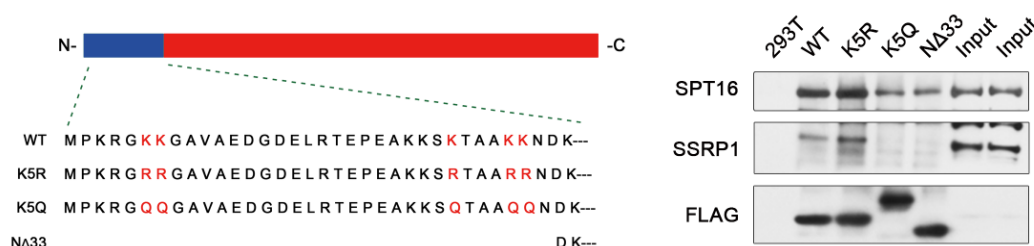


Figure 10. APE1 forms complex with FACT, and acetylation is not essential for this interaction.

(Left) Schematic diagram showing the mutation (red) and deletion sites in the N-terminus of APE1. Lysine residues K6,7,27,31,32 were mutated to glutamine (K5Q) or arginine (K5R) in FLAG-tagged WT APE1 using a site-directed mutagenesis Kit (Stratagene). Both K5Q and K5R are nonacetylatable mutants of APE1, with the latter maintains a positive charge. To examine whether acetylation of APE1 is required for its interaction with FACT complex, we immunoprecipitated FLAG-tagged WT-APE1 and nonacetylatable K5R mutant from whole cell extract. No significant differences were observed in the amount of SPT16 bound with WT and non-acetylatable K5R APE1 IPs, indicating that acetylation of APE1 is not essential for its interaction with FACT complex. In comparison, K5Q had less association with FACT complex in the IP complex, indicating a role of positive charge in the interaction. We also used the FLAG-tagged N-terminal 33 amino acids deleted N Δ 33 mutant and found that inhibition of localization significantly reduced the amount of SPT16 or SSRP1 in APE1 IP. Together, these data indicate that APE1 forms complex with FACT

in chromatin. While acetylation is not essential for this interaction, positive charge of APE1 may play a role.

Induction of AP sites enhances colocalization of AcAPE1 and FACT in chromatin

To determine whether induction of DNA damage promotes interaction of APE1 and FACT at damage sites, we generated AP sites in the genome by 5-FU or MMS treatment (a widely used alkylating agent that induces AP sites in the genome) (94). Structured Illumination Microscopy (SIM) revealed enhanced colocalization of both subunits of FACT complex with APE1 or AcAPE1 upon treatment (**Fig. 11 & 12**). The Pearson correlation coefficient (PCC) was used to quantify the degree (+1 perfect correlation to -1 perfect but negative correlation) of colocalization between fluorophores (**Fig. 13**). There was significant increase of colocalization of APE1 or AcAPE1 with FACT complex upon induction of DNA damages, raising the possibility that recruitment of FACT to the damage sites may promote binding and acetylation of APE1 during the DNA repair process. We examined the levels of FACT and AcAPE1 in chromatin fraction at several time points following MMS treatment. Treatment of MMS resulted in increasing levels of AcAPE1 and both subunits of FACT complex in chromatin fraction in a time-dependent manner (**Fig. 14**). Our Co-IP data showed that there was an increasing association of AcAPE1 and FACT complex upon induction of DNA damage (**Fig. 15**). Previously, we showed that APE1 regulates p21 expression via binding to the p21 and DTL proximal promoter regions and functions as a coactivator or corepressor depending on the p53 status of the cells (95). To understand if FACT facilitates the recruitment and/or binding of APE1 to damage sites in p21 and DTL promoters, we treated the cells with MMS and cross-linked the chromatin. We performed CHIP assays with AcAPE1 and SPT16 antibodies. We found

that induction of DNA damage significantly increased the binding/occupancy of AcAPE1 and SPT16 to the p21 and DTL gene promoter regions (**Fig. 16**).

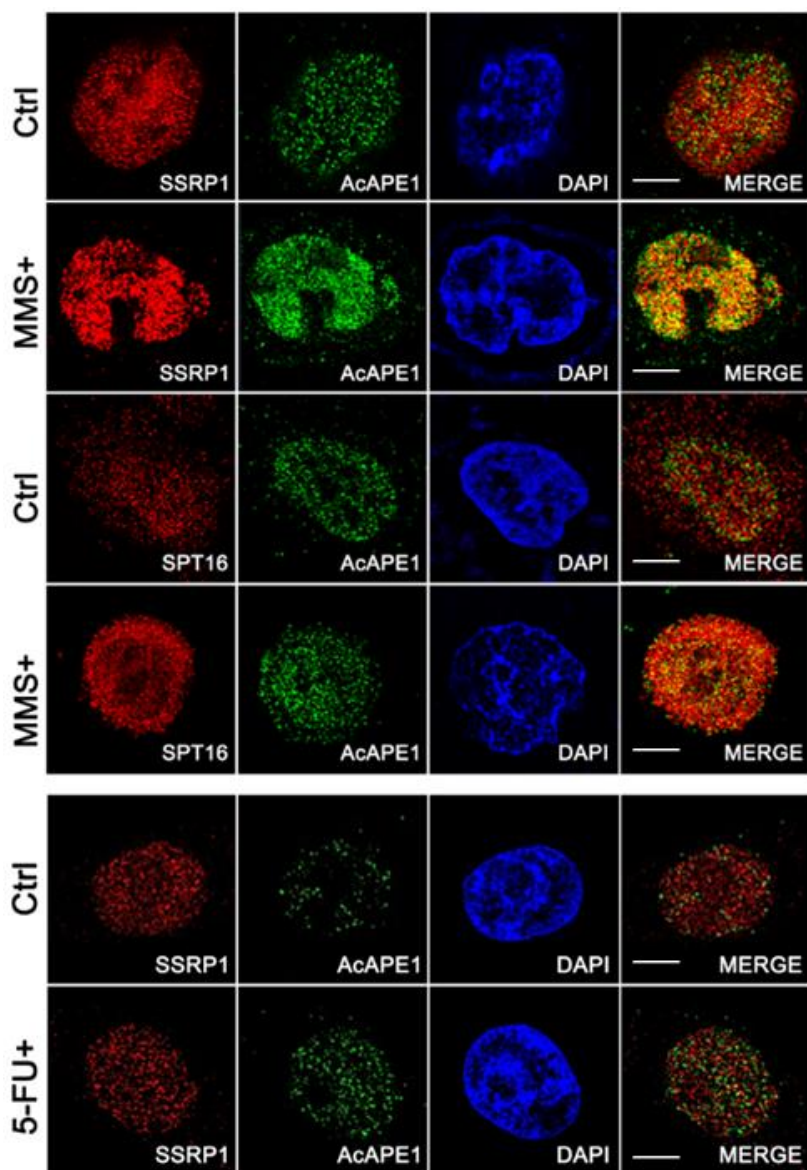


Figure 11. Colocalization of AcAPE1 and FACT complex increases upon induced DNA damages.

To investigate whether induced DNA damage affects the interaction, HCT116 cells were treated with MMS (1 mM) for 30 minutes or 5-FU (10 μ M) for 24 hours and cells were fixed

with paraformaldehyde submitted for immunofluorescence staining. Colocalization of SSRP1 or SPT16 with AcAPE1 was examined in multiple cells by Structured-Illumination Microscopy (SIM). MMS and 5-FU significantly induced the interaction of AcAPE1 and FACT complex. Three technical repeats were performed per sample and three biological replicates were analyzed. Representative images were shown. Bar = 5 μ m.

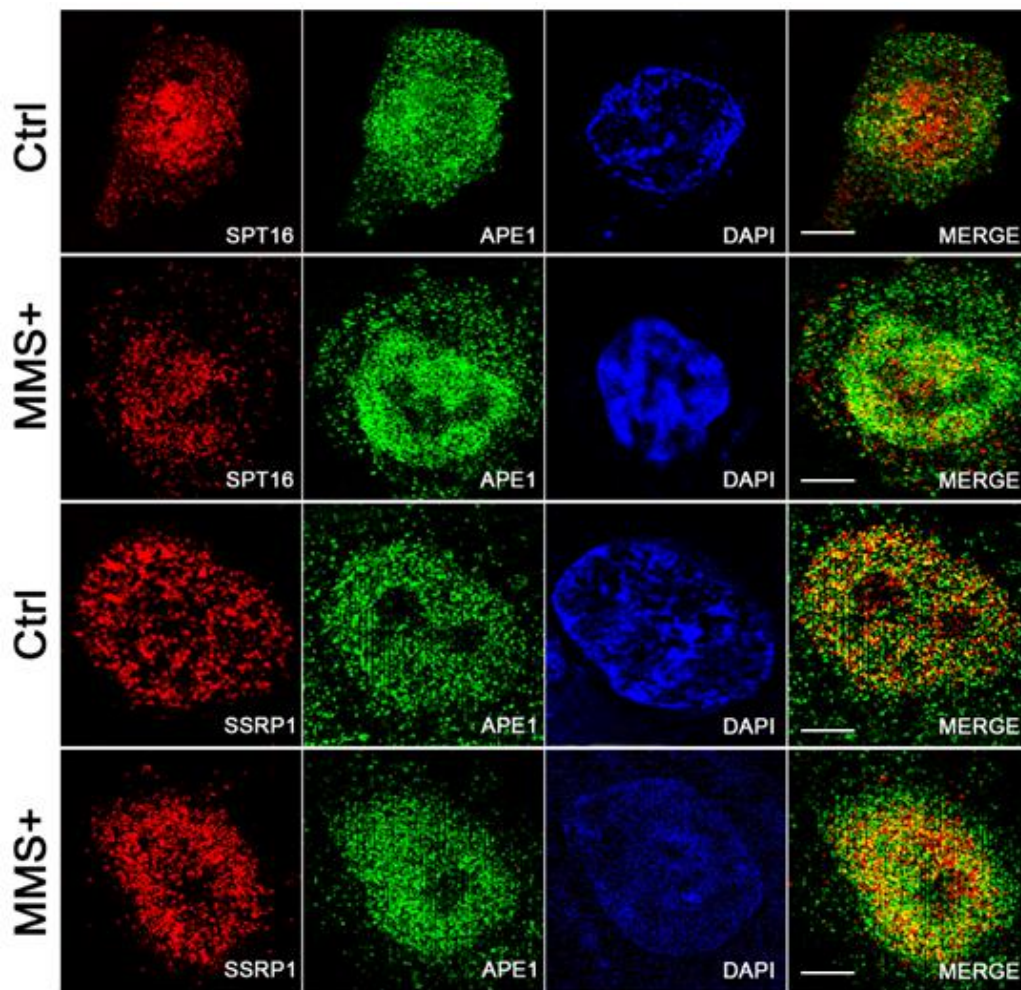


Figure 12. Colocalization of APE1 and FACT complex remains unchanged upon MMS treatment.

Following the above immunofluorescence analysis, we examined if MMS has effects on the interaction of APE1 (instead of acetylated form of APE1) and FACT. HCT116 cells were treated with MMS for 30 minutes or 5-FU for 24 hours. The colocalization of APE1 with SPT16 and SSRP1 remained stable without detectable changes under SIM. Three technical repeats were performed per sample and three biological replicates were analyzed. Representative images were shown.

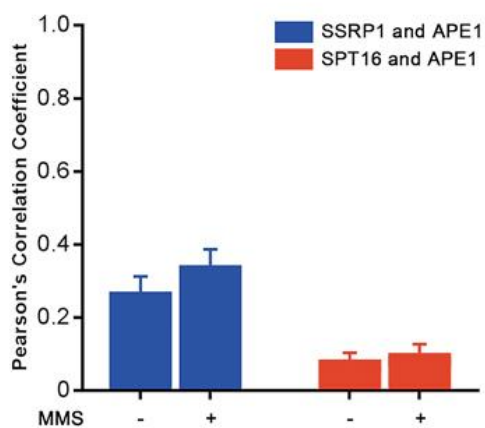
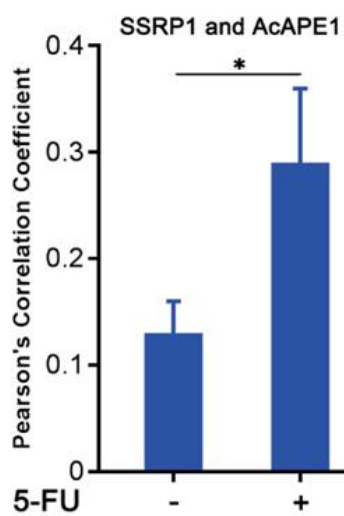
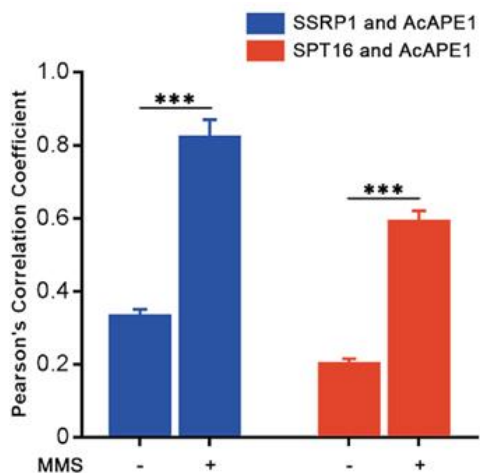


Figure 13. Pearson correlation coefficient of AcAPE1 and FACT complex increases upon induction of DNA damages.

To quantify the colocalization of the proteins of interest, we used Pearson correlation coefficient (PCC) which is a measure of the strength of the association between the two variables (96). The correlation coefficient ranges from -1 to $+1$, with $+1$ being perfect correlation and -1 being perfect but negative correlation. PCC of AcAPE1 and SSRP1 or SPT16 increased significantly upon induction of DNA damages either by MMS (top panel) or 5-FU (middle panel). The change in PCC of APE1 with SSRP1 or SPT16 did not demonstrate any statistical significance (bottom panel). Data from ten cells were analyzed. Top and bottom panels, MANOVA with Tukey's HSD test; middle panel, Student's t test; * $p=0.035$; *** $p<0.001$.

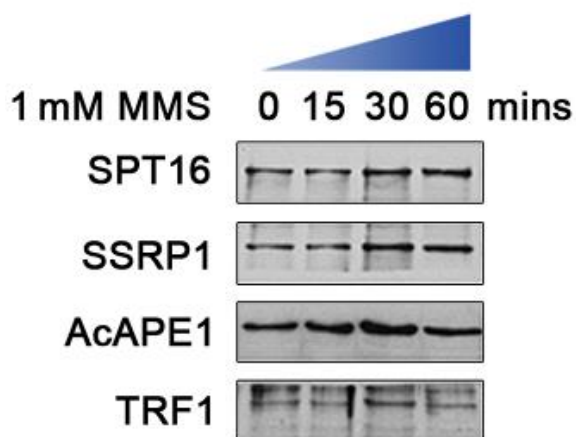


Figure 14. MMS treatment increases the expression of FACT complex and AcAPE1 in chromatin fraction.

To investigate whether MMS treatment has an effect on the AcAPE1 and FACT complex expression, HCT116 cells were treated with 1 mM MMS for various time periods as indicated. AcAPE1, SSRP1 and SPT16 proteins levels increased in chromatin extracts after MMS treatment in a time-dependent manner.

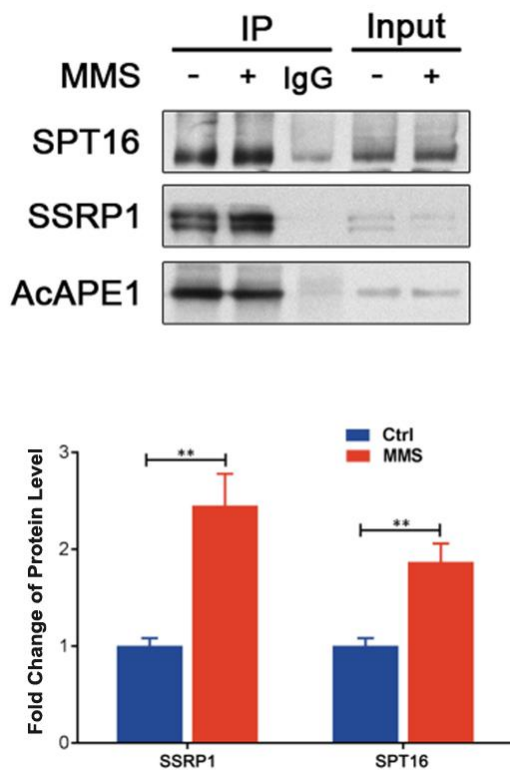


Figure 15. Interaction of AcAPE1 and FACT complex increases upon induction of DNA damages.

To understand if MMS treatment increases the association between AcAPE1 and FACT complex, HCT116 cells were treated with 1 mM MMS and the chromatin extract was immunoprecipitated with AcAPE1 antibody, followed by immunoblot analysis of SSRP1 and SPT16 antibodies (Top). MMS significantly induced the interaction of AcAPE1 and SSRP1 as well as SPT16. (Bottom) Quantification SPT16 and SSRP1 in IP was done by Image J software and average of three independent co-IP experiments demonstrated that the fold change of SSRP1 and SPT16 levels before and after MMS treatment. MANOVA with Tukey's HSD test, ** $p < 0.01$.

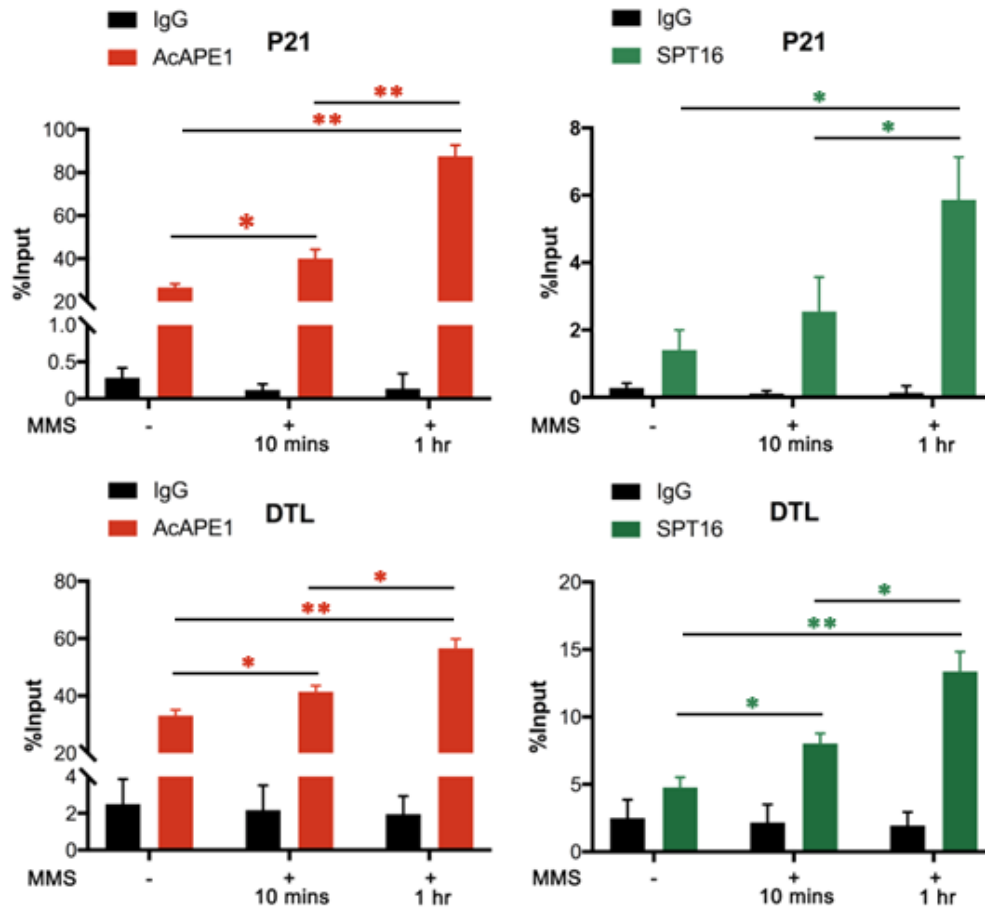


Figure 16. Occupancy of AcAPE1 and SPT16 to p21 and DTL promoter regions significantly increases upon MMS treatment.

To understand whether MMS treatment affects the occupancy of AcAPE1 and SPT16 to p21 and DTL promoter regions, cells were treated with 1 mM MMS and fixed with formaldehyde. Protein-DNA was crosslinked, followed by lysis of cells. Chromatin was harvested and fragmented, which was then subjected to immunoprecipitation with AcAPE1 and SPT16 antibodies. PCR of p21 and DTL sequences revealed that the binding of AcAPE1 and SPT16 significantly increased upon MMS treatment. Three technical repeats were performed per sample and three biological replicates were analyzed. Results are shown as the mean \pm SEM. The difference was noted both at 10 minutes and 1-hour time points. One-way ANOVA with Tukey's HSD test, * $p < 0.05$, ** $p < 0.01$.

FACT complex facilitates the binding and acetylation of APE1 to damage site in chromatin.

To examine if FACT is required for facilitating the binding and acetylation of APE1 at damage sites in chromatin, we used siRNA to downregulate SPT16 and SSRP1 individually and both together (**Fig. 17**). Consistent with prior report, we found that downregulation of either subunit SPT16 or SSRP1 affected the level of the other subunit in cells (97). We found a significant decrease of AcAPE1 level when both subunits of FACT were downregulated (**Fig. 17**). SIM demonstrated that FACT knockdown reduced the AcAPE1 level but did not alter total APE1 level in cells (**Fig. 18 & 19**). As acetylation of APE1 occurs after binding to AP site in chromatin, these data indicate that the absence of FACT complex significantly reduced the access or binding of APE1 to damage sites and its subsequent acetylation in chromatin. We examined the binding or occupancy of unmodified APE1 and AcAPE1 to p21 and DTL promoter in FACT downregulated cells by CHIP assays. CHIP assays revealed that FACT downregulation significantly abrogated the occupancy of APE1 and AcAPE1 to p21 and DTL promoters upon DNA damages (**Fig. 20 & 21**). Together, these data provide evidence that the FACT complex promotes the binding and subsequent acetylation of APE1 to damage sites in chromatin.

To further examine the role of FACT in regulating APE1 binding dynamics to damage sites, we used Fluorescence Recovery After Photobleaching (FRAP) (98) to quantify the mobility of GFP-tagged APE1 in the presence or absence of FACT complex. Fluorescence was bleached using an excitation laser, and the recovery of fluorescence in that region due to binding of new GFP-tagged APE1 into chromatin was monitored (98). The mobile fraction represents the fraction of recovered fluorescence and the half-life ($T_{1/2}$) is the time it takes for fluorescence intensity to reach half the maximum of the plateau

level. In the presence of MMS, the mobile fraction of APE1 in FACT downregulated cells was significantly lower compared to control cells (**Fig. 22**), suggesting that FACT regulates the mobility and binding dynamics of APE1 to damage sites in chromatin.

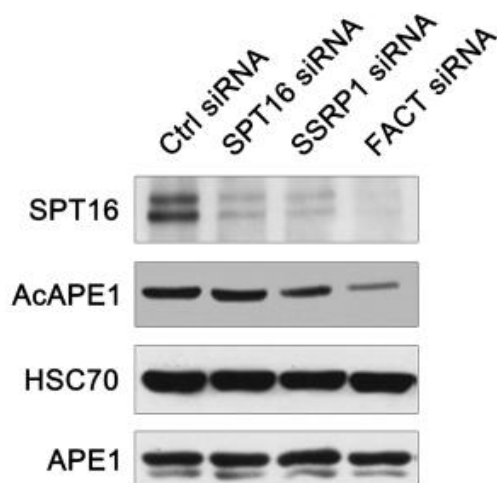


Figure 17. FACT KD decreases the level of AcApe1 but has no effect on total Ape1 level.

To examine if FACT is required for facilitating the binding and acetylation of APE1 at damage sites in chromatin, HCT116 cells were transfected with SPT16 or SSRP1 siRNA individually or both together (FACT) and the levels of AcApe1 and Ape1 were measured by Immunoblot analysis after 48 hours. Note that FACT siRNA means siRNAs of SSRP1 plus SPT16. We found that KD of either unit, SPT16 or SSRP1, decreased the AcApe1 level (more apparent in SSRP1 KD cells). Such effect was most evident when both subunits of FACT complex were depleted. We also found that the Ape1 level had stayed unchanged with SPT16 and/or SSRP1 treatment. Three biological replicates were analyzed. Representative images were shown.

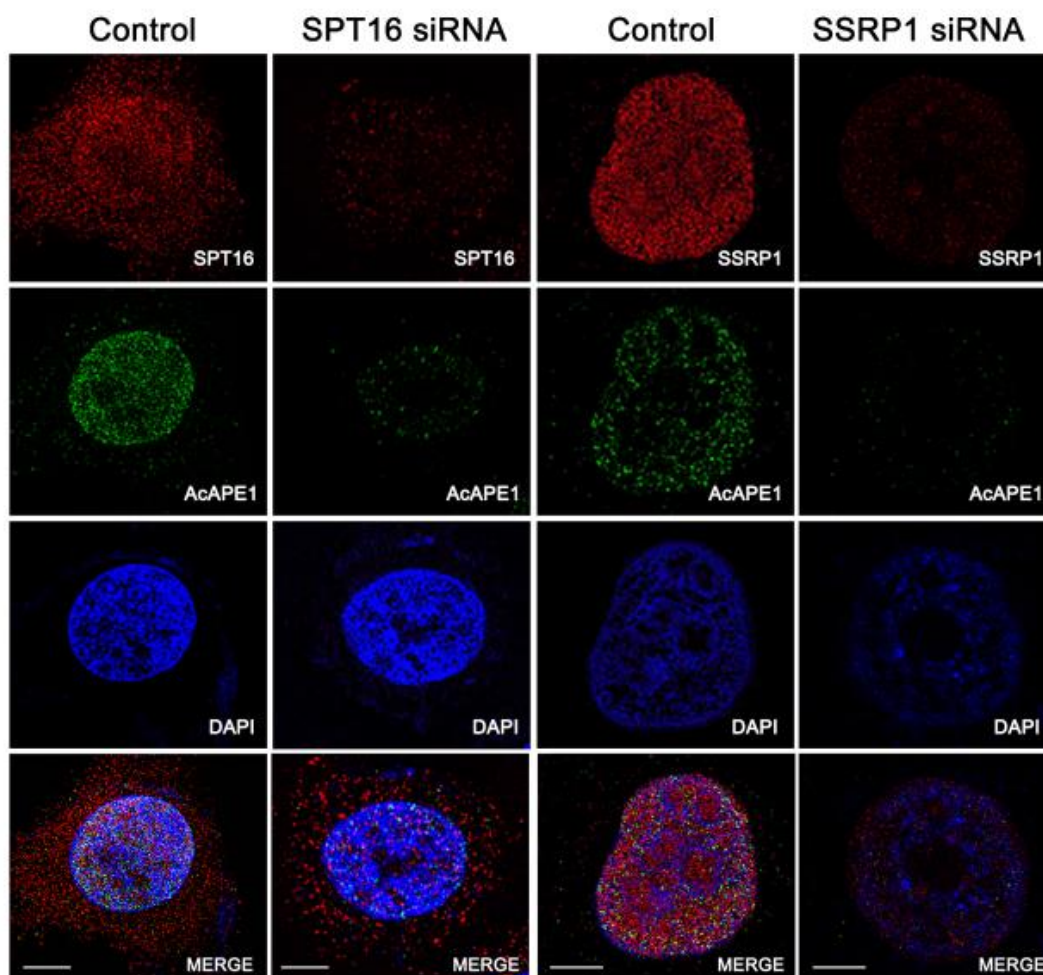


Figure 18. AcAPE1 level decreases upon knockdown of FACT complex.

To confirm our finding of the effect of FACT KD on APE1 and AcAPE1 levels, we used immunofluorescence staining. SPT16 or SSRP1 level individually or both together (FACT) was downregulated by siRNA for 48 hours and the levels of AcAPE1 and APE1 were examined by immunofluorescence. The decrease in the fluorophores detected in SPT16 and SSRP1 staining cells proves successful knockdown. Images of one representative cell is shown. Consistent with our IP result, the AcAPE1 staining reduced markedly after knockdown of SSRP1 or SPT16. Bar = 5 μ m.

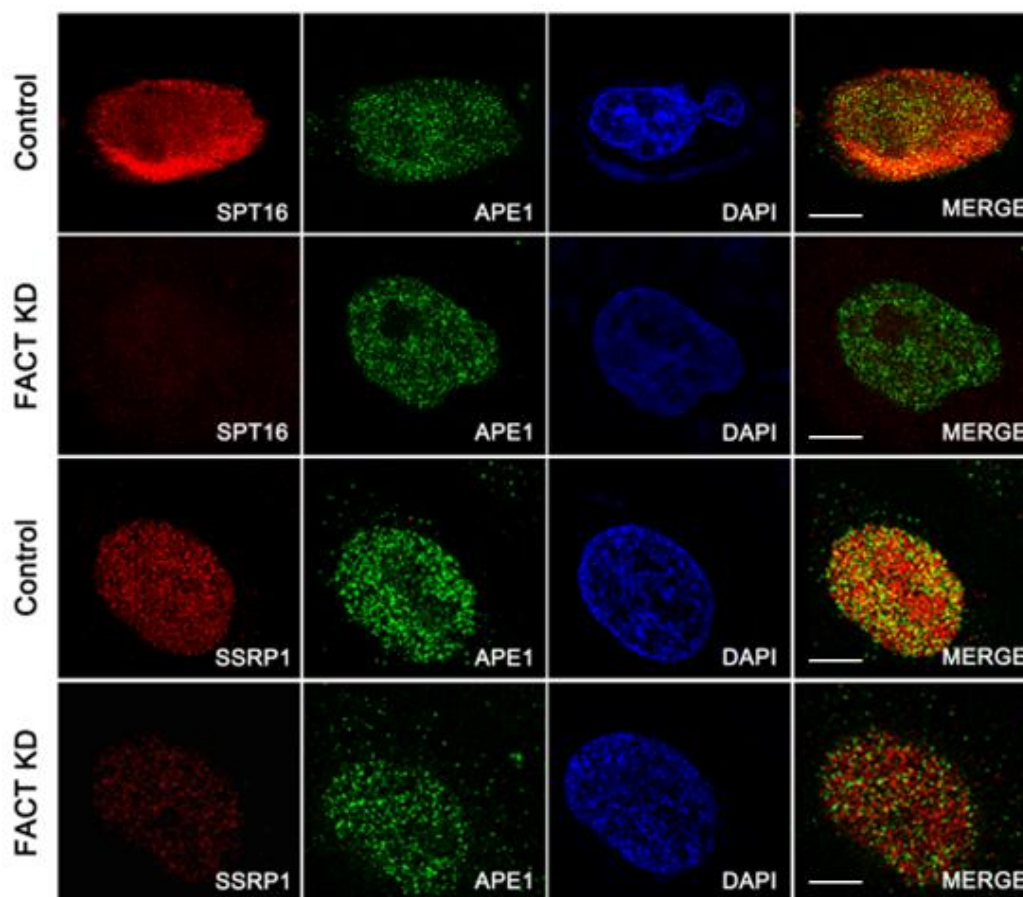


Figure 19. APE1 expression remains unchanged upon FACT KD.

This is in continuation of the previous experiment. After we demonstrated that FACT KD had no effect on total APE1 level by IP, we sought to confirm this finding using immunofluorescence staining. As compared to control cells, FACT KD cells demonstrated no change in staining of APE1. Three biological replicates were analyzed. Representative images were shown. As acetylation of APE1 occurs after binding to AP site in chromatin, these data (Fig. 17-19) indicate that the absence of FACT complex significantly reduced the access or binding of APE1 to damage sites and its subsequent acetylation in chromatin.

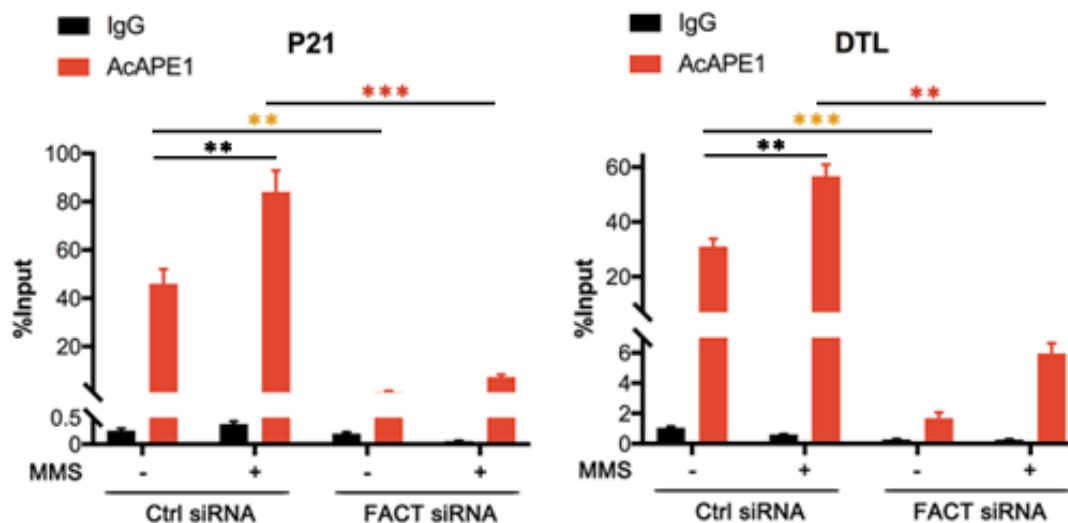


Figure 20. FACT KD prevents the increase of occupancy of AcAPE1 to p21 and DTL promoter regions upon MMS treatment.

Earlier we have shown that induction of DNA damage by MMS significantly increased the binding of AcAPE1 to p21 and DTL promoter regions (Fig. 16). We also showed that FACT KD had decreased the binding and subsequent acetylation of APE1 at chromatin. To assess if FACT KD affects the occupancy of AcAPE1 to p21 and DTL promoters, cells were treated with FACT siRNA for 48 hours and 1 mM MMS treatment for 1 hour, followed by ChIP analysis. Consistent with our prior result, MMS treatment increased the binding of AcAPE1 to p21 and DTL promoter regions. However, this effect was abrogated by depletion of FACT complex. Yellow asterisks mark the comparisons between ctrl siRNA and FACT siRNA without MMS treatment. This indicates that FACT KD alone (without induced DNA damage by MMS) decreases the AcAPE1 occupancy to both promoter regions, suggesting a role of FACT in the access and binding of AcAPE1 in normal cellular process. Red asterisks mark the comparisons between ctrl siRNA and FACT siRNA at the presence of MMS. This indicates that the effect of increased AcAPE1 occupancy induced by MMS is blunted if FACT complex is depleted, and further confirms the role of FACT complex in the access and binding of AcAPE1 to chromatin. Average enrichment relative

to % of input from three independent ChIP assays were shown. One-way ANOVA with Tukey's HSD test, ** $p < 0.01$, *** $p < 0.001$.

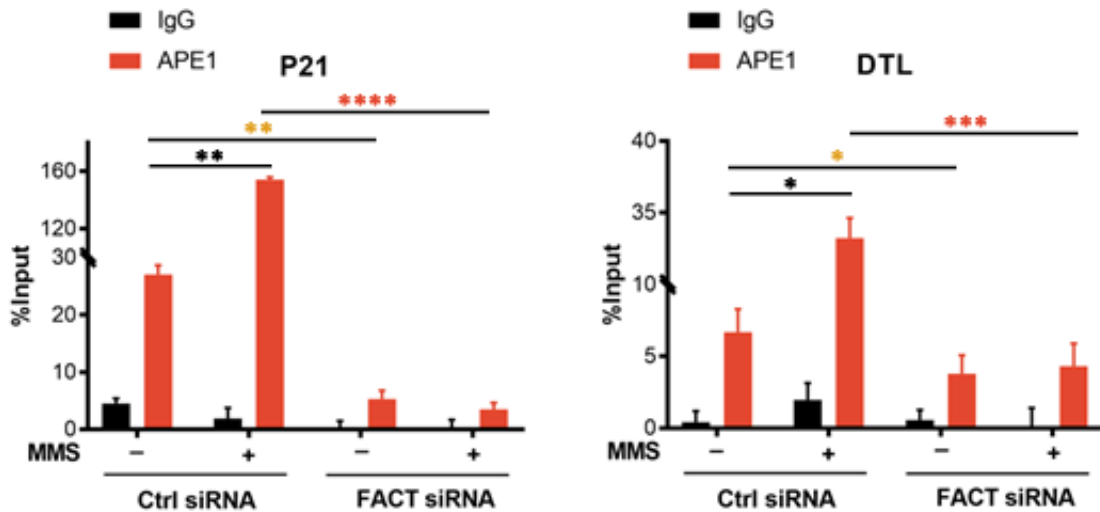


Figure 21. FACT KD prevents the increase of occupancy of APE1 to p21 and DTL promoter regions upon MMS treatment.

The previous ChIP analysis use antibody targeting acetylated APE1. However, the total APE1 may have different binding and occupancy to p21 and DTL promoter regions. Therefore, we performed ChIP analysis using total APE1 antibody which identifies all forms of APE1 in cells including acetylated APE1. There was some variation of how the APE1 occupancy changed in response to FACT knockdown and MMS treatment compared to the analysis where we used AcAPE1 antibody. The trend of changes, however, was consistent. As noted in the above figure, MMS treatment increased the APE1 occupancy to both promoter regions. When FACT complex was depleted, the APE1 occupancy reduced significantly which was marked as yellow asterisks (ctrl siRNA vs FACT siRNA without MMS treatment). Red asterisks mark the comparisons between ctrl siRNA and FACT siRNA at the presence of MMS, which demonstrated significant reduction of APE1 binding/occupancy to these promoter regions despite MMS induced

damage. Average enrichment relative to % of input from three independent ChIP assays data were shown. One-way ANOVA with Tukey's HSD test, * $p < 0.05$, ** $p < 0.01$, *** $p < 0.001$, **** $p < 0.0001$.

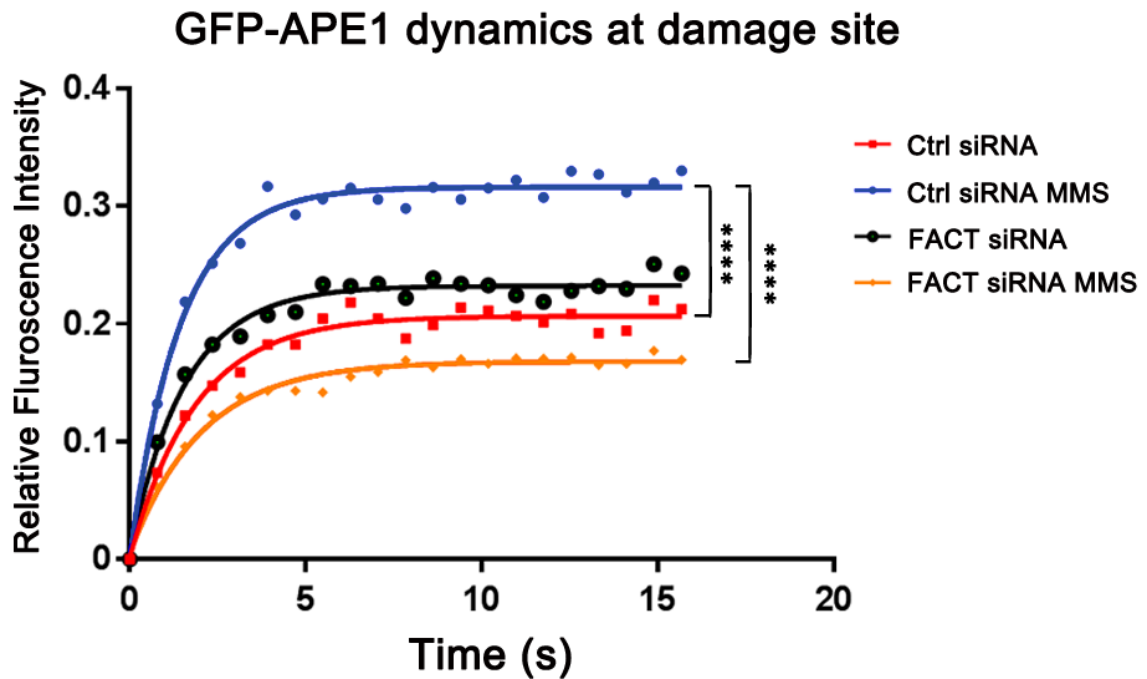


Figure 22. APE1 dynamics decreases after FACT KD.

Fluorescence recovery after photobleaching (FRAP) is a microscopy-based method used to study the mobility of fluorescent molecules. To determine if FACT complex plays a role in the mobility of APE1, N-terminal GFP tagged-APE1 was transfected into HCT116 cells. 48 hours after transfection of control and FACT siRNAs, cells were treated with DMSO or MMS. Specific regions were bleached with laser and the recovery of GFP fluorescence was examined. As expected, MMS treatment increased APE1 mobility while FACT KD decreased it. In FACT KD cells, however, the mobility of APE1 failed to increase despite MMS treatment, indicating that FACT complex facilitates the access and mobility in

damage regions. We performed FRAP experiments on at least 20 cells per condition and three biological replicates were performed. Individual FRAP measurement curves were averaged to get a single FRAP curve (99). One-way ANOVA with Dunnett's post-hoc test, **** $p < 0.0001$.

FACT is required for efficient repair of AP site damages in cells and downregulation of FACT sensitizes CRC cells to 5-FU

As FACT promotes binding and subsequent acetylation of APE1, we deduced that cells would accumulate AP sites in the absence of FACT. We depleted FACT complex by siRNA and quantitated AP sites in the genome. As expected, depleting FACT complex significantly increased the number of AP sites in the genome compared to control (**Fig. 23**). We also treated these cells with MMS to induce AP site damages. As shown in **Fig. 23**, AP sites accumulated significantly in the genome after MMS treatment in both control and FACT downregulated cells. However, after 6 hours of release, FACT knockdown cells retained significantly more AP sites, indicating that efficient AP site repair depends on the function of FACT complex. To provide further evidence for the role of FACT in facilitating the AP site or SSBs repair in cells, we used single cell alkaline comet assay which detects the SSBs and DSBs damages in the genome in cells. Knockdown of FACT significantly delayed the repair of MMS-induced DNA damages in the genome compared to control cells (**Fig. 24**). Consistently, we found that downregulation of FACT sensitizes HCT116 and RKO cell lines to 5-FU (**Fig. 25**). Together, these data indicate that FACT complex plays a crucial role in AP site or SSBs repair in cells.

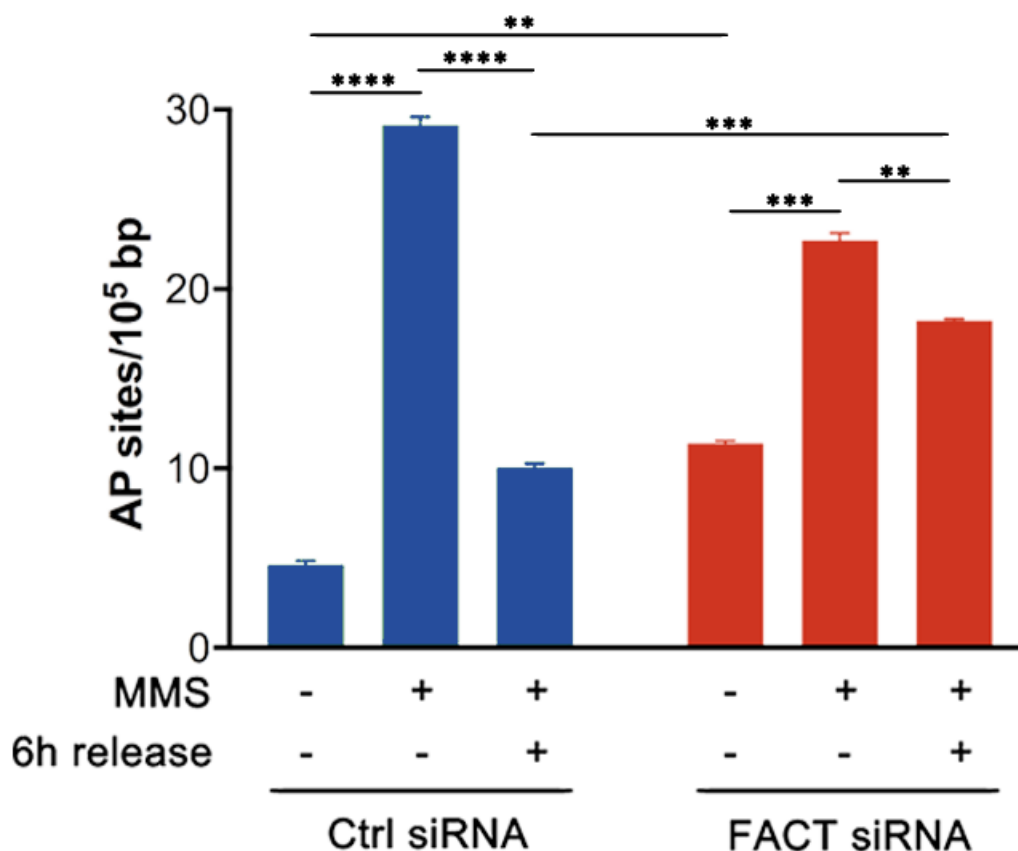


Figure 23. MMS treatment increases AP sites, and FACT KD cells retains significantly more AP sites after recovery.

MMS is a classic BER substrate-generating compound that modifies both guanine (to 7-methylguanine) and adenine (to 3-methyladenine) to cause base mispairing and replication blocks (100). The damaged bases are removed by glycosylases, producing AP sites. To investigate whether FACT complex affects the APE1 repair activity, control and FACT downregulated cells were treated with MMS and then release for 6 hours. The number of AP sites in the genomic DNA was quantitated using aldehyde reactive probe in triplicates under each condition (38). Without MMS to induce AP site, FACT KD cells had larger amount of AP sites as compared to control cells, indicating that normal BER function requires FACT complex under physiological condition. MMS treatment significantly increased the number of AP sites. After 6-hour release, cells were allowed for BER activity

and AP sites decreased. However, FACT siRNA treated cells retained significantly more AP sites despite 6-hour release, indicating that FACT depletion has negative impact on the BER function. This is consistent with our biochemical finding that FACT complex facilitates the access and mobility of APE1. Average of three independent experiments is shown. One-way ANOVA with Tukey's HSD test, ** $p < 0.01$, *** $p < 0.001$, **** $p < 0.0001$.

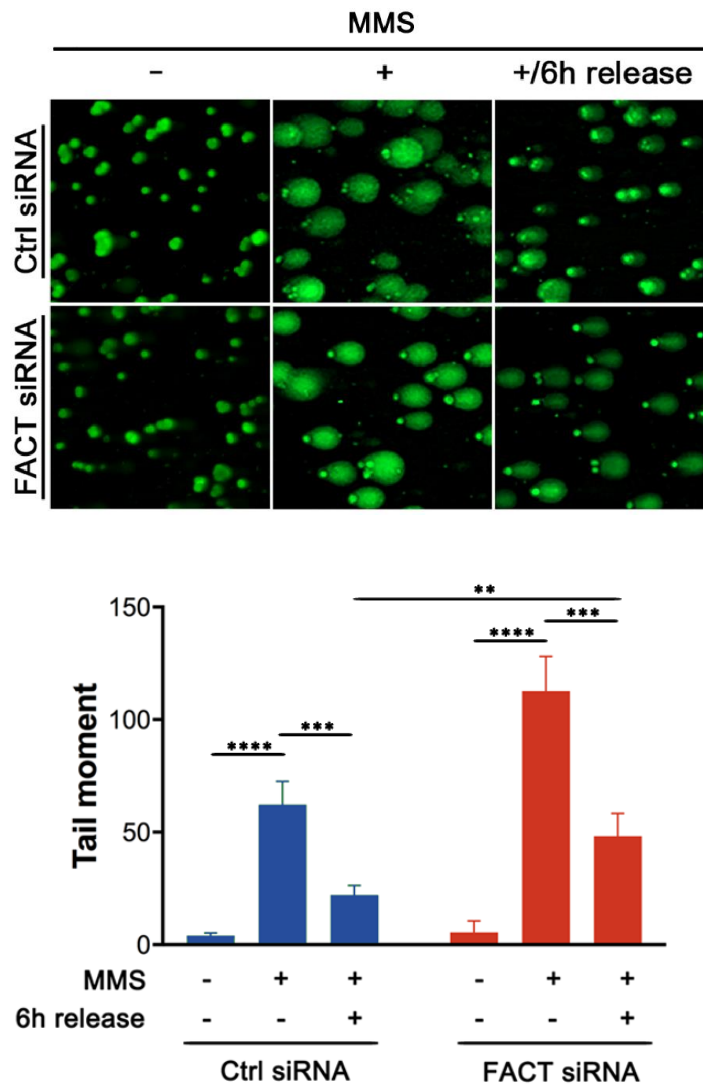


Figure 24. FACT KD impairs BER activity after MMS treatment as demonstrated by alkaline comet assay.

To further examine the effect of FACT complex in BER function, we used alkaline comet assay which detects the SSBs and DSBs damages in the genome (101). Control and FACT downregulated cells were treated with MMS (1 mM for 30 min) and release for 6 hours. The DNA damage was quantified by measuring the displacement between the comet head (which represent undamaged DNA) and the tail (resulting from damaged DNA). The tail moment has been suggested to be an appropriate index of induced DNA damage in considering both the migration of the genetic material as well as the relative amount of DNA in the tail. MMS treatment induced DNA damage, as reflected by the markedly increased tail moment. Cells were allowed for 6-hour recovery and tail moment decreased. In contrary, FACT KD cells failed to repair the damages after 6-hour release. Average tail moment was calculated from 100 cells using open comet software. One-way ANOVA with Tukey's HSD test, ** $p < 0.01$, *** $p < 0.001$, **** $p < 0.0001$.

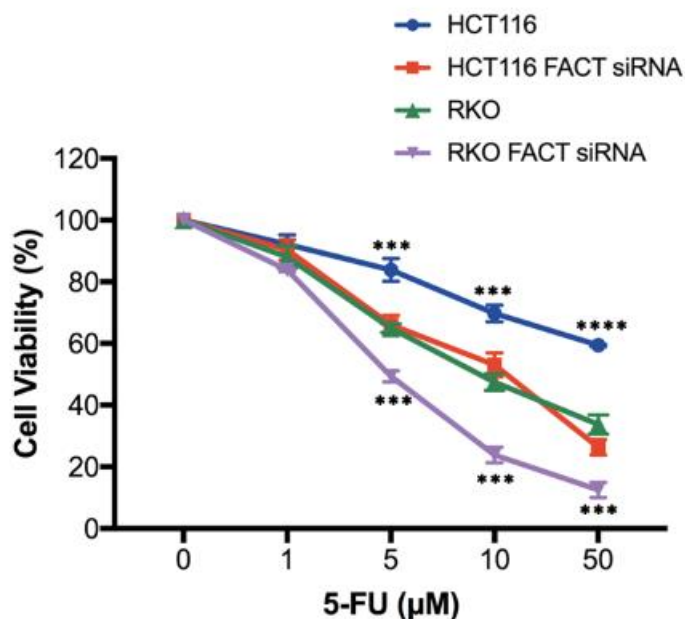


Figure 25. Downregulation of FACT sensitizes HCT116 and RKO cell lines to 5-FU.

To examine whether FACT KD sensitizes cells to 5-FU, HCT116 and RKO cells were treated with FACT siRNA and exposed to indicated doses of 5-FU for 72 hours. Cell viability were examined by MTT assay. FACT KD significantly improved the treatment efficacy of 5-FU, starting as low as from 5 μ M. Average of three independent experiments is shown. One-way ANOVA with Dunnett's post-hoc test, *** $p < 0.001$, **** $p < 0.0001$.

Targeting FACT with curaxins enhances the efficacy of 5-FU in dMMR CRC cells in vitro

Several studies have shown that curaxins, a class of small molecule drugs (**Fig. 26**), have broad anticancer activity and function as an inhibitor of FACT complex (102-104). FACT binds to unfolded nucleosomes and curaxins trap FACT in chromatin (102). Consistent with previous studies, our data show that Quinacrine (QC) (105), a first generation curaxin, reduced SSRP1 and SPT16 levels from soluble nuclear fraction but had no effect on the chromatin-bound fraction (**Fig. 27**). CBL0137, a second generation curaxin (106), exhibited a similar effect on FACT complex and decreased the level of AcAPE1 while total APE1 level remained unchanged (**Fig. 28, 29 & 30**). Of note, we found that HCT116 cells were unable to repair 5-FU- or MMS induced damage in the presence of FACT inhibitor CBL0137 (**Fig. 31 & 32**). Since our studies and others show that FACT is involved in AP site or SSBs repair in cells, we examined whether targeting FACT with CBL0137 enhanced the efficacy of 5-FU in dMMR CRC in vitro. To eliminate the possibility that QC or CBL0137 show cytotoxic effect per se by inducing DNA damages, cells were treated with different doses of QC or CBL0137 alone. We found minimal DNA damage with treatment of increasing doses of CBL0137 treatment on comet assay (**Fig. 33**). Moreover, 4 μ M CBL0137 or 10 μ M QC alone had a minimal effect (20% cell death) on cell viability (**Fig. 34**). However, combination of 2 μ M CBL0137 or 5 μ M QC with 5-FU

significantly enhanced the sensitivity (~50-fold decrease in IC_{50}) of 5-FU resistant dMMR HCT116 and RKO cells to 5-FU (**Fig. 35**), suggesting that targeting FACT complex with curaxins could be a promising strategy to overcome 5-FU resistance in dMMR CRC cells in vivo.

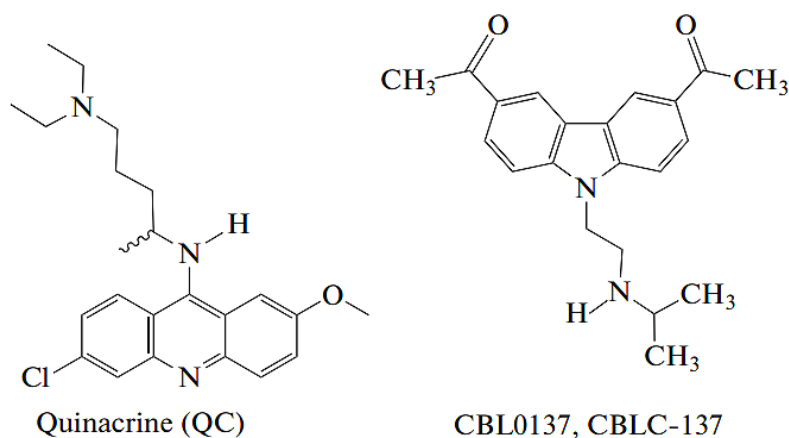


Figure 26. Chemical structures of QC and CBL0137.

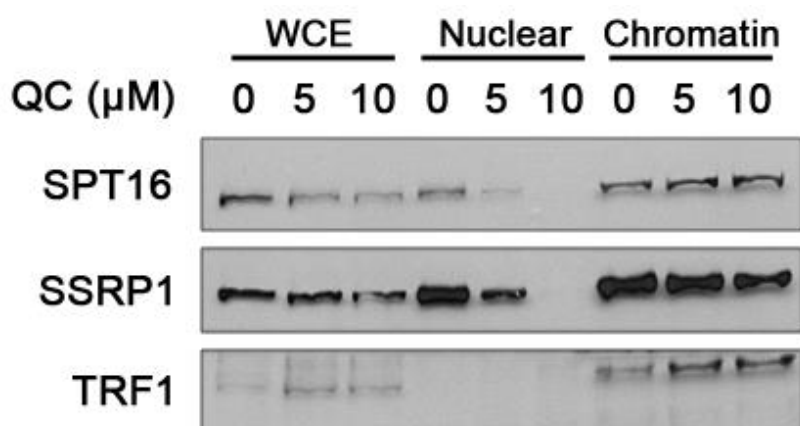


Figure 27. QC causes chromatin trapping effect on FACT complex.

To verify the effect of QC, the first generation curaxins, on the expression profile of FACT complex, HCT116 cells were treated with indicated doses of QC for 1 hour and whole cell

extract (WCE), soluble nuclear and chromatin-bound fractions were prepared. SSRP1 and SPT16 levels in these extracts were examined by immunoblot analysis. QC treatment resulted in reduced levels of SPT16 and SSRP1 both in WCE and nuclear extracts. In chromatin extract, the opposite effect of QC on SPT16 and SSRP1 levels were noted. This is referred to as 'chromatin trapping' effect of curaxins.

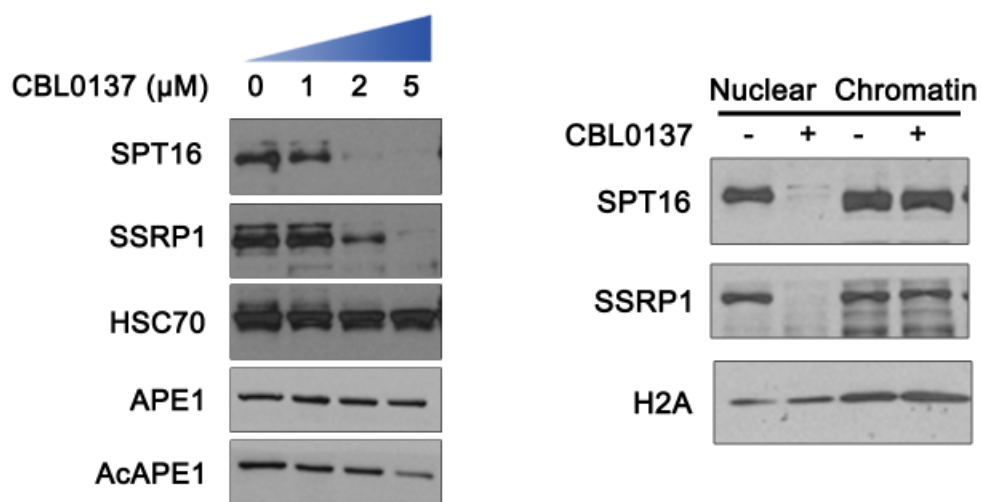


Figure 28. CBL0137 causes chromatin trapping effect on FACT complex and decreases AcAPE1 level.

In continuation of the previous experiment, we used second generation curaxins, namely CBL0137, to confirm its effect on FACT complex. HCT116 cells were treated with indicated doses of CBL0137 for 1 hour and whole cell extract (WCE), soluble nuclear and chromatin-bound fractions were prepared. SSRP1 and SPT16 levels in these extracts were examined by immunoblot analysis. A similar effect was noted with CBL0137, in which SPT16 and SSRP1 levels decreased in WCE and nuclear extracts while increased in chromatin fraction. In addition, we found that the AcAPE1 level decreased upon CBL0137

treatment. The total APE1 level, however, remained unchanged. Three biological replicates were analyzed. Representative images were shown.

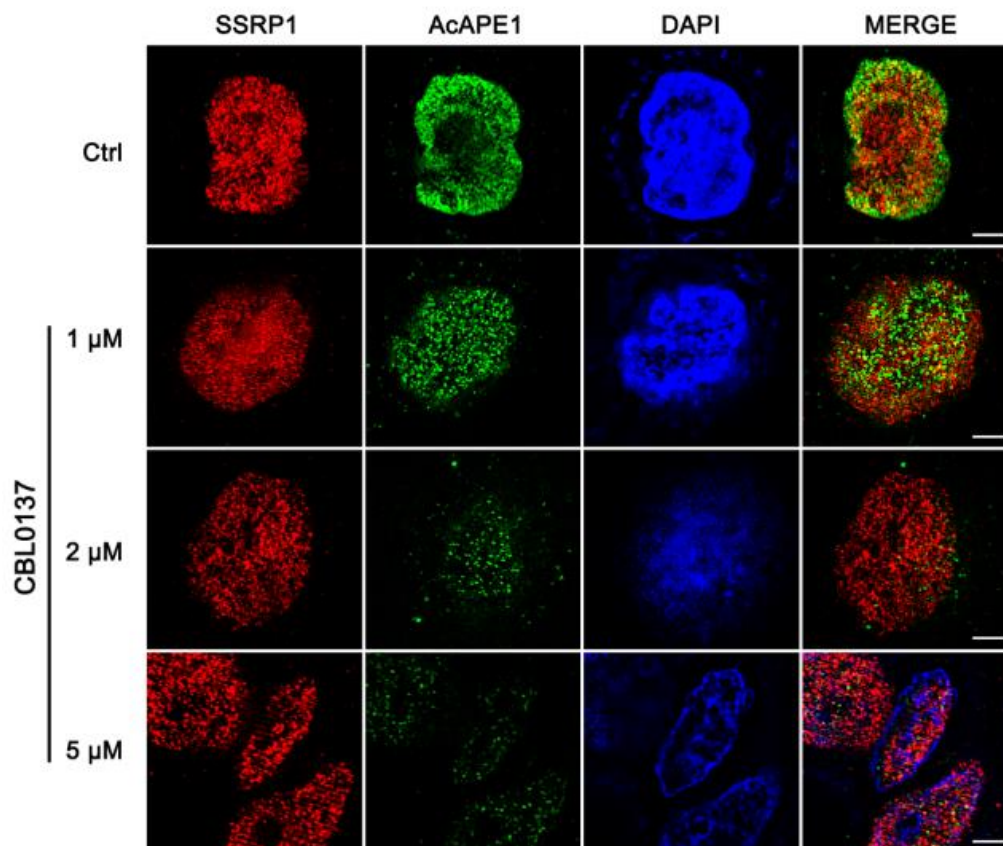


Figure 29. CBL0137 decreases the expression level of AcAPE1 in a dose-dependent manner.

The observation that CBL0137 decreased the AcAPE1 level was further confirmed by immunofluorescence staining. Cells were treated with indicated doses of CBL0137 for 1 hour and the AcAPE1 level in cells was examined by SIM. CBL0137 treatment caused reduction of AcAPE1 level in a dose-dependent manner. Multiple cells from three biological replicates were analyzed. Representative images were shown. Bar = 5 μM.

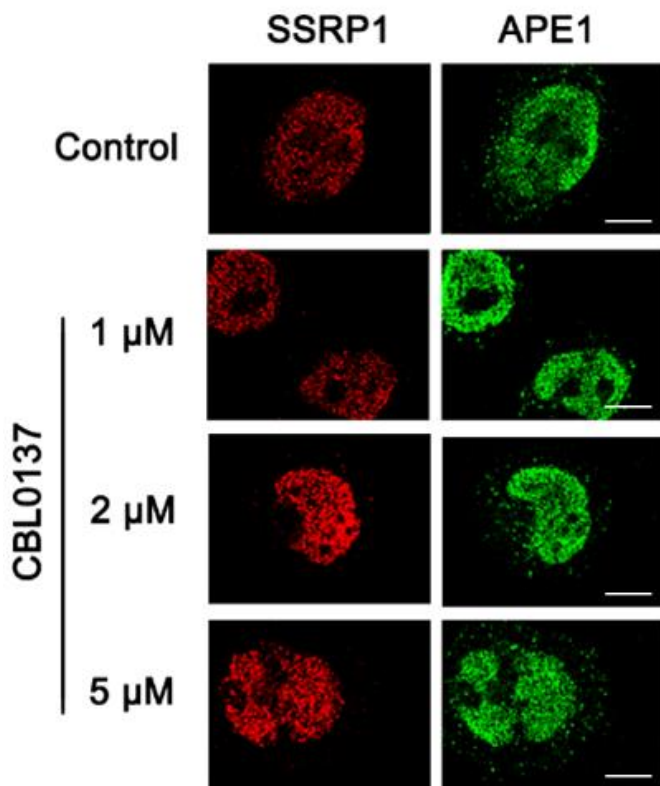


Figure 30. CBL0137 has no effect on the expression of total APE1.

We have shown that FACT KD does not affect the total APE1 level. Here, we examined the APE1 level in HCT116 cells after treatment with indicated doses of CBL0137. At tested doses of CBL0137, the total APE1 level remained unchanged as demonstrated by SIM. Multiple cells in three biological replicates were analyzed. Representative images were shown. Bar = 5 μ M.

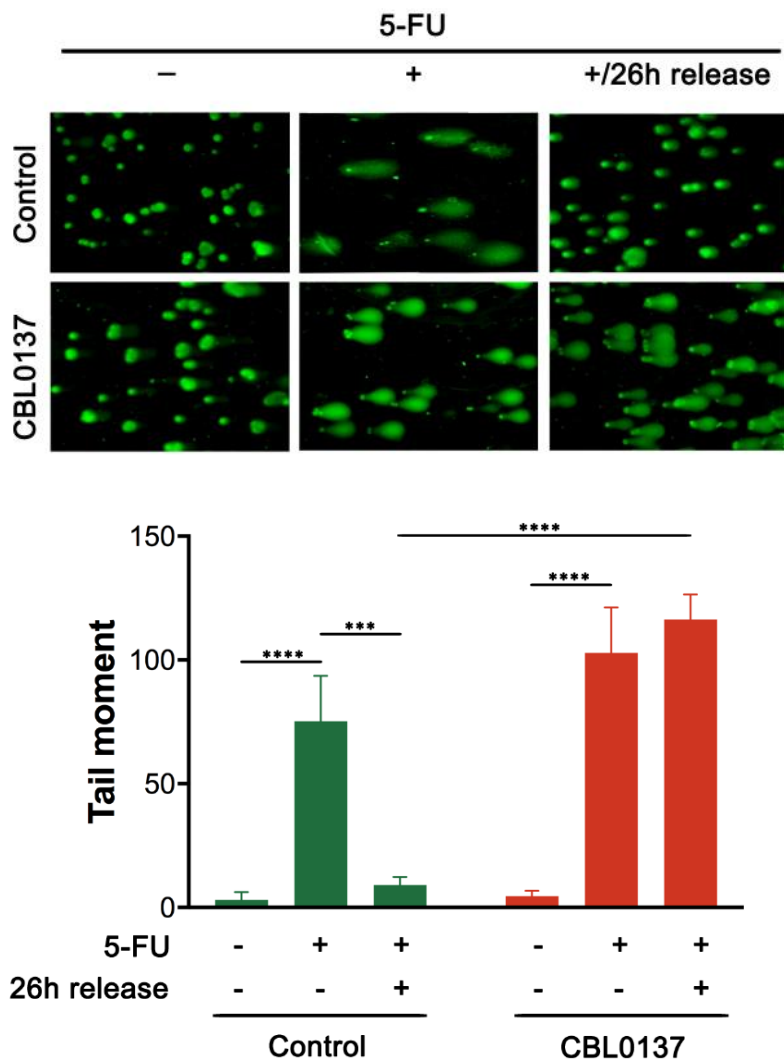


Figure 31. CBL0137 inhibits BER function on 5-FU induced DNA damage repair.

In previous experiments, we have demonstrated that FACT KD significantly impaired BER activity. To investigate whether CBL0137 produces similar inhibitory effect on BER function, we pretreated HCT116 cells with CBL0137 for 1 hour. Cells were then exposed to 5-FU for 6 hours and allowed to recover for 26 hours. DNA damage was examined by alkaline comet assay. In both groups, 5-FU treatment induced a rise in tail moment. As compared to control cells which successfully repaired the majority of induced damages at 26-hour release, CBL0137 treated cells retained the damages despite recovery. Tail moment of 100 cells per sample was calculated using open comet software. Three

independent biological replicates were analyzed. Results are shown as the mean \pm SEM. One-way ANOVA with Tukey's HSD test, *** $p < 0.001$, **** $p < 0.0001$.

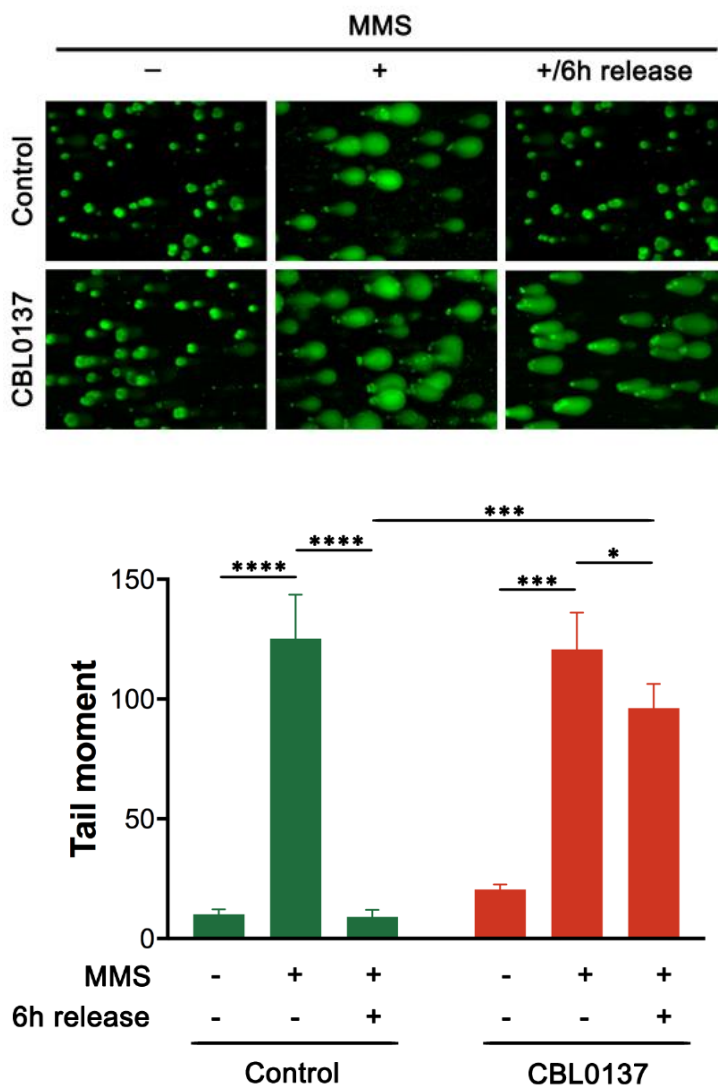


Figure 32. CBL0137 inhibits BER function on MMS induced DNA damage repair.

BER and MMR are both involved in 5-FU damage repair (discussed in detail in Introduction). While the previous experiment showed cells retained 5-FU damage after CBL0137 pretreatment, the possibility of MMR being dysfunction cannot be eliminated. In continuation of the previous experiment, to provide further evidence that CBL0137 inhibits BER repair activity, we pretreated HCT116 cells with CBL0137 for 1 hour. Cells were then

exposed to MMS (a classic BER substrate–generating compound) for 30 minutes and allowed to recover for 6 hours. DNA damage was examined by alkaline comet assay. Consistently, we found that cells failed to repair MMS induced damages after 6-hour release. Along the previous experiment, these data suggest that CBL0137 inhibits BER repair activity in cells. Tail moment of 100 cells was calculated per sample using open comet software. Three biological replicates were analyzed. Results are shown as the mean \pm SEM. One-way ANOVA with Tukey's HSD test, * $p < 0.05$, *** $p < 0.001$, **** $p < 0.0001$.

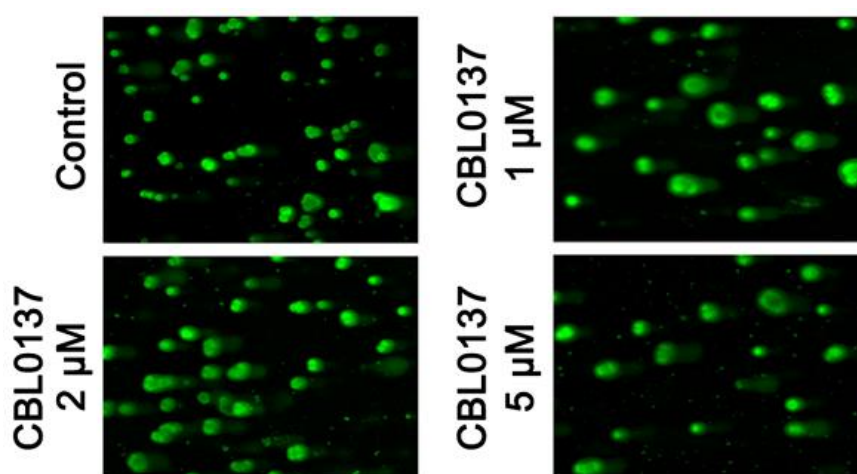


Figure 33. CBL0137 alone does not induce DNA damage.

To eliminate the possibility that CBL0137 induce DNA damages which would bias our above findings, cells were treated with indicated doses of CBL0137 for 1 hour and alkaline comet assay was performed. We found that CBL0137 alone did not induce significant DNA damages. Three biological replicates were performed. Representative images were shown.

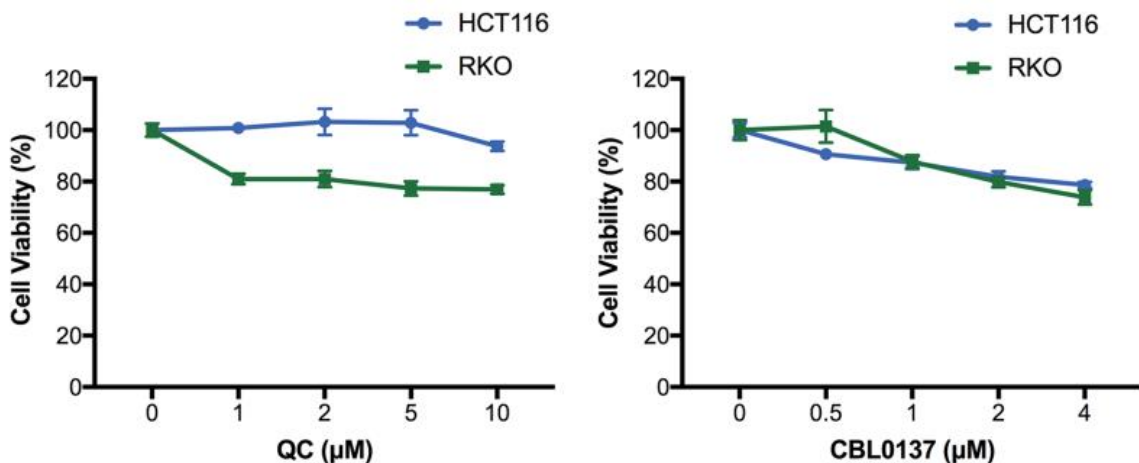


Figure 34. QC or CBL0137 alone has minimal effect on cell viability.

To examine if QC or CBL0137 has inhibitory effect on cell viability, HCT116 and RKO cells were treated with QC (Left) or CBL0137 (Right). MTT assays showed that high dose of QC (10 μM) or CBL0137 (4 μM) had minimal effect on cell viability. Six technical repeats were performed per sample and three biological replicates were analyzed. Results are shown as the mean \pm SEM.

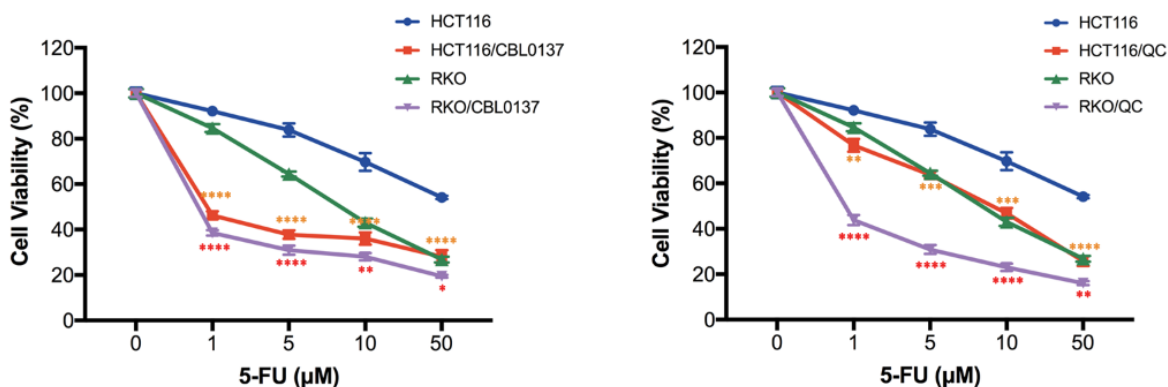


Figure 35. Combination of 5-FU plus curaxins demonstrated synergistic effect on inhibition of cell viability.

To investigate whether curaxins sensitizes colon cancer cells to 5-FU, HCT116 and RKO were treated with 2 μ M CBL0137 (Left) or 5 μ M QC (Right) for 1 hour then exposed to various doses of 5-FU. RKO is a mismatch repair deficient cell line and intermediate resistant to 5-FU. Cell viability was measure in six replicates by MTT assay. We found that combination therapy significantly inhibited cell viability and demonstrated synergistic effect. Yellow asterisks mark the comparisons between HCT116 and HCT116/CBL0137 (Left) or HCT116 and HCT116/QC (Right). Red asterisks mark the comparisons between RKO and RKO/CBL0137 (Left) or RKO and RKO/QC (Right). Average of three independent experiments are shown. One-way ANOVA with Dunnett's post-hoc test, * $p < 0.05$, ** $p < 0.01$, *** $p < 0.001$, **** $p < 0.0001$.

FACT inhibitor Curaxin sensitizes dMMR-CRC tumor to 5-FU in vivo

To examine whether the combination of curaxins and 5-FU inhibits dMMR-CRC tumor growth in vivo, we utilized tumor xenograft models. The effects of QC and CBL0137 were tested alone and in combination of 5-FU. HCT116 and DLD-1 cells were used to generate xenograft models. Tumor growth curve showed that single agent treatment with 5-FU, QC or CBL0137 alone had very little or moderate effect on tumor growth compared to vehicle group (**Fig. 36-39**), while combination group significantly inhibited tumor growth, demonstrating a synergistic effect. The combination of QC with 5-FU was well tolerated at the scheduled doses. All mice were weighted at each time point of treatment during the study, and there was 10-15% total weight loss at the end of study period. No cachectic appearance was noted (**Fig. 40**). Moreover, no major histological abnormality was identified in vital organs including lung, liver and kidney (**Fig. 41**). Further analysis showed that combination group suppressed the proliferation and induced apoptosis in these tumors (**Fig. 42-43**). Additionally, long-term QC treatment resulted in decreased SSRP1

level in nucleus and the residual SSRP1 was trapped in chromatin (**Fig. 44**), suggesting that QC alters FACT expression and localization in vivo. These data together demonstrate that inhibition of FACT function with curaxins can overcome 5-FU resistance and inhibits dMMR CRC growth both in vitro and in vivo.

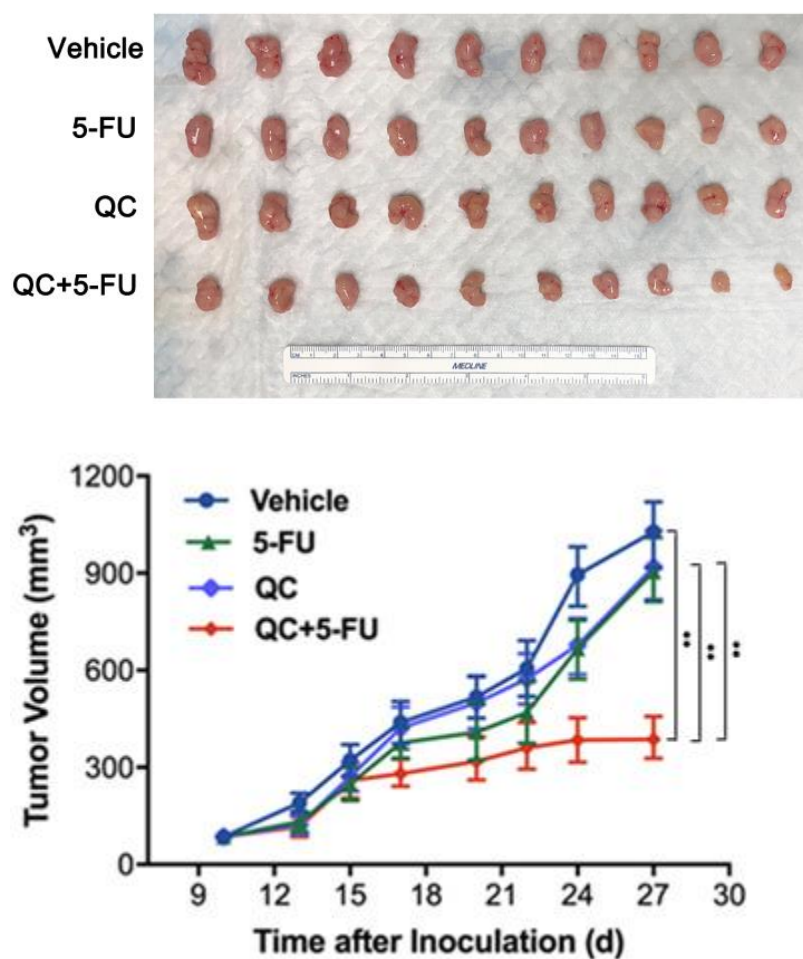


Figure 36. Combination of 5-FU plus QC significantly inhibits HCT116 xenograft growth with synergistic effect when compared to monotherapy of 5-FU or QC.

To test the treatment efficacy of combination therapy in vivo, one million of HCT116 cells (in 100 μ L culture medium) were implanted subcutaneously in the flanks of seven weeks

old athymic nude male mice to generate xenografts. When average tumor volume reached 100 mm³, mice were randomized into four groups (n=5 in each group). Vehicle (100 µL PBS), 5-FU, QC and combination of 5-FU and QC were administered to mice intraperitoneally for 3 weeks. Weight of each mice and tumor size were measured each time before treatment and every 3 days after completion of treatment. Tumor volume= ($\pi \times \text{length} \times \text{width}^2$) / 6, where length represents the largest tumor diameter and width represents the perpendicular tumor diameter. Although we measured the ten xenograft tumors' volume in each group, caution should be taken when interpreting the results as we used 5 mice (independent biological samples) in each group; the pair of tumors (technical replicates) in each mouse should be considered as one as the microenvironment and drug delivery was nearly identical. In our final analysis, we used the average volume of the pair of xenografts in the same mice as an independent sample. We found that 5-FU or QC alone had minimal inhibitory effect on xenograft growth. This is consistent with the fact that HCT116 cells are highly 5-FU resistant. In contrast, when combining with QC, 5-FU inhibited tumor growth with significantly ($p < 0.01$) smaller tumor volume at the end of the study, demonstrating synergistic effect. The drug combination effect was calculated in SynergyFinder to examine the presence of additive or synergistic effect. Kruskal-Wallis test with Games-Howell post-hoc test, ** $p < 0.01$.

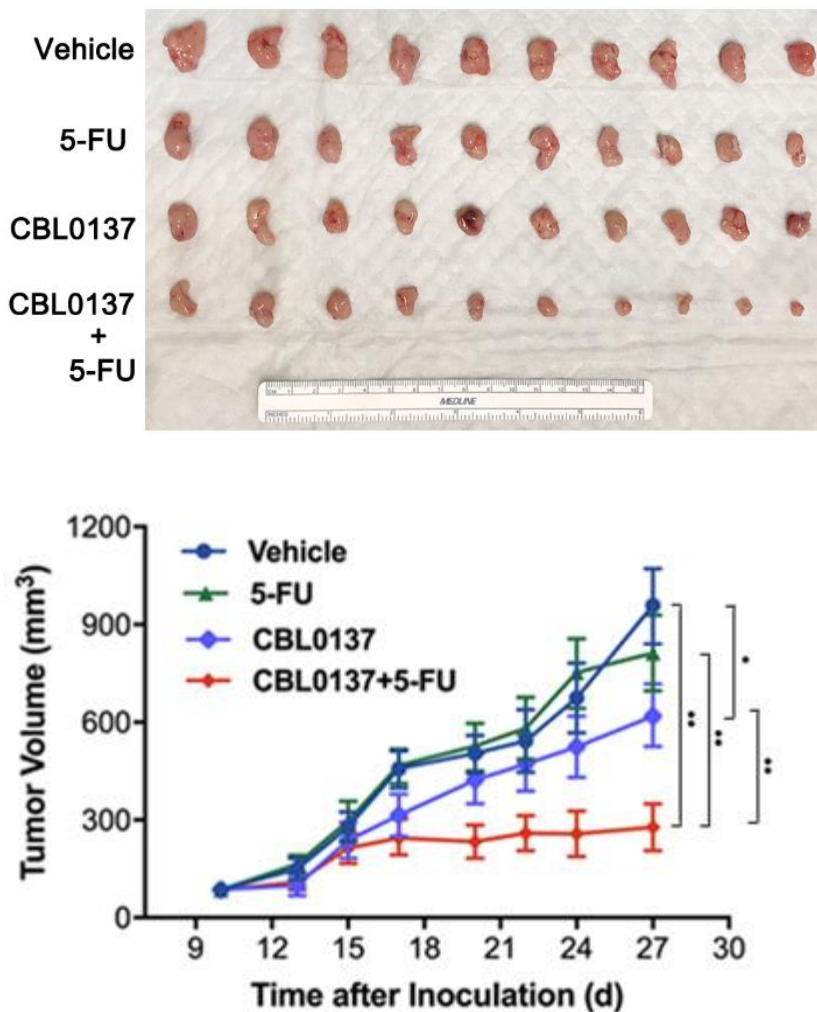


Figure 37. Combination of 5-FU plus CBL0137 significantly inhibits HCT116 xenograft growth with synergistic effect when compared to monotherapy of 5-FU or CBL0137.

In another experiment, we used CBL0137 to replace QC and repeat the xenograft study. One million of HCT116 cells were used to generate xenograft tumors as described above. We found that CBL0137 alone had inhibitory effect on tumor growth, as evident from final tumor volume. Similar to prior experiment, combination therapy of 5-FU and CBL0137 exhibited synergistic effect on final tumor volume. Statistical analysis was performed as described in figure 36. Kruskal-Wallis test with Games-Howell post-hoc test, * $p < 0.05$, ** $p < 0.01$.

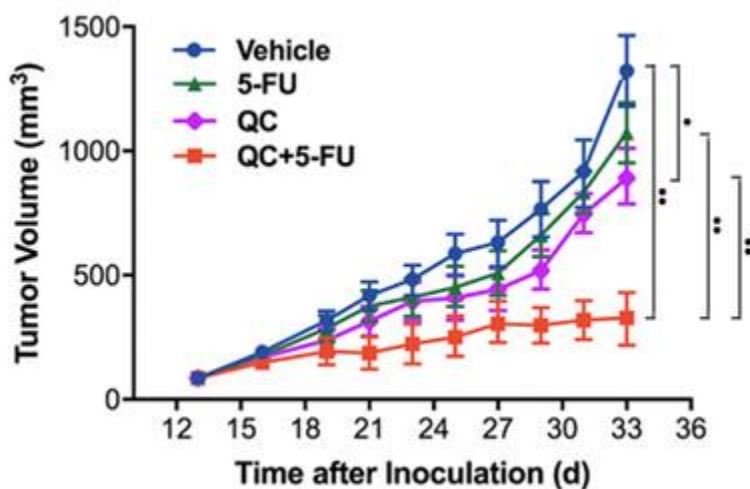
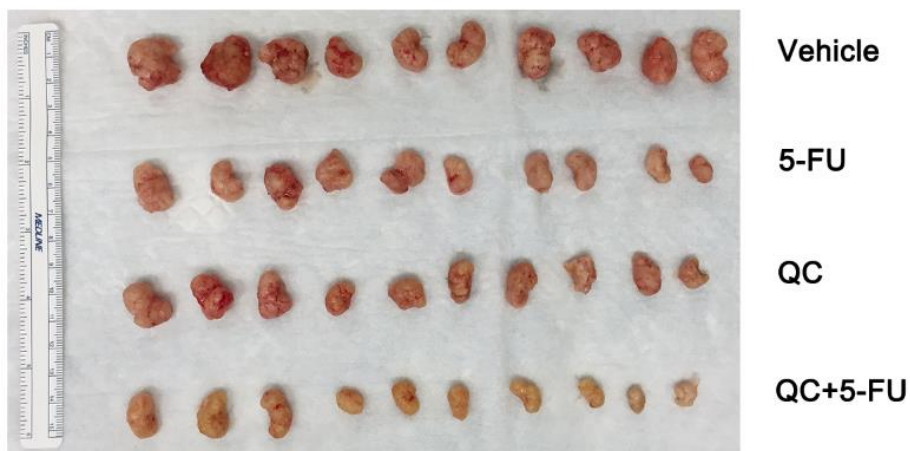


Figure 38. Combination of 5-FU plus QC significantly inhibits DLD-1 xenograft growth with synergistic effect when compared to monotherapy of 5-FU or QC.

To further provide evidence that combination therapy overcomes 5-FU resistance, we used DLD-1 cells (5-FU resistant cell line) to perform xenograft study per our protocol. One million DLD-1 cells were injected subcutaneously in the flanks of mice. Vehicle, 5-FU, QC and combination of 5-FU and QC were administered to mice (n=5) intraperitoneally for 3 weeks. While 5-FU alone did not produce significant inhibition on tumor growth, QC alone demonstrated statistically significant inhibitory effect. Combination therapy, on the

other hand, exhibited superior treatment efficacy with synergistic effect as demonstrated by significantly smaller tumor volume at the end of study when compared to monotherapy either of 5-FU or QC. Statistical analysis was performed as described in figure 36. Kruskal-Wallis test with Games-Howell post-hoc test, * $p < 0.05$, ** $p < 0.01$.

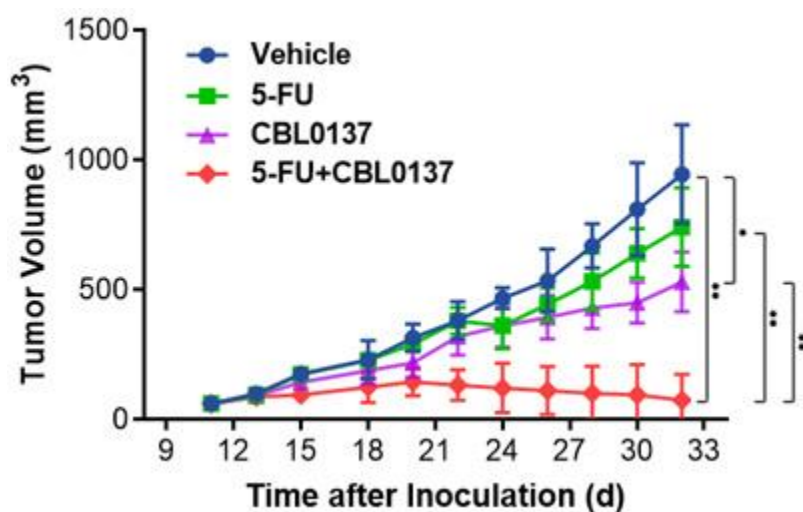
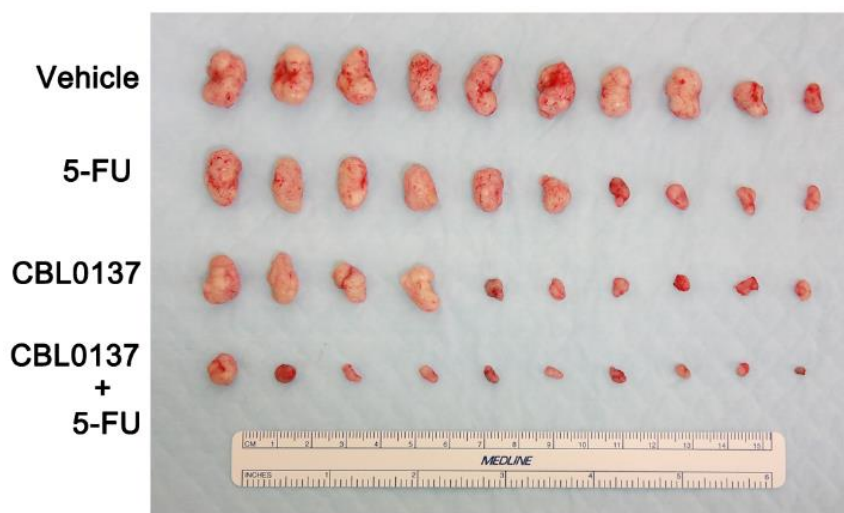


Figure 39. Combination of 5-FU plus CBL0137 significantly inhibits DLD-1 xenograft growth with synergistic effect when compared to monotherapy of 5-FU or CBL0137.

As CBL0137 has been introduced in clinical phase I and II trials, we are interested in the effect of CBL0137. Similar to our prior experiment, we generated xenograft tumor model using DLD-1 cells. Vehicle, 5-FU, CBL0137 and combination of 5-FU and CBL0137 were administered to mice (n=5) intraperitoneally for 3 weeks. While 5-FU failed to inhibit tumor growth as demonstrated by similar tumor volume at the end of the study, we found that addition of CBL0137 sensitized the DLD-1 cells to 5-FU and the combination group demonstrated synergistic effect on inhibition of tumor growth. Statistical analysis was performed as described in figure 36. Kruskal-Wallis test with Games-Howell post-hoc test, * $p < 0.05$, ** $p < 0.01$.

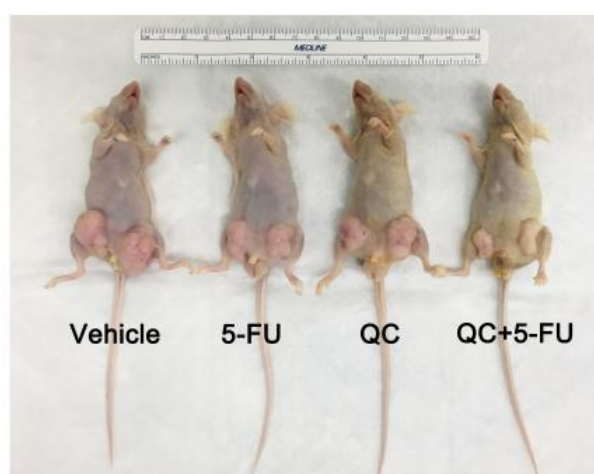


Figure 40. Representative xenograft mice picture demonstrates no gross weight change noted at the completion of study.

One of the considerations in the evaluation of treatment effect is the toxicity of drugs. If the drug causes severe toxicity, it will lead to weight loss and cachectic appearance. In our study, we measured body weight each time before treatment. Representative images of mice from each treatment group at the completion of experiment showed no significant differences in weight among groups.

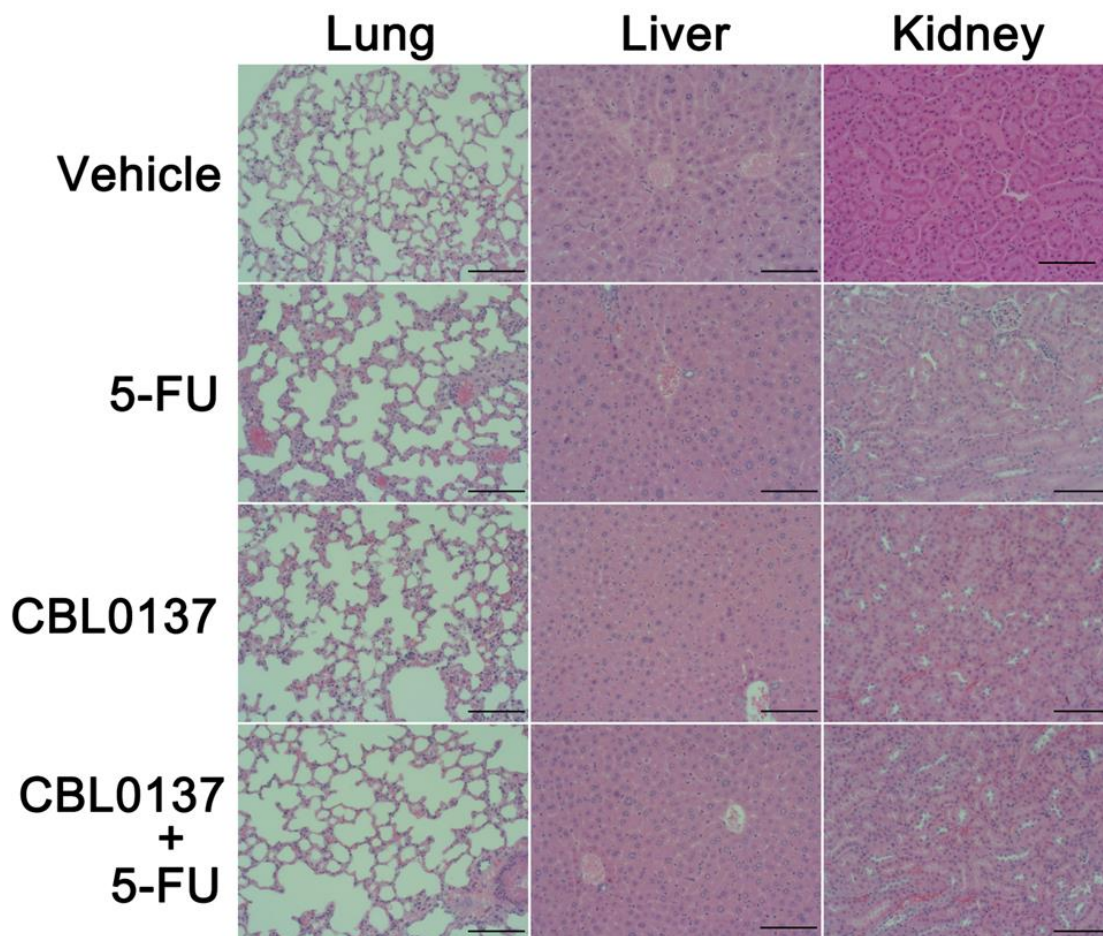


Figure 41. No major organ toxicity is noted on H&E staining after treatment.

To examine if the monotherapy or combination drugs has toxicity effect, we harvested major organs after completion of the treatment and performed H&E staining. We found that there was no alteration of tissue histology in major organs after a series of 3-week treatment. Original magnification x 400. Bar=100 μ M.

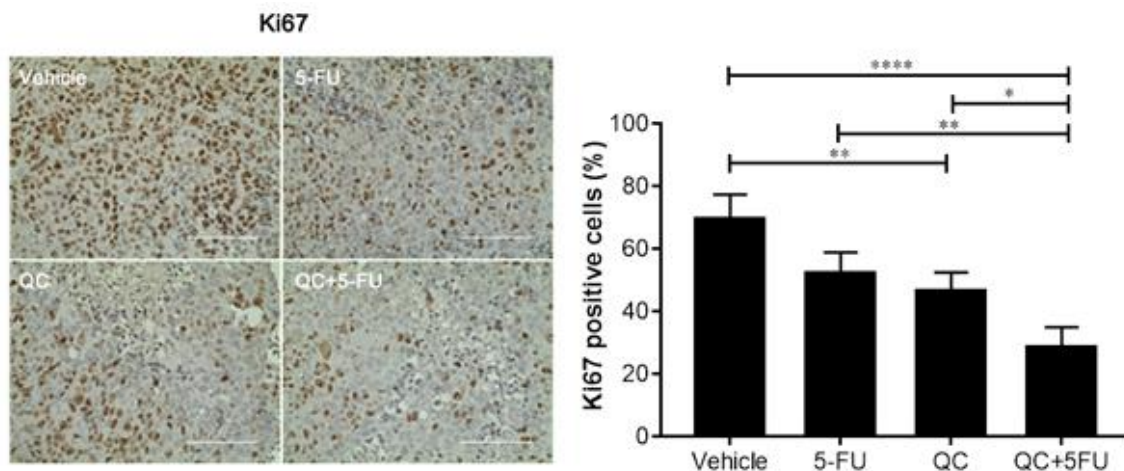


Figure 42. Combining 5-FU with QC significantly decreases percentage of positive Ki-67 staining in xenograft.

To understand the mechanism of the inhibitory effect of combination therapy, we examined proliferative marker (Ki-67) and apoptotic marker (TUNEL staining) in xenograft section. The percentage of positive staining cells were quantified with 10 random high-power field images using TMARKER. On the right side was bar graph depicting the Ki67 positive cell percentage among groups. We found that monotherapy with QC had some inhibitory effect on cell proliferation. Combination therapy demonstrated significant reduction of Ki67 staining, indicating that at least part of the effect on tumor growth could be attributed to anti-proliferative activity. Data report the mean \pm SEM of percentages of positive cells (107). One-way ANOVA with Tukey's HSD test, * $p < 0.05$, ** $p < 0.01$, *** $p < 0.001$.

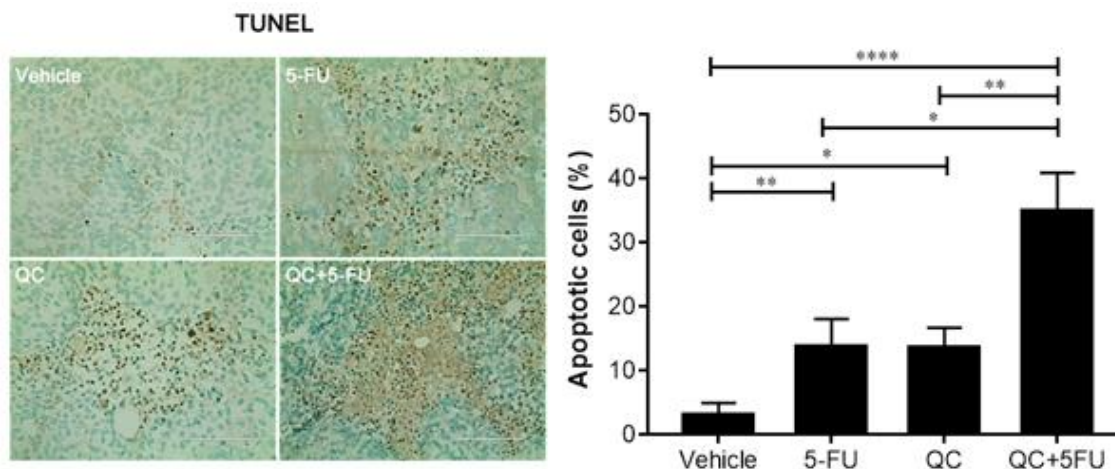


Figure 43. Combination therapy induces apoptosis in xenograft tumor.

(Left) TUNEL assay was performed in tumor sections and the representative images are shown. (Right) Bar graph depicts the TUNEL positive cell percentage among groups. In contrary to the tumor growth result where 5-FU alone had no effect, 5-FU treated group had higher percentage of cells undergoing apoptosis when compared to vehicle group. Combination therapy induced apoptosis in a significantly higher percentage of cells when compared with vehicle or monotherapy. This suggests that the inhibitory effect on xenograft growth is partly derived from apoptosis. Data report the mean \pm SEM of percentages of positive cells. One-way ANOVA with Tukey's HSD test, * $p < 0.05$, ** $p < 0.01$, **** $p < 0.0001$.

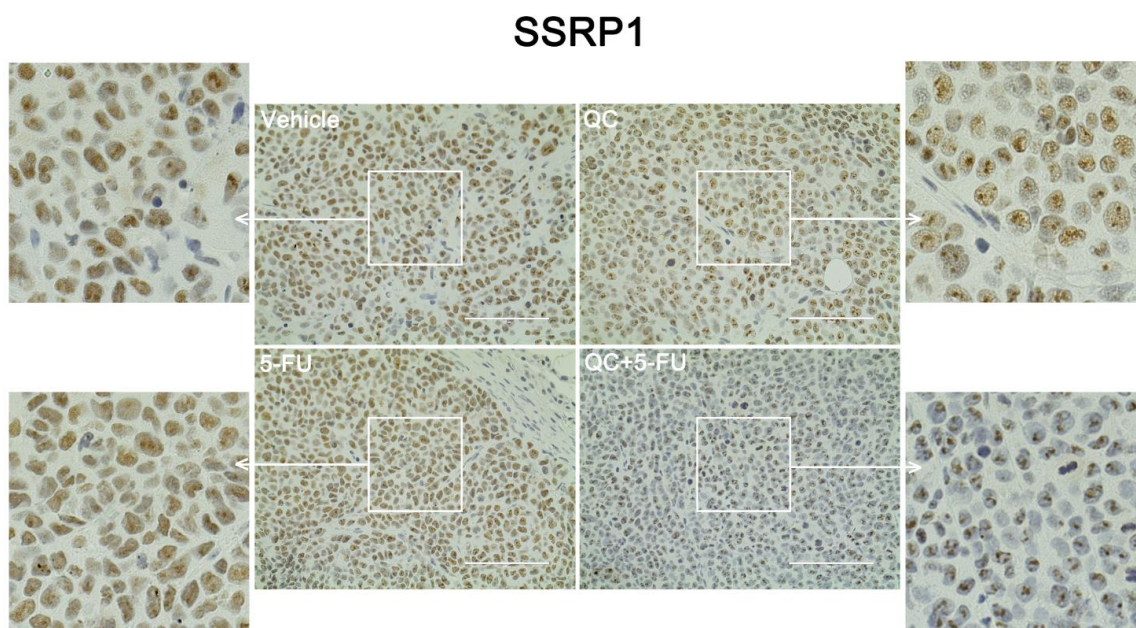


Figure 44. The staining of SSRP1 decreases in the combination treatment group.

We have provided biochemical evidence that QC causes chromatin trapping of FACT complex (Fig. 27). Here, we investigated if such effect could be detected in xenograft section. Tumor sections from each treatment groups were stained with SSRP1 antibody. Zoomed images of portions of the IHC staining indicate the chromatin trapping of FACT complex due to QC treatment. Notably, the combination group markedly decreased the expression level of SSRP1. It is an interesting finding that we could not fully understand and explained. Indeed, we have verified the finding several times in our animal studies and observed the same results. It is clearly evident from Western blot data that QC can trap FACT in chromatin in vitro. However, the in vivo finding is not quite obvious when using QC alone. As shown here, QC treatment leads to mild decrease of SSRP1 in the nucleus. The effect of chromatin trapping is very clear in the combination group, which could be due some reasons that are not fully understood at present.

FACT is overexpressed in colon cancer tissue and cell lines

Previously, we showed that primary tumor tissues of CRC and other types of cancer patients have higher AcAPE1 levels compared to adjacent-non-tumor tissues (44,108). Recent reports demonstrate that FACT expression is strongly associated with poorly differentiated cancers and low overall survival (97,103,104,106). Here we examined the levels of SSRP1 and AcAPE1 in CRC patients' tumor tissues. Both subunits of FACT complex and AcAPE1 were overexpressed in tumor but not in adjacent normal tissues (**Fig. 45**). This finding was confirmed in various colon cancer cell lines using HCEC cells for comparison (**Fig. 46**). These data indicate a potential role of overexpression of FACT and AcAPE1 in inducing chemoresistance.

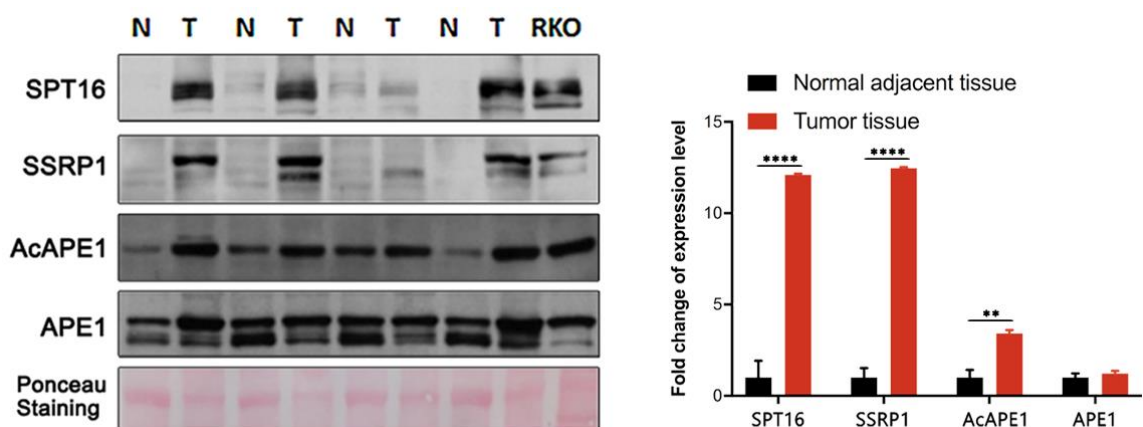


Figure 45. Expression of FACT complex and AcAPE1 is elevated in colon cancer tissues.

To investigate the expression levels of AcAPE1 and FACT complex in human colon cancer, we used colon cancer samples and performed western blot analysis. (Left) Levels of APE1, AcAPE1, SSRP1 and SPT16 were elevated in tumor (T) as compared to the adjacent normal (N) tissue extracts of CRC patients. (Right) The expression level of each protein

in tumor was presented in fold change compared to normal adjacent tissues. Data were expressed as mean \pm SEM of three independent experiments. MANOVA with Tukey's HSD test, ** $p < 0.01$, **** $p < 0.0001$.

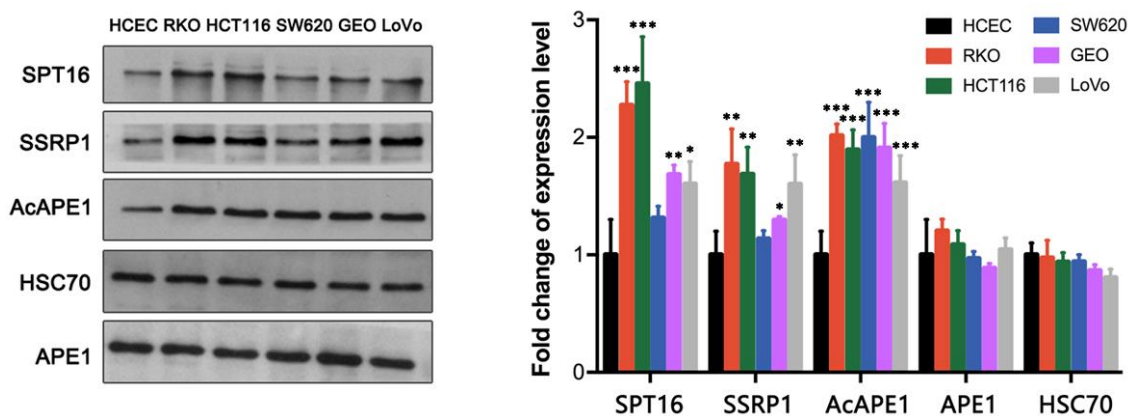


Figure 46. Expression of FACT complex and AcAPE1 is elevated in multiple colon cancer cell lines.

After we demonstrated that the human colon cancer samples had higher levels of AcAPE1 and FACT complex, we sought to determine the expression levels in most commonly used colon cancer cells lines, including RKO, HCT116, SW620, GEO, and LoVo. (Left) The levels of AcAPE1, SSRP1, and SPT16 were elevated in various colon cancer cell lines as compared to normal colon cell line HCEC. (Right) Bar graph showing elevated levels of SPT16, SSRP1 and AcAPE1 in multiple CRC cell lines compared to normal HCEC cells. Expression levels were presented in fold change with respect to normal HCEC cells. Data were expressed as mean \pm SEM of three independent experiments. One-way ANOVA with Tukey's HSD test, * $p < 0.05$, ** $p < 0.01$, *** $p < 0.001$.

FACT (SSRP1) expression and AcAPE1 levels positively correlate with chemoresistance in CRC patients

To determine the clinical significance of elevated levels of FACT and AcAPE1 in CRC, we extended our analyses by assessing SSRP1 and AcAPE1 levels in 39 CRC patients at different T stages. Among them, 19 patients had a moderate response and the other 20 had no response or minimal response to chemotherapy. Four (10.3%) were characterized as microsatellite instable or MMR deficient. This is consistent with prior reports that sporadic, noninherited dMMR CRC constitutes 10-15% of all CRCs (109). The percentages of positive cells and the staining intensity of SSRP1 and AcAPE1 level were significantly higher in CRC tumor tissue compared to control (**Fig. 47**). Although SSRP1 or AcAPE1 staining varied among the samples within a particular stage of CRC, we found a significant increase in percentage of positive SSRP1 and AcAPE1 staining cells from stage T2 to T4, indicating that SSRP1 and AcAPE1 level increases with tumor depth invasion (**Fig. 48**). Analysis of staining intensity of AcAPE1 and SSRP1 in tumor samples (characterized as low, medium and high intensity) revealed higher numbers of positive cells exhibiting high intensity staining with increasing tumor stage (**Fig. 49**).

Next, we determined the relationship between FACT expression and acetylation of APE1 across all patient's samples. We revealed a moderate but significantly positive correlation between SSRP1 and AcAPE1 levels in CRC samples (**Fig. 50**). We found that patients exhibiting no or minimal response to 5-FU had distinct staining patterns compared to patients exhibiting moderate responses (**Fig. 51**). Quantitation of the percentage of positive staining cells showed that the percentage of positive SSRP1 or AcAPE1 was two-fold higher in non- or minimal responders compared to moderate responders (**Fig. 52**). Additionally, three out of four patients who have loss of MSH2 and MSH6 were found to have minimal or no response and they had high levels of AcAPE1 and FACT (**Fig. 53**).

Overall, these data indicate that the expression levels of SSRP1 and AcAPE1 positively correlates with 5-FU resistance in CRC patients.

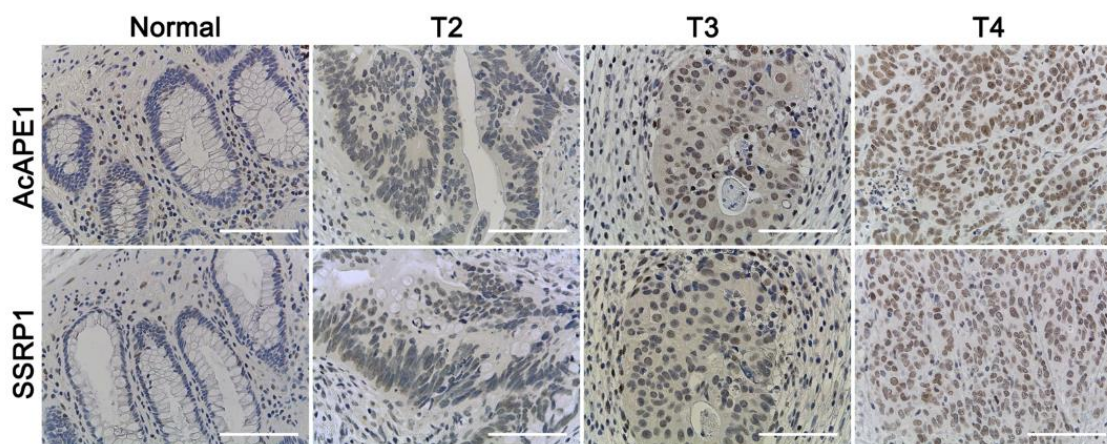


Figure 47. AcAPE1 and SSRP1 expression increases in tumors of higher T stage.

To investigate the prognostic value of AcAPE1 and SSRP1 in colon cancer, we first collected invasive colon cancer samples (T2 or above). These patients received chemotherapy before surgery and underwent surgery to remove residual tumor. We performed IHC staining of AcAPE1 and SSRP1. A total of 39 CRC patients with different T stages were included. Note that T stage pertains to tumor invasion depth. T2 means tumor invading muscularis propria, and T3 means tumor invading through muscularis propria into subserosa or nonperitonealized pericolic or perirectal tissues. T4 indicates that tumor directly invades other organs or structures and/or perforates visceral peritoneum. Normal colon tissue was used as control. Grossly we noted that the staining intensity and percentage of cells with positive staining increased as tumor invasion depth increased. The quantification was performed and presented in next figure.

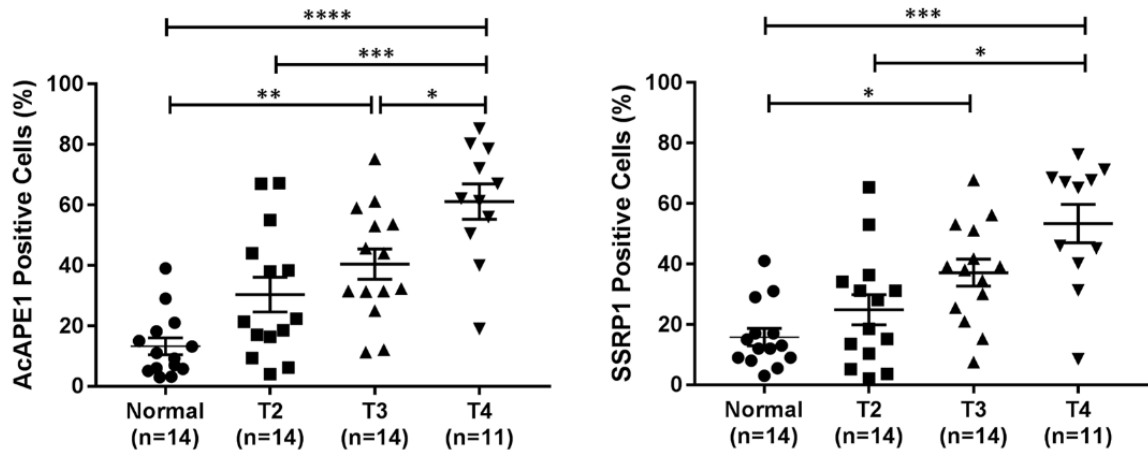


Figure 48. Percentage of AcAPE1 and SSRP1 positive staining cells increases as tumor progresses in terms of invasion depth.

To quantify the staining result, the percentage of positive staining cells and staining intensity (next figure) were analyzed by Definiens Releases Tissue Studio® 4.3 which is available at the UNMC Tissue Science core facility. The percentage of cells positive for AcAPE1 (Left) or SSRP1 (Right) from ten random high field in each sample was pooled and average for each sample was plotted. The percentage of AcAPE1 and SSRP1 positive staining increases as tumor invasion increases. Kruskal-Wallis test with Games-Howell post-hoc test, * $p < 0.05$, ** $p < 0.01$, *** $p < 0.001$, **** $p < 0.0001$.

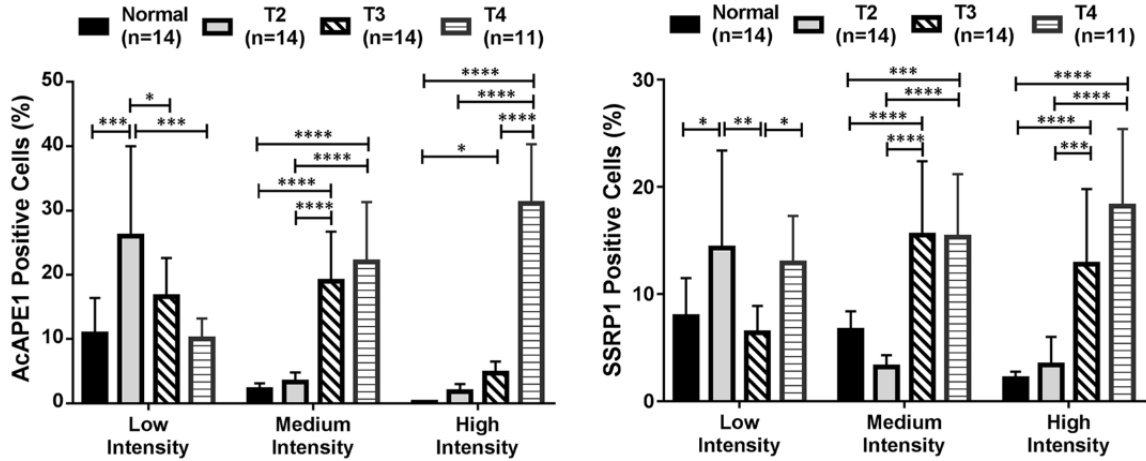


Figure 49. Tumors of higher stage demonstrate higher portion of cells with high intensity.

We further characterized the staining intensity of the IHC sections. The staining intensity was analyzed by Definiens Releases Tissue Studio® 4.3. We used a stain deconvolution algorithm to separate the DAB chromogen stain and the hematoxylin counterstain in all tissue cores. We then measured the brown chromogen intensity across all tissues to obtain the range of pixel density. Based on the range, we divided the staining intensity into 3 categories using one third threshold increment in the range. The percentage of cells with low, medium and high staining intensity in each group for AcAPE1 (Left) and SSRP1 (Right) was analyzed and plotted. We found that higher numbers of positive cells exhibiting high intensity staining of AcAPE1 and SSRP1 with increasing tumor stage. Kruskal-Wallis test with Games-Howell post-hoc test, * $p < 0.05$, ** $p < 0.01$, *** $p < 0.001$, **** $p < 0.0001$.

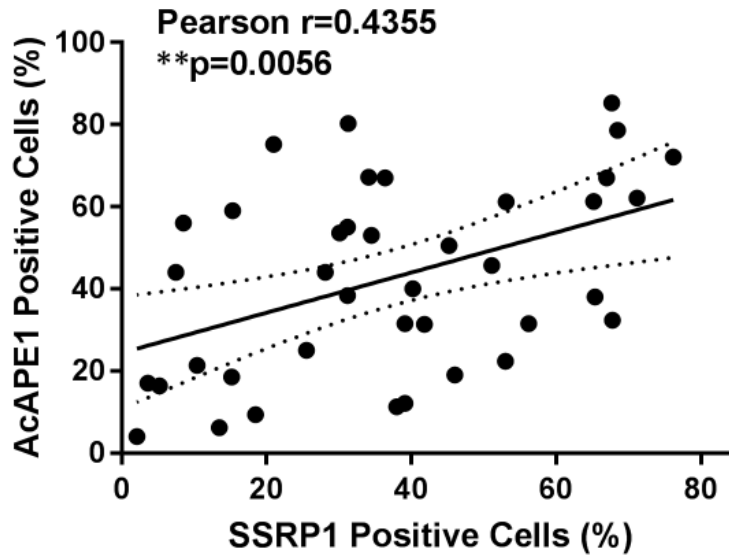


Figure 50. The AcAPE1 and SSRP1 expression is correlated in colon cancer.

As AcAPE1 is overexpressed in colon cancer, and FACT complex facilitates its function, we examined whether the expression of these two proteins was correlated. Percentage of AcAPE1 and SSRP1 positive cells in each sample were plotted and linear regression was performed which demonstrated that the expression of AcAPE1 was correlated with SSRP1 with Pearson r of 0.4355.

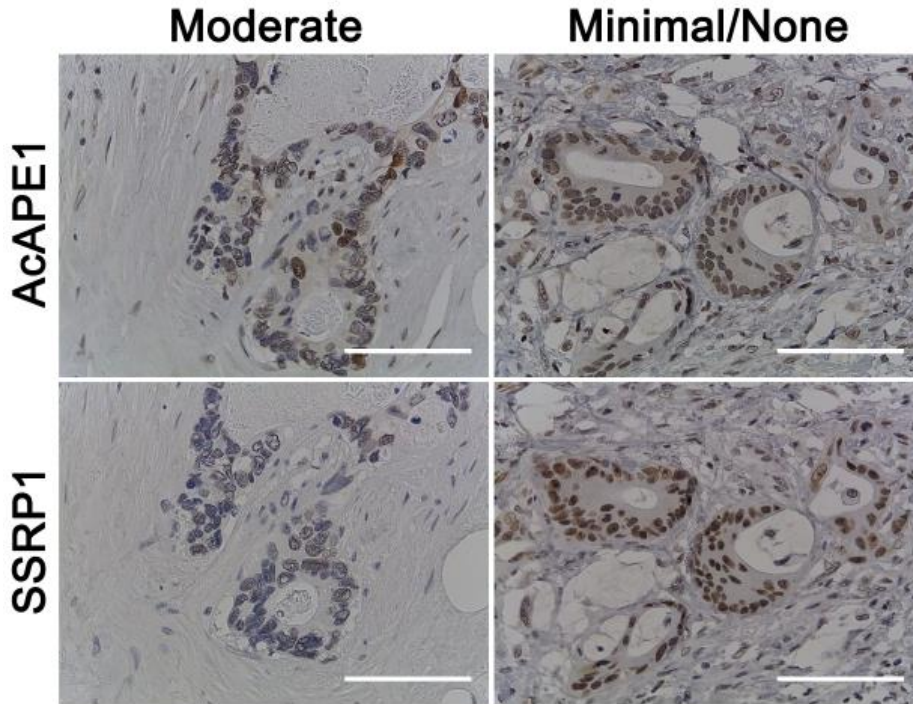


Figure 51. Minimal or none responders have significantly higher percentage of AcAPE1 and SSRP1 staining.

As all the tumor samples we included in this study were from patients with invasive cancer, and the fact that all invasive cancer received neoadjuvant chemotherapy, they represented ideal post-treatment samples for analyzing the tumor after chemotherapy drugs. We divided the samples into two groups, moderate responder (n=19) vs none/minimal responder (n=20). Treatment response is assessed by clinician using modified Ryan Tumor Regression Grading System. We found that none/minimal responders had strong staining of AcAPE1 and SSRP1. The IHC staining was then quantified for percentage of positive staining and presented in the next figure.

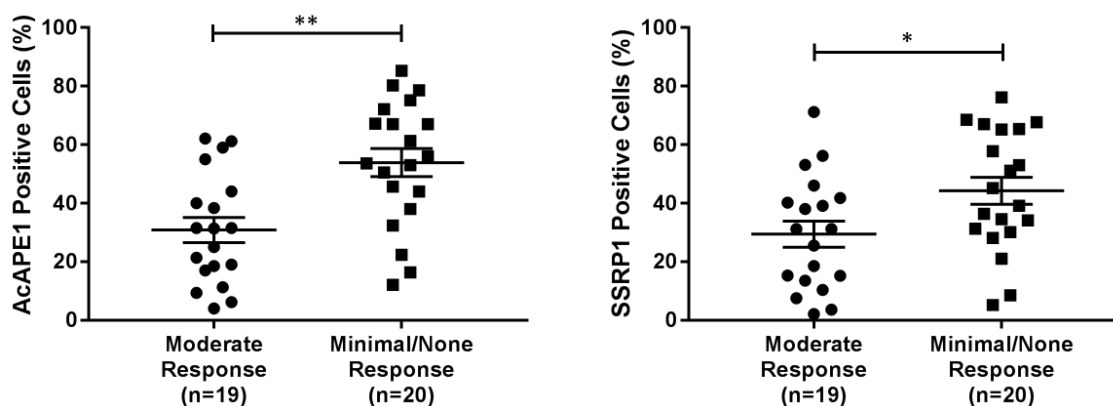


Figure 52. Minimal or none responders have significantly higher percentage of AcAPE1 and SSRP1 staining.

The percentages of cells with positive AcAPE1 and SSRP1 staining were compared between moderate and minimal/none response groups. Similarly, we used Definiens Releases Tissue Studio® 4.3 to quantify the percentage of positive staining of AcAPE1 and SSRP1 in 10 random high power field images. We found that compared to moderate responders, none/minimal responders had significantly higher percentage of AcAPE1 and SSRP1 staining. Together these data suggest that AcAPE1 and SSRP1 is elevated in colon cancer, and the expression is correlated. The none/minimal responders have higher percentage of positive staining for both proteins, indicating a potential role of chemoresistance derived from the overexpression of AcAPE1 of which the activity is enhanced by concurrent overexpression of SSRP1. The finding is consistent with our in vitro and in vivo study that targeting AcAPE1 and FACT complex may represent a novel therapeutic strategy for chemosensitization. Mann–Whitney U test, * $p < 0.05$, ** $p < 0.01$.

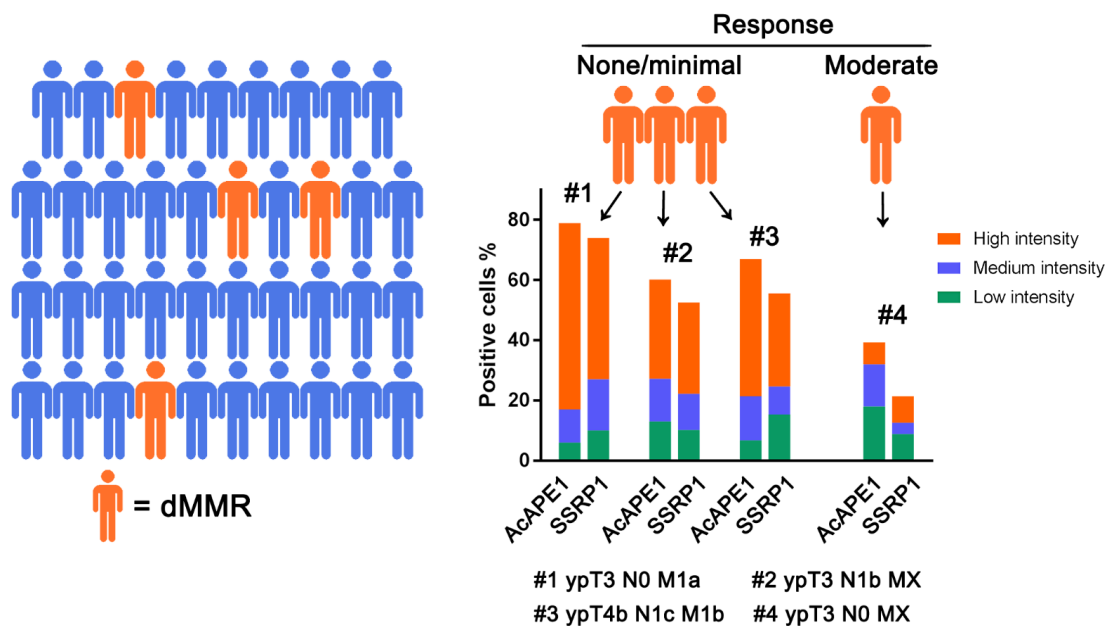


Figure 53. Illustration of MMR deficient patient in our cohort and their staining of AcAPE1 and SSRP1.

Among all 39 CRC patients, 4 were previously identified as MMR deficient. 75% of them (3 out of 4) had minimal or none response to neoadjuvant chemotherapy (details of therapy regimens was not provided), and IHC staining revealed that these patients had high percentage of positive staining for AcAPE1 and SSRP1. Stacked column chart showed staining intensity characterization of positive staining cells. Note that a higher portion of the positive staining was characterized as high intensity in minimal or none response patients. The post-therapy pathologic stages (T=primary tumor, N=lymph node, M=metastasis) of these patients are also included.

Discussion

Resistance to 5-FU remains a major challenge in the treatment of dMMR CRC. Several mechanisms are believed to be responsible for 5-FU resistance, including overexpression of TS enzyme due to gene amplification, deficient MMR pathway and enhanced DNA damage repair resulting in reduced apoptosis (70,110). However, TS levels cannot explain the therapeutic resistance to 5-FU in dMMR-CRC (111), and several clinical studies have shown that defective mismatch repair is a strong predictor for lack of response of 5-FU-based adjuvant therapy in dMMR CRC (109,112,113). This study reveals a novel mechanism of histone chaperone FACT complex in inducing 5-FU resistance in dMMR CRC. Our data show that FACT facilitates the recruitment and acetylation APE1 to the damage sites, and promotes repair of 5-FU-induced DNA damages via BER pathway. Additionally, we demonstrate extensively that targeting FACT with small molecules curaxins significantly improve the efficacy of 5-FU in dMMR CRC both in vivo and in vitro. We found a strong clinical correlation between FACT or AcAPE1 levels with CRC patient's response to chemotherapy. Therefore, FACT complex is a promising target to increase 5-FU treatment response, and our study provides a compelling rationale to combine CBL0137 with 5-FU to provide synergistic effects to overcome the 5-FU resistance in dMMR CRC.

Overexpression of APE1 in various cancer types including colon, lung and breast and its association with chemotherapeutic resistance as well as patients' poor prognosis are well documented (2,43,114). AP site or SSB is a common intermediate in the BER pathway that is generated after treatment with many chemotherapeutic drugs including 5-FU and alkylating agents (2). The repair of AP sites/SSBs by APE1 on naked DNA or nucleosomal DNA substrate has been extensively investigated in vitro (115,116), however, till to date, how APE1 repair AP sites in the context of the nucleosome in

chromatin remains largely unknown. Earlier, we discovered that human APE1 could be acetylated (AcAPE1) at multiple lysine (Lys 6, 7, 27, 31, 32 & 35) residues in the N-terminal domain by p300 (38,117). Acetylation of these Lys residues modulates both DNA damage repair function of APE1 and the expression of multiple genes (26,35,38,44,84,117,118). We have recently shown that acetylation of APE1 occurs at AP sites damage in chromatin which enhances the AP-endonuclease activity of APE1 (38). Furthermore, we demonstrated that primary tumor tissues of diverse origins have higher levels of acetylated APE1 and absence of APE1 acetylation sensitizes cells to many chemotherapeutic agents (44). In this study, we discover that APE1 interacts with FACT complex and induction of DNA damages with 5-FU enhances their recruitment and colocalization at damage sites in chromatin. FACT complex, as a histone chaperone, facilitates the removal and deposit of histone H2A/H2B in nucleosome at the promoter, which in turn stimulating the formation of the preinitiation complex, and at the coding sequence for RNA pol II elongation (93,119). Increasing evidence suggests that FACT plays a role in DNA damage repair in evicting and depositing H2A and H2B, at sites of UV damage and single-strand breaks in DNA (91,92). Our results, using multiple approaches, show that FACT facilitates the access and subsequent acetylation of APE1 to the damage sites and promotes efficient repair of 5-FU-induced DNA damages. (1) Our ChIP assays show that downregulation of FACT complex significantly reduced the occupancy of AcAPE1 to the p21 and DTL promoter regions upon induction of DNA damages. (2) Our biochemical and confocal SIM data show that FACT knockdown reduced APE1 acetylation levels. As acetylation of APE1 occurs after binding to AP sites in chromatin, this data indicates that absence of FACT complex significantly reduced binding of APE1 at damage sites in chromatin. (3) Our FRAP data show that absence of FACT significantly reduces the mobility of GFP-tagged APE1 in chromatin upon induced DNA damages. (4) Depletion of endogenous FACT complex significantly delays the repair of MMS-induced damages and results in accumulation of

AP sites/SSBs in the genome compared to control cells. (5) CRC cells are unable to repair 5-FU induced SSBs in the absence of FACT or in the presence of FACT inhibitor CBL0137. Thus multiple lines of compelling evidence establish a key role of the histone chaperone FACT in the repair of AP site damage in chromatin and FACT complex as a novel regulator of BER pathway. It is likely that at the initiating steps of repair, DNA glycosylase responsible for removing the incorporated 5-FU facilitates recruitment of FACT to sites of damage through physical interaction. Consistent with this, SSRP1 was shown to interact with DNA glycosylase (120). We predict that FACT remains at damage sites and might cooperate to facilitate complete repair by promoting chromatin relaxation and subsequent recruitment of downstream repair protein APE1 and XRCC1 through physical interaction (92). Consistently, a recent study shows that SSRP1 cooperates with PARP1 and XRCC1 to facilitate SSBs repair by chromatin priming (92). This may also facilitate the recruitment of histone acetyltransferase p300 to acetylate APE1 and acetylation in turn enhances the endonuclease activity of APE1 and promotes faster repair. Our current study establishes a key role of FACT complex in BER pathway via regulating APE1 activity which contributes to drug resistance.

Earlier study showed that downregulation of UNG or SMUG 1 responsible for removing 5-FU from DNA did not enhance the 5-FU sensitivity in murine cells (121). This observation can be explained by the fact that the enzymes removing 5-FU from DNA are functionally redundant, the loss of one of these enzyme would not affect the sensitivity. On the other hand, AP site or SSB, a common intermediate in the BER pathway that are generated after removal of incorporated 5-FU, are primarily repaired by APE1. Indeed, our data show that downregulation of APE1 significantly sensitizes a panel of 5-FU resistant CRC cells in vitro. In the absence of MMR pathway, APE1-dependent BER is primarily responsible for removing 5-FU from DNA in dMMR-CRC cells and higher levels of APE1

and FACT would promote 5-FU resistance. Thus, targeting APE1 or FACT represents an opportunity for sensitizing dMMR CRC to 5-FU. However, in the absence of any selective and nontoxic small molecules inhibitor of APE1, we propose that CBL0137, an inhibitor of FACT, could be used for sensitizing dMMR CRC patients to 5-FU. Our data show that in the presence of CBL0137, cells were unable to repair the 5-FU-induced DNA breaks and the addition of CBL0137 sensitizes 5-FU resistant dMMR CRC cell lines in vitro. Importantly, we demonstrate that this therapeutic strategy is also effective in vivo. Our data show that while treatment with 5-FU alone or CBL0137 alone had minimal effects, combination of CBL0137 (or the first generation drug QC) and 5-FU significantly reduced tumor growth in vivo. These data reveal that curaxin helps overcome 5-FU resistance in dMMR CRC. The second generation curaxin CBL0137 is in the final stage of multi-center phase I clinical trial for metastatic or unresectable advanced solid malignancies (NCT01905228), and it has not yet exhibited dose-limiting toxicity. It modulates several important signaling pathways through inhibition of FACT function (103,104,122-124). Increasing evidence suggests that CBL0137 itself has very less cytotoxic effect (102,106,125). Our data also support that combination of CBL0137 with 5-FU has no major toxicity in vital organs in mice. Our studies and others have identified curaxins as a new class of drugs that can be used to sensitize cells to many chemotherapeutic agents (102,106). The mechanism of action is fundamentally different from current chemotherapeutic drugs. By binding DNA within chromatin and altering FACT activities, curaxins can modulate multiple DNA damage repair pathways to sensitizes cells to 5-FU. Studies have shown that curaxins do not cause DNA damage and affect general transcription and are therefore expected to be well tolerated, as we have shown in mice experiments. We propose that combination of CBL0137 has several advantages, including extremely efficient in reaching nuclear DNA as they are not substrate for multidrug

transporters, and high DNA affinity that facilitates binding to bent nucleosome without causing DNA damage.

Although our data show that combination of CBL0137 with 5-FU provides better control of xenograft growth in vivo, we cannot eliminate the possibility that curaxins also affect the expression of other genes involved in modulating the tumor growth or sensitivity to 5-FU. FACT inhibitor CBL0137 has been shown to synergize with cisplatin in small cell lung cancer by increasing Notch signaling and targeting tumor initiating cells (126). It has been shown that curaxins simultaneously suppress NF- κ B and activates p53 (106). Targeting FACT with CB0137 has also been shown to eliminate glioblastoma stem cells and prolong survival in a preclinical model (103). Nonetheless, here we add to the current knowledge by providing compelling evidence that curaxins exhibit strong synergy with 5-FU by interference of BER pathway. We showed that AcAPE1 and SSRP1 levels were elevated in colon cancer samples and could serve as a predictor for CRC patients' response to 5-FU. Patients with minimal or none response demonstrated a distinct expression profile as compared to those with moderate response. However, the use of AcAPE1 and SSRP1 levels as a predictor for treatment response requires a larger number of patient samples and ideally should be tested prospectively. We identified four patients (10.3%) with MMR deficiency and found three of them had minimal or none response to 5-FU-based chemotherapy. These patients have high levels of AcAPE1 and FACT which is consistent with our in vitro and animal studies. Because of the rarity of sporadic dMMR CRC and Lynch syndrome in nature, we are in the process of collecting more clinical samples prospectively to validate our results and would propose that further analysis at a larger population basis is necessary to safely draw the conclusion that FACT can be targeted for chemosensitization in dMMR CRCs.

In conclusion, our study has identified a novel role of FACT complex in BER pathway, and advanced the understanding on how nucleosome remodeling FACT complex contributes to 5-FU resistance in CRC via promoting DNA damage repair. Our study reveals that targeting FACT by combining CBL0137 with 5-FU is a promising strategy to overcome the 5-FU resistance in dMMR CRC.

CHAPTER 2. TARGETING FACT COMPLEX INTERFERES DNA DAMAGE REPAIR AND TRANSCRIPTION AND SENSITIZES MEDULLOBLASTOMA TO CHEMOTHERAPY AND RADIATION

Introduction

Medulloblastoma (MB) is the most common malignant brain tumor in childhood, accounting for nearly 20-25% of all pediatric brain tumors (127,128). Genetically, MB is a heterogeneous tumor that consists of four molecular subtypes: Wingless (WNT), Sonic Hedgehog (SHH), Groups 3 and Group 4 (129,130). A multimodal approach that consists of surgical resection, preceded or followed by craniospinal radiation and cisplatin-based chemotherapy, is the standard of care (131-134). High doses of chemotherapy and radiation cause delayed complications that result in debilitating cognitive, neurologic, and endocrinologic sequelae which severely impacts the quality of life of pediatric cancer survivors (135-138). Additionally, overall survival rate is still poor despite the cure rates are improving in 75% of patients (139). Research efforts directing at reducing treatment toxicity while remaining high cure rate is of importance.

Chemotherapeutic drugs and radiation therapy act, in part, by generating DNA damages in proliferating tumor cells. Apurinic/aprimidinic (AP) sites are one of the most common types of DNA damage that occur following treatments (140). Both radiation and chemotherapeutic drug cisplatin exert their cytotoxic effects by directly inducing DNA damages in cells. Cisplatin induces intrastrand and interstrand crosslinks (ICLs) in DNA which are primarily repaired by nucleotide excision repair (NER) pathway (141,142). On the other hand, radiation induces isolated DNA lesions including AP sites and single-strand breaks (SSBs) and double-strand breaks (DSBs) (143,144). The multifunctional DNA repair enzyme AP-endonuclease (APE1) initiates the repair of AP sites and SSBs,

which constitute ~65% of the DNA damage caused by radiotherapy via the base excision repair (BER) pathway (145). Previous report has demonstrated that APE1 is overexpressed and its activity is associated with response to radiation and chemotherapy in MB. Recent evidence has also demonstrated the role of BER pathway (146-148), where targeting BER showed enhanced sensitivity to cisplatin (149). Altered or efficient repair of DNA damages could play a major role in chemotherapy resistance (150). The mechanisms of repair of AP sites or SSBs and cisplatin-induced DNA cross-link damages via BER and NER have been extensively investigated in naked DNA in vitro. However, how these damages are repaired in the context of nucleosome in chromatin in cells and whether these repair pathways can be targeted to increase the efficacy of chemo and radiation therapy in MB remain an open question.

DNA in the eukaryotic cell is packaged into nucleosome in chromatin. Thus cells must repair DNA lesions including AP sites or SSBs within the context of nucleosome in chromatin. Facilitates chromatin transcription (FACT) complex is a nucleosome remodeling protein complex that has histone chaperone activity and facilitates transcription through chromatin. The FACT complex, a heterodimer of Structure-Specific Recognition Protein1 (SSRP1) and Suppressor of Ty (SPT16) (151), was originally identified as a histone chaperone complex that facilitates the removal and deposition of histone H2A/H2B in nucleosomes during transcription initiation and elongation (63,93). Furthermore, increasing evidence suggests that the FACT complex plays a role at sites of UV damage and single-strand breaks (SSB) in cells (91,92). SSRP1 is recruited to SSB in PARP-dependent manner and retained at DNA damage sites by N-terminal interactions with the DNA repair protein XRCC1 (152). On the other hand, SPT16 is found to accelerate the exchange of H2A/H2B at sites of UV-induced DNA damage and is involved in NER pathway (64). Curaxins, a class of small molecule drugs with broad anticancer activity,

destabilize nucleosomes and inhibits FACT in chromatin (102,125). The second generation curaxin CBL0137, has been utilized in phase II clinical trial for metastatic or unresectable advanced solid malignancies, modulates several important pathways through inhibition of FACT function.

In this study, we seek to investigate whether FACT interacts with APE1 and functional cooperation between FACT and APE1 induces radiation and cisplatin resistance in MB, and whether targeting FACT with curaxin can sensitize MB to cisplatin and radiation. Our study show that FACT complex interacts with APE1 and FACT facilitates repair of radiation and cisplatin-induced DNA in BER pathway via promoting the recruitment and acetylation of APE1 (AcAPE1) to damage sites in chromatin. We show that primary tumor tissues of MB patients have higher FACT and AcAPE1 levels. Targeting FACT complex with Curaxin/CBL0137, inhibits DNA repair and alters gene expression. Curaxin/CBL0137 significantly improves efficacy of cisplatin in MB in vitro and in vivo xenograft models. Together, our study unveils a novel role of FACT complex in promoting radiation and cisplatin resistance in MB, and demonstrate that FACT inhibitor curaxins/CBL0137 can be used as a radiation and chemotherapy sensitizer to augment treatment efficacy and reduce the treatment toxicity in MB patients.

Materials and methods:

Cell culture, plasmids, siRNAs, transfection and treatments

HD-MB03 and UW228 cells were grown in RPMI 1640 Medium (ATCC modification) (Gibco) supplemented with 10% fetal calf serum (FCS; Sigma) and antibiotic mixture of 100 U/ml penicillin and 100 µg/ml streptomycin (Gibco). ONS-76 cells were cultured in RPMI 1640 Medium (ATCC modification) (Gibco) supplemented with 10% fetal calf serum (FCS; Sigma), antibiotic mixture of 100 U/ml penicillin and 100 µg/ml

streptomycin with 2 mL-Glutamine (Gibco). DAOY, D283 and SVG p12 cells were grown in Eagle's Minimum Essential Medium (Gibco) supplemented with 10% fetal calf serum (FCS; Sigma) and antibiotic mixture of 100 U/ml penicillin and 100 µg/ml streptomycin (Gibco). All cell lines were kindly provided by Dr. Sutapa Ray (Division of Pediatric Cancer Research Group at UNMC) and authenticated using STR DNA profiling by Genetica DNA laboratories (Burlington, NC) two years ago before being used in this study.

Western Blot Analysis

Cell fractionation was performed as described previously (81). Whole cell lysates or cell fractions were resolved on 10 to 12.5 % SDS-PAGE gel and transferred to nylon membranes for blotting. Primary antibodies were used including SPT16 (Abcam, 204343), SSRP1 (Biolegend, 609702), α -HSC70 (B6-Sc7298, Santa Cruz Biotechnology), H2A (Abcam, 26350), GAPDH(CST, 8884s), APE1 (Novus Biologicals, NB100-116), α -tubulin (Abcam, 52666) and AcAPE1 (35,84). Immunoblot signals were detected using Super Signal West pico chemiluminescent substrate (Thermo Scientific) after treating with HRP-conjugated secondary Ab (GE Healthcare).

Patient tissue samples and analysis

Tissues were collected in accordance with institution's review board approval and informed consent was waived. 12 of the Medulloblastoma cancer samples were obtained from tissue bank at UNMC. 59 of the deidentified Medulloblastoma cancer patients' samples were obtained from Department of Pathology of Sun Yat-sen University Cancer Center. The deparaffinized sections were stained per standard IHC protocol. The antibodies used were: AcAPE1 (1:200) and SSRP1 (1:100). Staining percentage of positive cells were analyzed by Definiens Releases Tissue Studio® 4.3. The data were plotted using GraphPad Prism 7.

Immunoprecipitation (IP)

Whole cell extracts of HD-MB03 or ONS-76 cells were pre-cleared with protein A/G Plus agarose beads and IP was performed with AcAPE1 antibody or control IgG (Santa Cruz, sc-2003). The whole cell extracts of control and IR-treated cells were immunoprecipitated with the same antibody. The immunoprecipitated proteins were resolved in SDS-PAGE and identified by Western Blot analysis with the indicated antibodies.

Immunofluorescence

Cells grown on coverslips were fixed with 4% formaldehyde (Sigma-Aldrich) and stained with immunofluorescence as described previously (38). Primary antibodies used were mouse monoclonal anti-APE1 (1:100; Novus Biologicals, NB100-116), anti-AcAPE1 (1:50; Ref. 27, 31,32), SSRP1, SPT16 (1:50; Abcam, 204343). Images were acquired by use of a fluorescence microscope with a 63x oil immersion lens (LSM 510; Zeiss), and structured illumination microscopy (SIM) was done with an Elyra PS.1 microscope (Carl Zeiss) by using a 63x objective with a numerical aperture of 1.4. ImageJ software was used to measure Manders colocalization using the JaCoP plug-in.

Chromatin Immunoprecipitation (ChIP) Assay

ChIP assay was performed after double crosslinking of cells with disuccinimidyl glutarate and formaldehyde, with protein A/G Plus agarose beads (Santa Cruz, sc-2003) using with AcAPE1 and control IgG (Santa Cruz) following the procedure as described earlier (38,84). The immunoprecipitated purified DNA was used to amplify the p21 and DTL promoter regions using SYBR GREEN-based (Thermo Scientific) Real Time PCR analysis. The following primers are used: p21 forward 5'-CAGGCTGTGGCTCTGATTGG-3', reverse 5'-TTCAGAGTAACAGGCTAAGG-3'; DTL forward 5'-

TCCTGCAAATTTCCCGCAAC-3', reverse 5'- GGCTATGGCGAACAGGAACT-3'. Data were represented as relative enrichment with respect to IgG control based on $2^{-\Delta\Delta CT}$ method.

Cell Viability Assay

Cell viability was evaluated by MTT assay per standard protocol. The IC₅₀ values were calculated using GraphPad Prism 7 (GraphPad Software Inc., San Diego, CA).

Single Cell Gel Electrophoresis (Alkaline comet assay)

Comet assay was performed following the manufacturer's protocol (Trevigen, # 4250-050-K). At least three independent experiments were performed for each condition. Tail moment was quantitated at least in 50 independent cells for each condition using the OpenComet v1.3.1 software.

Xenograft studies

All animal experiments were performed following the approval of Institutional Animal care and use committee (IACUC). HD-MB03 and ONS-76 cells (1×10^6 in 100 μ l medium) were injected subcutaneously over the left and right flanks in athymic nude mice (Charles Rivers, Wilmington, MA). Subcutaneous tumors were allowed to grow for 1-2 weeks before treatments. When tumor volume reached 100 mm³, the mice were divided into four treatment groups (each groups n=5 mice) and received treatments every other day for four weeks. The following drugs: cisplatin 2 mg/kg, CBL0137 30 mg/kg were injected intraperitoneally. Combination group received both cisplatin and CBL0137. 100 μ L PBS was given to control group. Body weight and tumors volume were measured before each treatment. The mice were euthanized after the end of treatment cycles. Xenograft tumor was fixed in formalin and paraffin-embedded tissue sections were used to perform IHC staining AcAPE1, Ki67 (1:500, CST, 9027), SSRP1, PARP1(1:100, Santa

Cruz, sc-8007), and Caspase 3(1:100, Santa Cruz, sc-7272). Statistical analyses and comparisons of tumor growth was calculated using ANOVA (GraphPad Prism 7). The percentage of positive staining was quantified with 10 random high-power field images using TMARKER (88). Additive or synergistic effect was examined using online tool SynergyFinder (<https://synergyfinder.fimm.fi>) (89).

Terminal dUTP nick-end labeling (TUNEL) assay

Xenograft tumor sections (4 μm thick) were deparaffinized, re-hydrated and submitted to apoptosis quantification analysis according to manufacturer's protocol (Abcam, ab206386).

Statistical analysis

Results are shown as the mean \pm SEM of three independent experiments. Shapiro-Wilk test was used to test for normality distribution. If the Sig. value of the Shapiro-Wilk Test is greater than 0.05, the data is considered normal. For comparison among multiple groups, one-way analysis of variance (ANOVA) followed by Dunnett's post-hoc test or Tukey's HSD test was used depending on the nature of comparison. When there were more than one continuous dependent variables, one-way multivariate analysis of variance (one-way MANOVA) was used to determine whether there were any differences between independent groups. If data did not distribute normally, Kruskal-Wallis test followed by Games-Howell post-hoc test was used as a non-parametric counterpart of ANOVA for multiple comparison. Statistical analyses were performed in SPSS v22.0 (IBM SPSS Statistics). A p-value of less than 0.05 is considered statistically significant. * $p < 0.05$, ** $p < 0.01$, *** $p < 0.001$, **** $p < 0.0001$.

Results

AcAPE1 and SSRP1 levels are elevated in medulloblastoma and associated with overall patients' survival

We have shown that APE1 is acetylated (AcAPE1) at AP site damage in chromatin by p300 and increased level of AcAPE1 in tumor cells promotes resistance to many chemotherapeutic agents (38,44). We examined the AcAPE1 and SSRP1 levels in a cohort of 71 MB patients' tissue specimens by IHC staining. Among these patient's, there were 44 children and 27 adults; clinicopathological characteristics of the cohort are shown in **Table 1**. We found that AcAPE1 and SSRP1 were significantly elevated in MB tissues compared to adjacent normal tissues (**Fig. 54**). Across all histology types, the percentage of positive cells of AcAPE1 and SSRP1 was significantly higher than normal adjacent tissues (**Fig. 55**). There was no statistical difference between classical and Desmoplastic/Nodular (D/N) groups. However, large cell/anaplastic (LCA) group demonstrated significantly higher percentage of positive staining cells as compared to other histology types and normal adjacent tissues. Furthermore, a positive correlation between AcAPE1 and SSRP1 levels ($r=0.57$, $p<0.0001$, **Fig. 56**) was observed. Kaplan-Meier survival analysis was used to compare the overall survival in patients with high and low AcAPE1 and SSRP1 levels. Results show that elevated expression of AcAPE1 and SSRP1 was associated with worse overall survival (**Fig. 57**). We tested this in a larger database, R2 Genomics (153). Consistent with our result, analysis of the database of 763 MB patients' mRNA expression profiles reveals a correlation between expression levels of APE1 or SSRP1 and the overall survival of these patients (**Fig. 58**). Together, these data suggest that APE1 and FACT are overexpressed in MB and levels of AcAPE1 and SSRP1 could serve as a prognostic marker for MB.

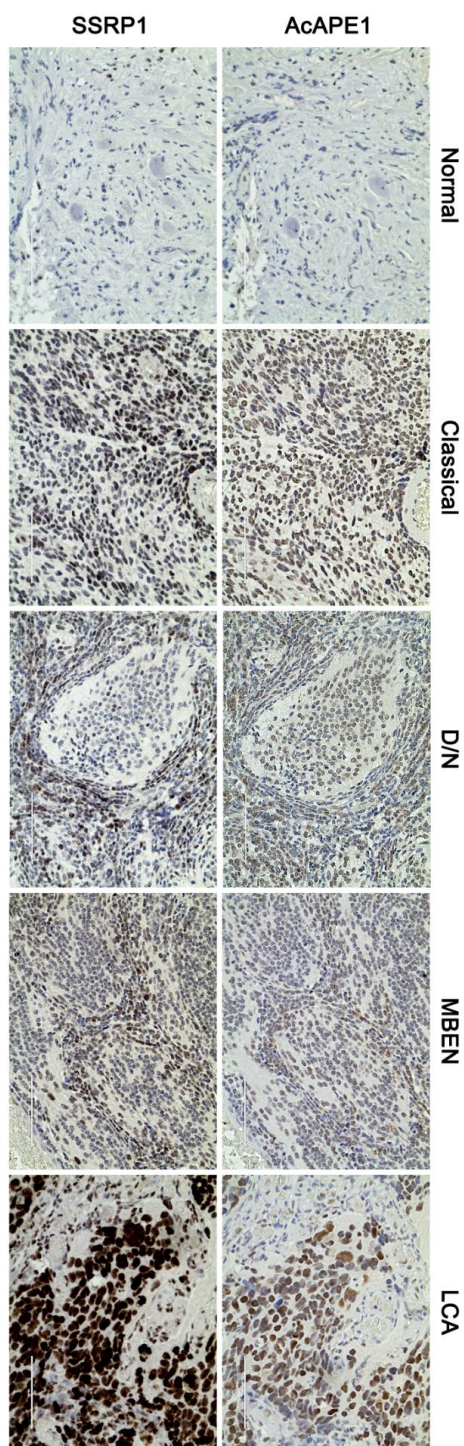


Figure 54. Overexpression of AcAPE1 and SSRP1 is observed in MB.

To investigate if AcAPE1 and SSRP1 may play a role in the treatment response and prognosis of MB, samples from medulloblastoma were submitted for IHC analysis. MB

can be divided into four different groups based on their histology: classical, desmoplastic/nodular (D/N), medulloblastoma extensive nodular (MBEN) and large cell/anaplasia (LCA). Overexpression of AcAPE1 and SSRP1 was observed in MB across all histology groups.

Table 1. Clinical characteristics of the medulloblastoma cohort.

Characteristics	Classical (n=43)	D/N (n=19)	MBEN (n=5)	LCA (n=4)
Age (median, range)	8.5 (2-35)	13 (4-35)	2 (0.5-38)	22.5 (3-33)
Age				
≤18	29	10	4	1
>18	14	9	1	3
Sex				
Male	25	11	3	4
Female	18	8	2	0
Tumor location				
Midline	18	6	1	2
Hemisphere	10	5	1	2
V4	15	8	3	0
Tumor size				
≥4 cm	25	14	3	4
<4 cm	14	5	2	0
V4 floor involvement				
Yes	15	5	2	2
No	28	12	3	2
Surgical resection				
GTR	25	14	4	3
STR	18	5	1	1
Recurrence				
Yes	8	3	1	2
No	35	16	4	2
PFS (median, range, months)	12 (1-168)	29 (1-120)	29 (3-30)	8 (1-14)
OS (median, range, months)	15 (1-168)	33 (1-120)	29 (3-30)	15 (1-21)
Death				
Yes	7	4	1	2
No	36	15	4	2

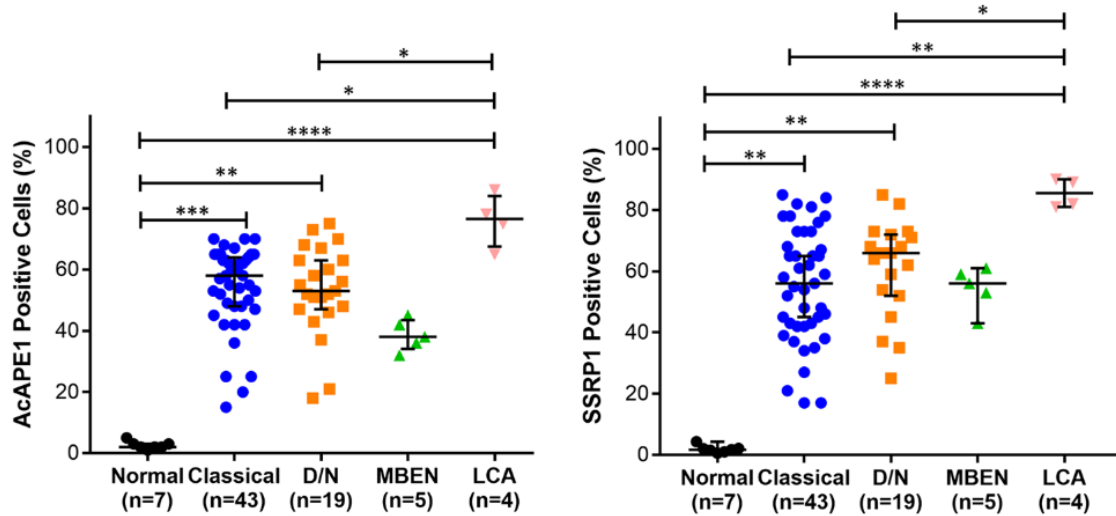


Figure 55. MB tissues have higher percentage of AcAPE1 and SSRP1 positive staining as compared to normal tissues.

The percentage of cells positive for AcAPE1 or SSRP1 from ten random high field in each sample was pooled. We found that all histology groups had higher percentage of positive staining of AcAPE1 and SSRP1. While the statistical difference was noted when comparing LCA group with other groups, caution must be taken when interpreting the result given the relatively small number of cases included. This is due to the rarity of MB in general population and majority is classical type. Additionally, unlike other solid tumor in human, the resection of brain tumor does not always include significant amount of surrounding normal tissue as this will cause devastating neurological consequences. Therefore, we were only able to include seven normal adjacent tissues for comparison. Kruskal-Wallis test with Games-Howell post-hoc test, * $p < 0.05$, ** $p < 0.01$, *** $p < 0.001$, **** $p < 0.0001$.

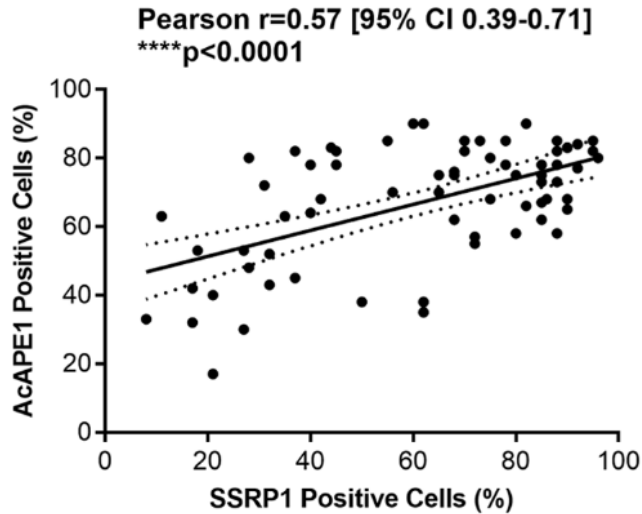
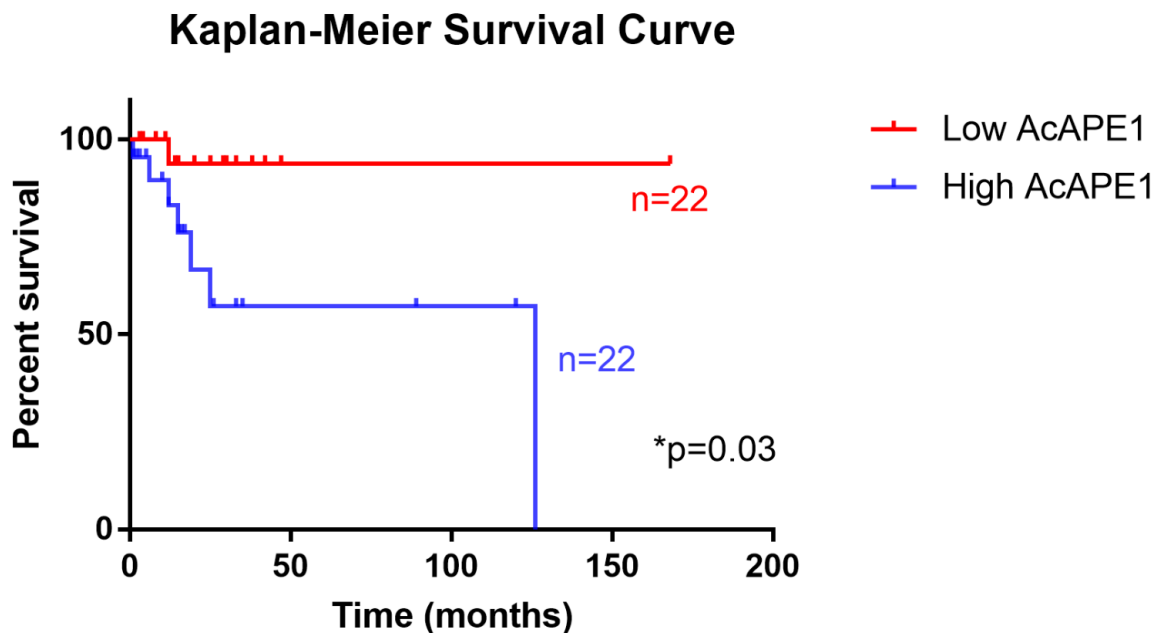


Figure 56. The expression of AcAPE1 and SSRP1 is correlated in MB.

Based on the quantification of IHC staining result, we analyzed the association between AcAPE1 and SSRP1 expression using linear regression. We found that the expression of AcAPE1 was correlated with SSRP1 with Pearson r of 0.57. This provides rationale for the following study to examine their interaction and prognostic features.



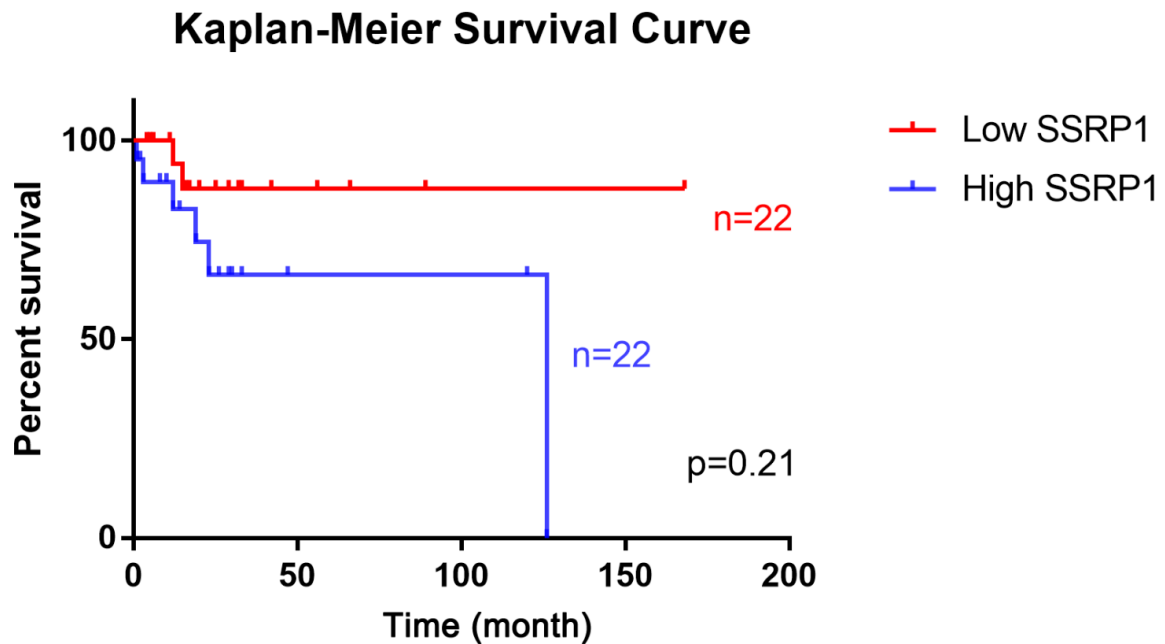


Figure 57. Survival analysis based on AcAPE1 and SSRP1 expression.

To investigate whether AcAPE1 and SSRP1 plays a role in the prognosis of MB patients, we performed Kaplan-Meier analysis to analyze the overall survival in relation to AcAPE1 and SSRP1 expression. We calculated the median of the percentage of positive staining cells and divided the cohort into two groups (high vs low expression). A total of 44 pediatric patients in our cohort were included. We found that high expression of AcAPE1 and SSRP1 was associated with poor overall survival. The p value is statistically significant in AcAPE1 but not in SSRP1. The high SSRP1 group did demonstrate worse overall survival. A possible explanation is the small number of samples available for analysis makes it difficult to detect statistical difference. Therefore, we sought to examine the prognostic significance of AcAPE1 and SSRP1 in a larger cohort (presented in next figure).

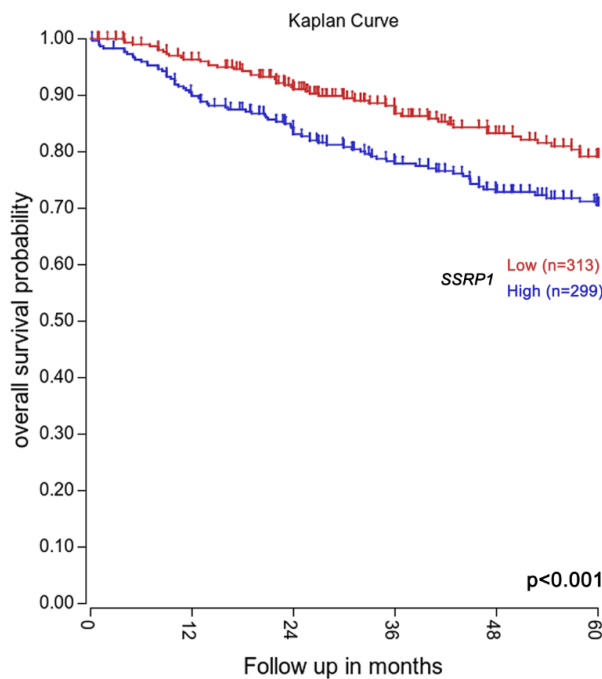
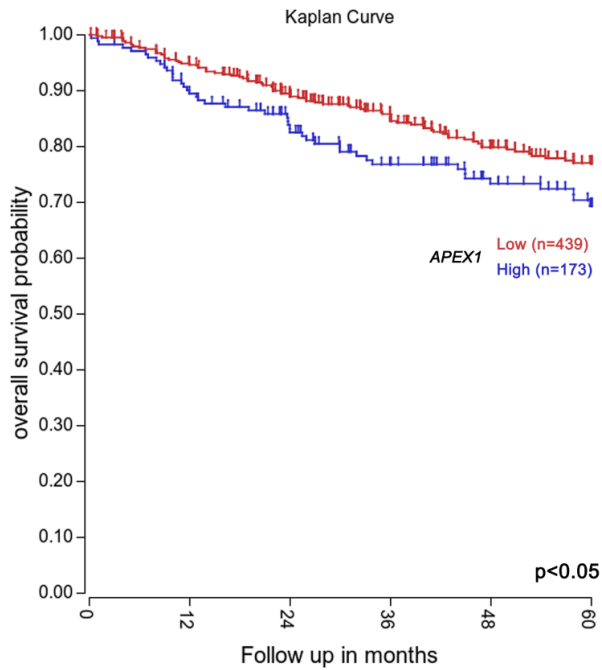


Figure 58. Survival analysis using R2 genomics demonstrates that high expression levels of AcAPE1 and SSRP1 is correlated with poor overall survival.

As our cohort was relatively small, we extended our survival analysis using R2 Genomics.

This is a freely accessible online genomics analysis and visualization tool which can

analyze a large collection of public data. In this database, there is a cohort of 612 MB patients that have survival and gene expression data available for analysis. We analyzed the prognostic significance of APE1 (aka. *APEX1*, Top) and SSRP1 (Bottom) gene expression by Kaplan-Meier plot and found that the expression levels of APE1 and SSRP1 were associated with poor overall survival. Together, these data suggest that the AcAPE1 and SSRP1 is overexpressed in MB, and their elevated expression plays a role in the prognosis.

AcAPE1 interacts with FACT complex and radiation enhances their colocalization

We used multiple MB cells line along with fetal glial cell line SVG p12 as normal control to determine the expression levels of FACT complex and APE1. As shown in **Fig. 59**, both subunits of FACT complex, SSRP1 and SPT16 were upregulated in MB cells lines. Concurrently, AcAPE1 showed overexpression in these tumor cell lines while the total APE1 had no change in expression. The quantification of WB result was shown in **Fig. 59**. As both FACT and AcAPE1 are elevated in MB and one recent study has shown that FACT complex is involved in DNA SSBs damage repair, we examined whether AcAPE1 interacts with FACT complex in MB cell lines. We immunoprecipitated (IP) endogenous AcAPE1 from HD-MB03 and ONS-76 cell extracts and examined the presence of FACT complex in AcAPE1 IP by Western blot analysis. We found both subunits of FACT in AcAPE1 IPs (**Fig. 60**). Confocal microscopy revealed colocalization of AcAPE1 with SPT16 and SSRP1 in the nucleus of MB cells (**Fig. 61**). To determine whether radiation therapy which induces SSBs and AP sites damages in the genome promotes interaction of AcAPE1 and FACT at damage sites, we exposed HD-MB03 cells to radiation. Our Co-IP data showed that there was an increasing association of AcAPE1 and FACT complex upon induction of DNA damage with radiation (**Fig. 62**). Confocal

microscopy revealed enhanced colocalization of both subunits of FACT complex with AcAPE1 after radiation (Fig. 63).

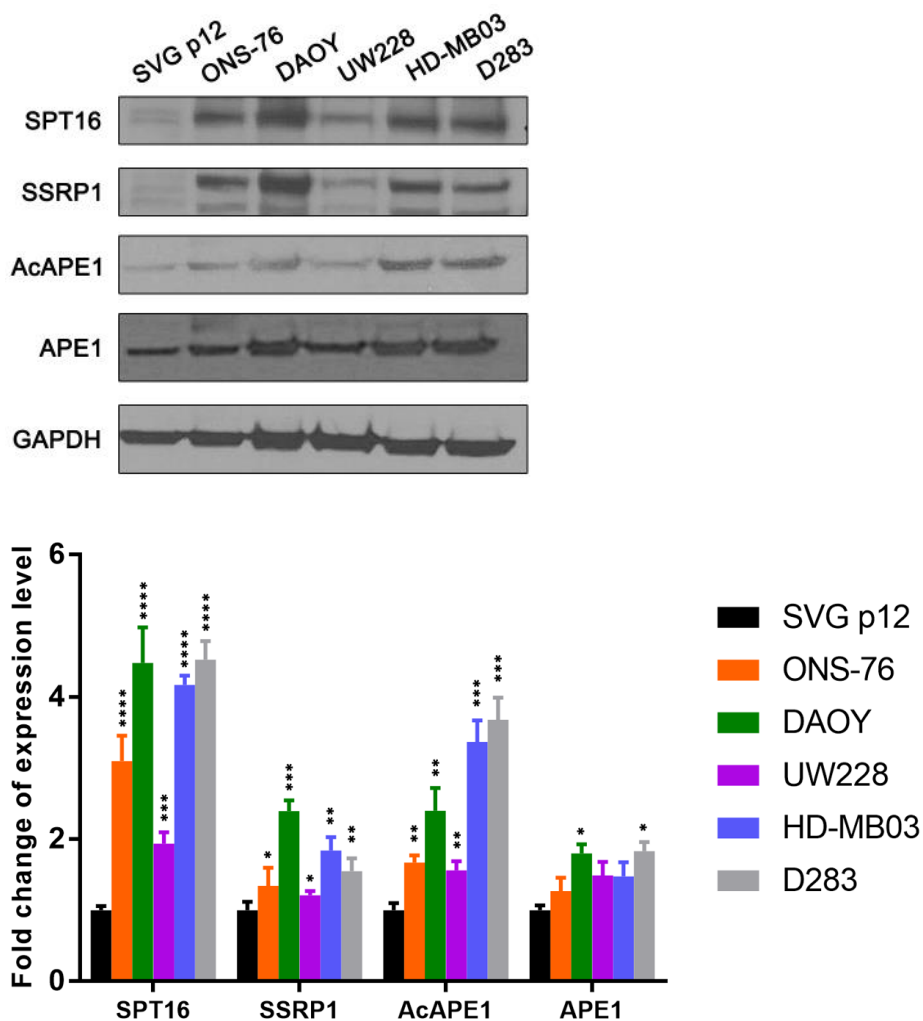


Figure 59. Elevated expression of AcAPE1 and FACT complex is observed in various MB cell lines.

We sought to determine the expression levels of both proteins in MB cell lines. The expression levels of SPT16, SSRP1, AcAPE1 and APE1 were determined using Western blotting in multiple MB cells lines. ONS-76, DAOY and UW228 are from Sonic-Hedgehog (SHH) group, HD-MB03 and D283 are from group 3. The expression levels of proteins

were semi-quantified using ImageJ. GAPDH was used as control. Compared to SVG p12 cells which were used as normal glial cell control, MB cells demonstrated significantly higher expression of AcAPE1 and SSRP1. Three biological replicates were performed. Results are shown as the mean \pm SEM. One-way ANOVA with Tukey's HSD test, * $p < 0.05$, ** $p < 0.01$, *** $p < 0.001$, **** $p < 0.0001$.

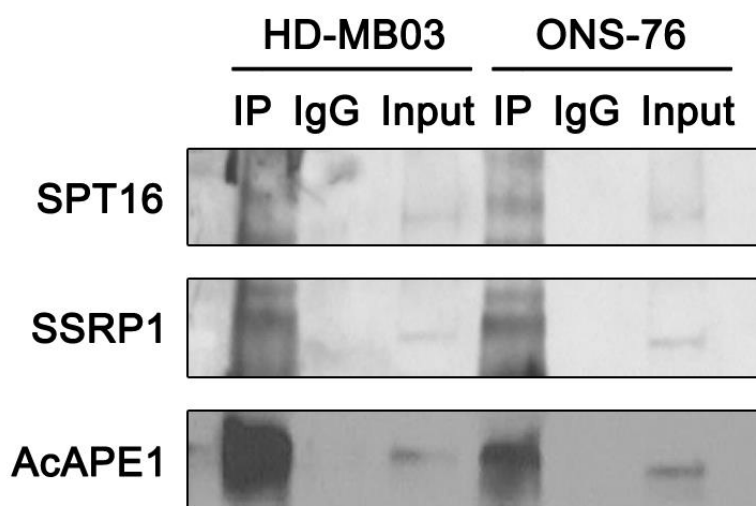


Figure 60. AcAPE1 is associated with FACT complex.

To investigate whether AcAPE1 interacts or associated with FACT complex, co-immunoprecipitation using AcAPE1 antibody was performed using HD-MB03 and ONS-76 cell extracts. ONS-76 and HD-MB03 are p53 WT cell lines. DAOY and UW228 have p53 mutations. IgG was used as negative control. We found that AcAPE1 was associated with FACT complex in both cell lines. Three biological replicates were performed and representative image was shown.

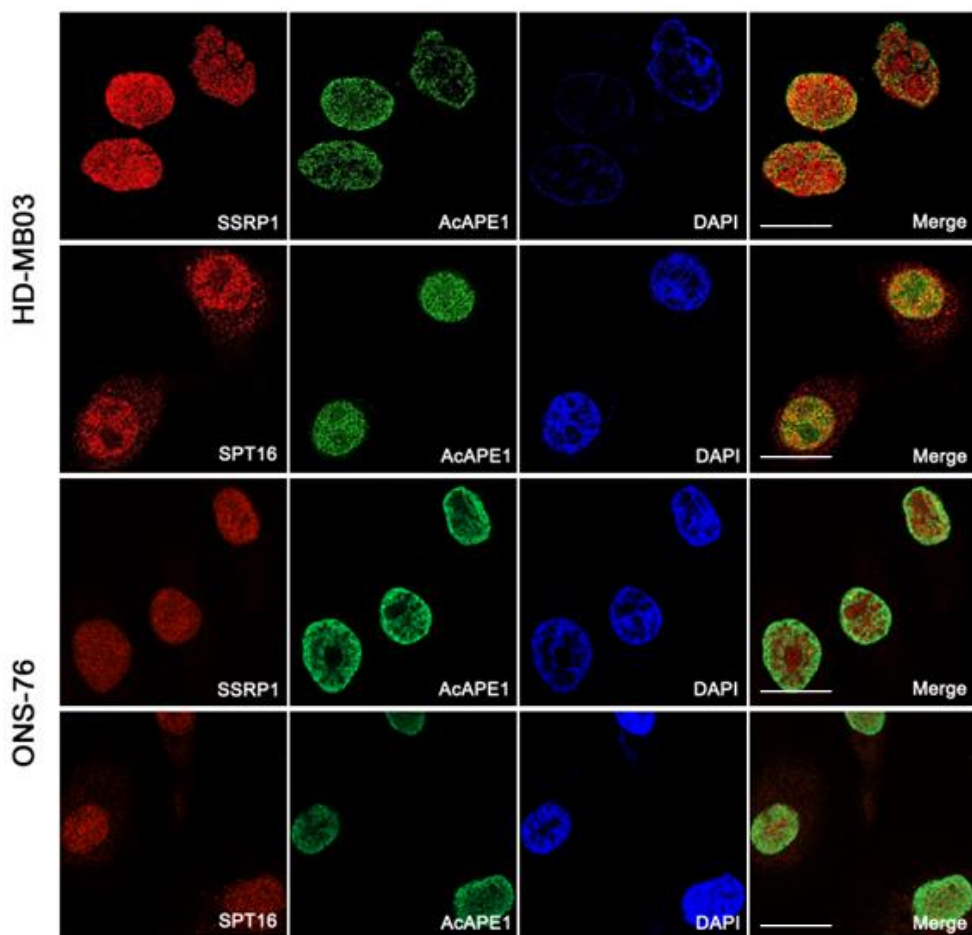


Figure 61. Confocal microscopy demonstrates the colocalization of AcAPE1 and FACT complex.

To provide further evidence of the interaction of AcAPE1 and FACT complex, HD-MB03 and ONS-76 cells were stained with AcAPE1, SSRP1 and SPT16 antibodies. The expression and co-localization of SSRP1, SPT and AcAPE1 was examined using confocal microscopy. The colocalization was visualized on merged images. Multiple cells from three biological replicates were analyzed. Representative images were shown. Bar = 25 μ M.

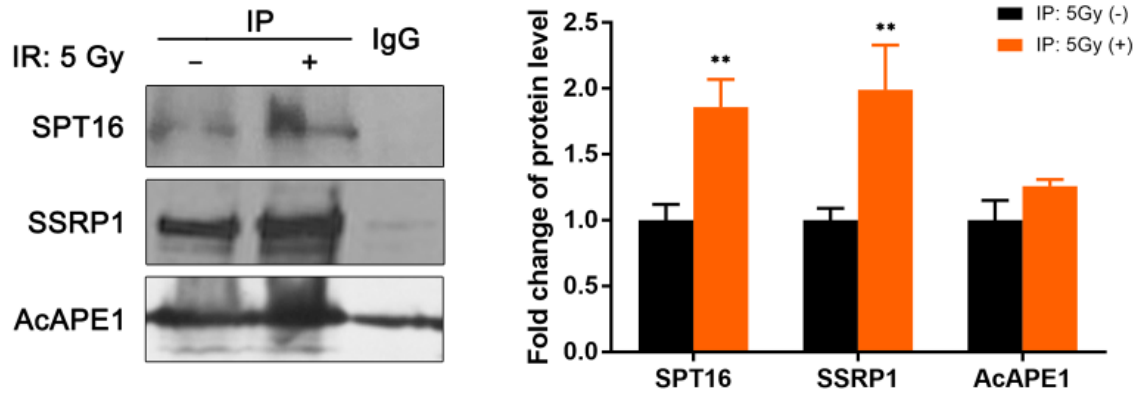


Figure 62. Increased association of AcAPE1 and FACT complex upon irradiation is observed.

To examine if radiation affects the interaction of AcAPE1 and FACT complex, we irradiated (5 Gy) HD-MB03 cells and performed immunoprecipitation using AcAPE1 antibody. IgG was used as negative control. We found that irradiation significantly increased the association of AcAPE1 and FACT complex. Three biological replicates were analyzed. Results are shown as the mean \pm SEM. One-way MANOVA with Tukey's HSD test, ** $p < 0.01$.

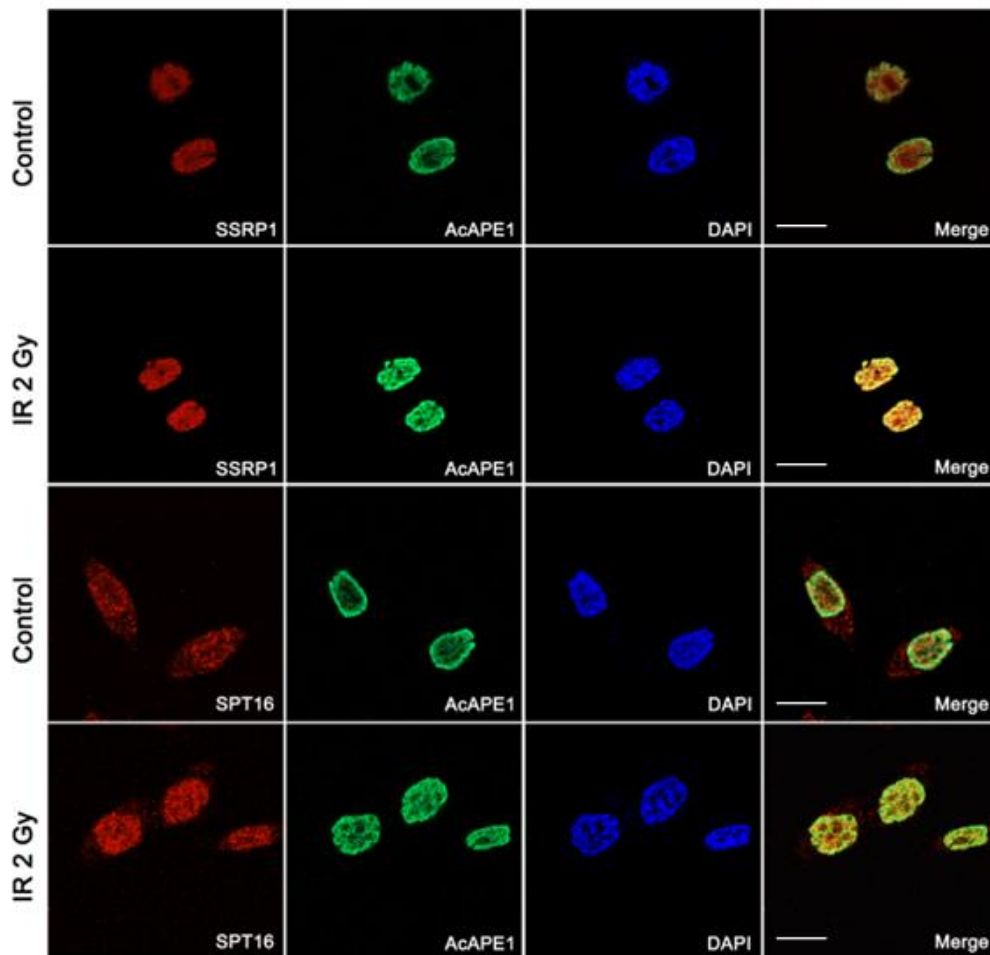


Figure 63. Confocal microscopy demonstrates increased colocalization of AcAPE1 and FACT complex upon irradiation treatment.

To provide further evidence that irradiation increases the interaction of AcAPE1 and FACT complex, cells were irradiated with 2 Gy and submitted for immunofluorescence staining with corresponding antibodies. We found that irradiation enhanced the colocalization of AcAPE1 and both subunits of FACT complex. Multiple cells in three biological replicates were analyzed. Representative images were shown. Bar = 25 μ M.

FACT is involved in facilitating the binding and acetylation of APE1 to damage site in chromatin

To examine whether FACT facilitates the binding and acetylation of APE1 at damage sites in chromatin, we used siRNA to downregulate SPT16 and SSRP1 together (FACT siRNA) (**Fig. 64**). FACT siRNA successfully decreased the expression of SPT16 and SSRP1 which resulted in reduction of AcAPE1 level. The total APE1 expression remained unchanged. As acetylation of APE1 occurs after binding to AP site in chromatin, these data indicate that the absence of FACT complex significantly reduced the access or binding of APE1 to damage sites and its subsequent acetylation in chromatin. Previously, we showed that APE1 regulates p21 expression via binding to the p21 and DTL proximal promoter regions and functions as a coactivator or corepressor depending on the p53 status of the cells (95). To understand if FACT facilitates the recruitment and/or binding of APE1 to damage sites in p21 and DTL promoters, we treated the cells with 5 Gy radiation with control and FACT siRNA, respectively. We performed ChIP assays with APE1 antibody. Consistently, ChIP assay revealed that FACT downregulation significantly abrogated the occupancy of APE1 to p21 and DTL promoters upon radiation damages (**Fig. 65**). Together, these data provide evidence that the FACT complex promotes the binding and subsequent acetylation of APE1 to damage sites in chromatin. Next, we tested if FACT knockdown impacted the DNA repair function of APE1. FACT knockdown cells demonstrated undetectable level of AcAPE1 as compared to normal cells (**Fig. 66**). While cisplatin increased the colocalization of SSRP1 and AcAPE1 in nucleus, FACT knockdown abrogated the effect of cisplatin on inducing AcAPE1. The interference of FACT knockdown on BER function was further examined using neutral comet assay which measures DNA double-strand breaks. Cells treated control siRNA showed DNA damage after 5 Gy radiation, and the damages were repaired at 24-hour release (**Fig. 67**). On the other hand, FACT siRNA treated cells failed to repair the DNA damage despite 24-hour release. These data indicate that the interaction of FACT complex and AcAPE1 can be targeted by knocking down FACT complex and it leads to functional interference of APE1.

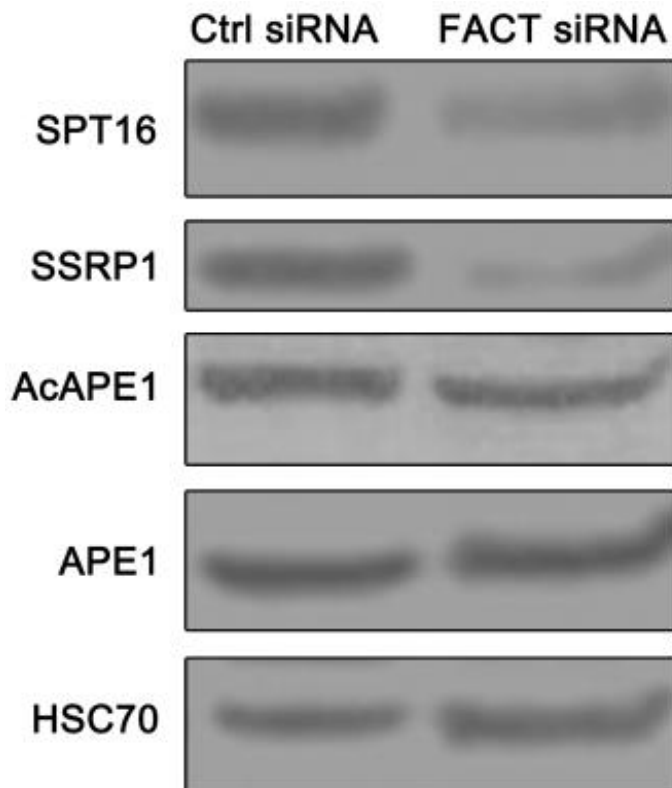


Figure 64. FACT KD decreases the expression of AcAPE1 but not total APE1.

To examine if FACT knockdown affects the level of AcAPE1, we used siRNAs of SPT16 and SSRP1 to deplete FACT complex. The expression levels of SPT16, SSRP1, AcAPE1 and APE1 were examined by Western blot analysis. We found that the level of AcAPE1 decreased upon FACT knockdown while total APE1 level stayed stable. Two biological replicates were analyzed. Representative images were shown.

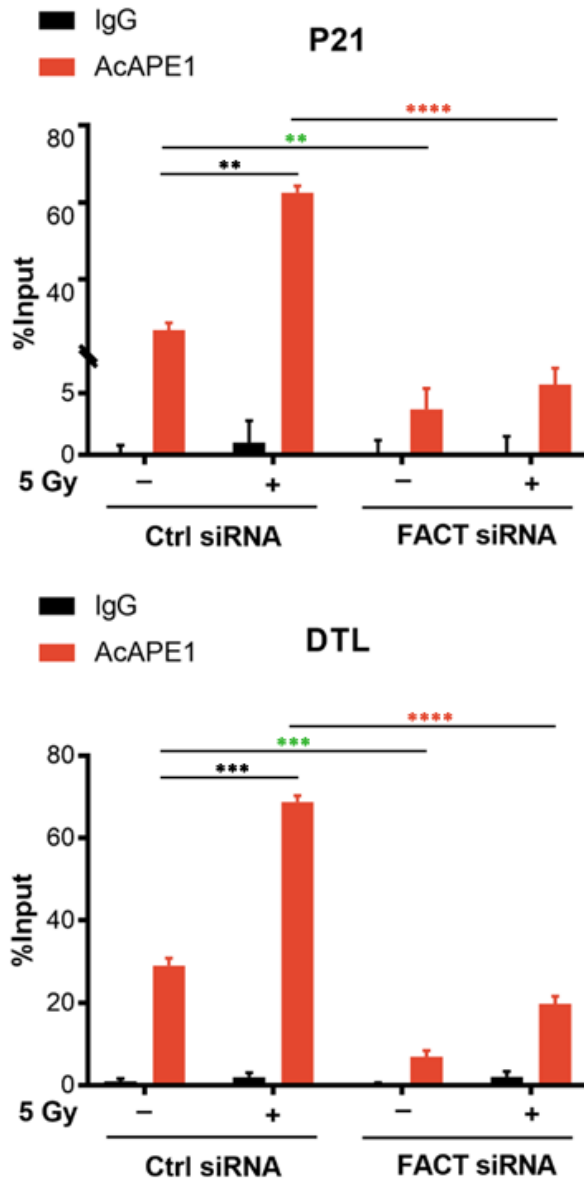


Figure 65. FACT KD abrogates the enhanced occupancy of AcAPE1 to p21 and DTL promoter regions upon irradiation.

To investigate whether FACT complex affects the binding of AcAPE1 to p21 and DTL promoter regions, the cells were transfected with siRNAs of FACT complex and 48 hours after transfection cells were then exposed to 5 Gy irradiation. The binding/occupancy of AcAPE1 to p21 (Top) and DTL (Bottom) promoter regions were examined using promoter-directed real-time PCR assay. Note that FACT siRNA means siRNAs of SPT16 plus

SSRP1. Green asterisks mark the comparisons between ctrl siRNA and FACT siRNA without irradiation treatment. This indicates that FACT depletion under physiological condition leads to decreased AcAPE1 occupancy to both promoter regions. Red asterisks mark the comparisons between ctrl siRNA and FACT siRNA at the presence of irradiation. While in control cells AcAPE1 occupancy increased upon irradiation, such effect was abrogated by FACT depletion. Three biological replicates were performed. Results are shown as the mean \pm SEM. One-way ANOVA with Tukey's HSD test, ** $p < 0.01$, *** $p < 0.001$, **** $p < 0.0001$.

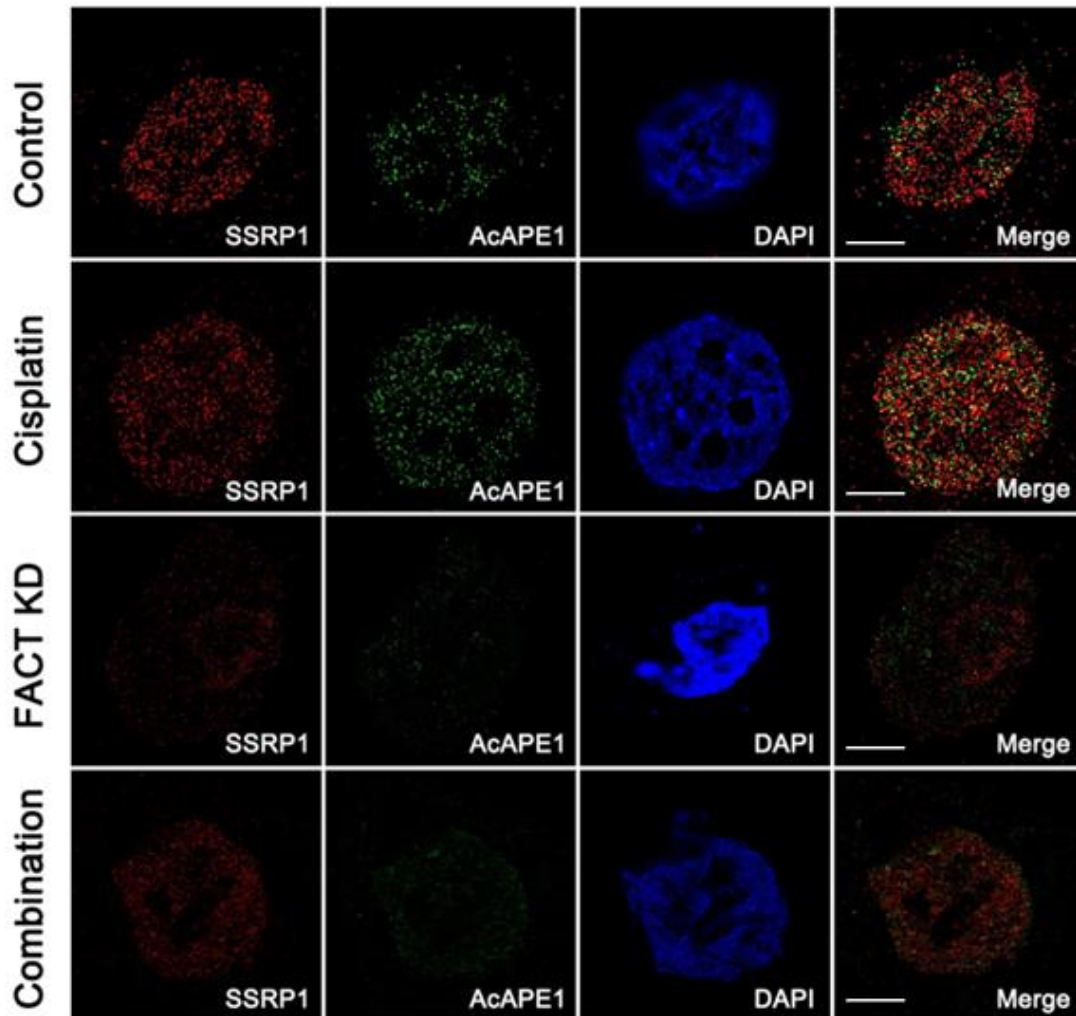


Figure 66. SIM demonstrates that the enhanced colocalization of SSRP1 and AcAPE1 upon cisplatin treatment is abrogated by FACT KD.

Beside irradiation, cisplatin-based chemotherapy is another mainstay of treatment for MB. We sought to test if cisplatin increased the colocalization of AcAPE1 and FACT complex, and if such effect would be affected by FACT knockdown. The expression of SSRP1 and AcAPE1 were examined after treatment with cisplatin or FACT knockdown, and combination (FACT knockdown plus cisplatin). As demonstrated by SIM, while cisplatin increased the colocalization of AcAPE1 and SSRP1, the enhancement was prevented by

FACT depletion. Three biological replicates were performed. Representative images were shown. Bar = 5 μ M.

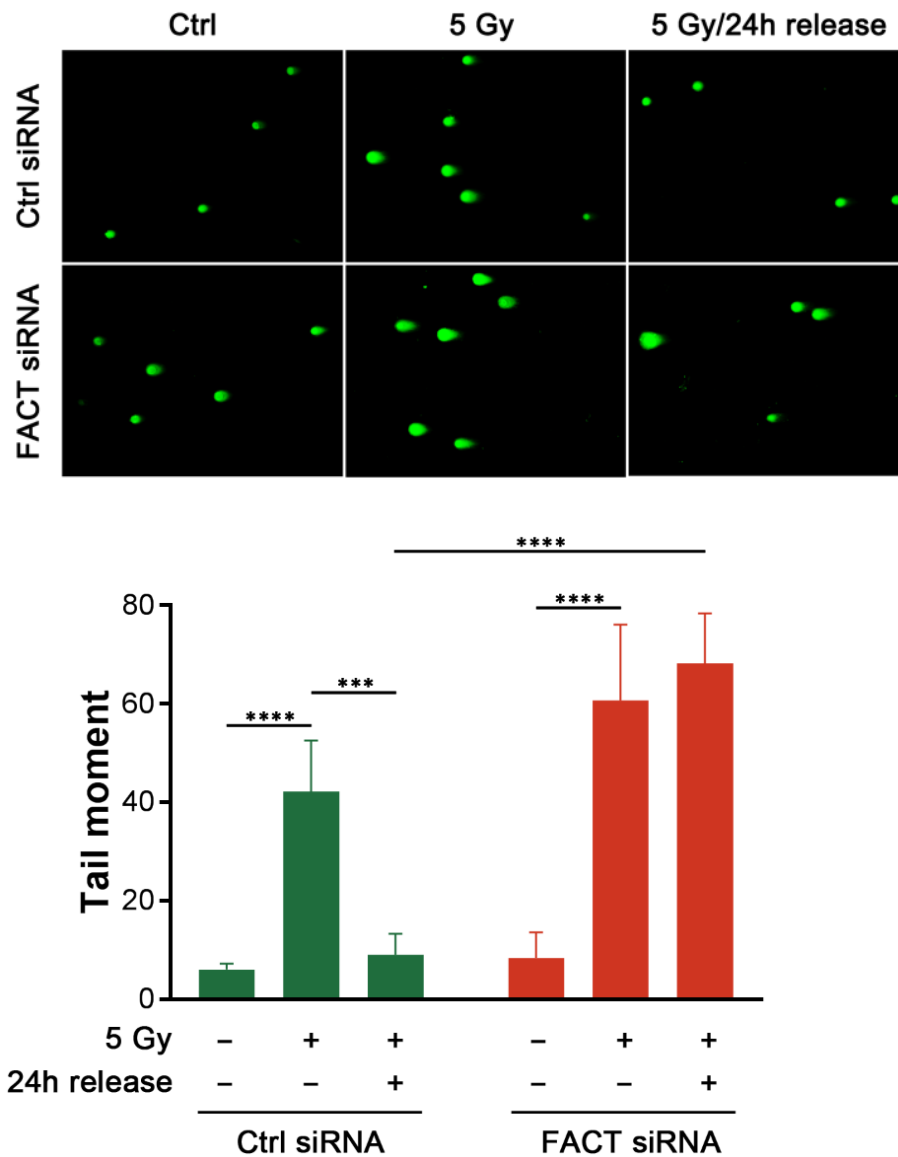


Figure 67. FACT KD significantly impairs BER repair on irradiation induced damage.

(Top) Neutral comet assay was performed to detect the DNA damage induced by irradiation. Note that we used neutral comet assay which allows the detection of double-strand breaks by subjecting lysed cell nuclei to an electrophoretic field at a neutral pH (7).

This is different from alkaline comet assay which was used in Chapter 1, in the way that it uses alkaline pH (13) to allow for single strand break detection. Cells were transfected with control or FACT siRNA and submitted to irradiation at indicated dose. 24-hour release was given to allow DNA repair. (Bottom) Tail moment of 50 cells was examined in each treatment group and the bar graph was shown. In control and FACT KD groups, 5 Gy irradiation induced a significant amount of DNA damage as evident by the rise of tail moment. The difference, however, was at 24-hour release. The FACT siRNA treatment resulted in failure to repair DNA damage, while control cells had recovered with baseline tail moment. Three biological replicates were analyzed. Results are shown as the mean \pm SEM. One-way ANOVA with Tukey's HSD test, *** $p < 0.001$, **** $p < 0.0001$.

Inhibition of FACT complex with Curaxin/CBL0137 abrogates the binding and acetylation of APE1 to damage site in chromatin.

We further examine if FACT complex can be targeted using a readily available agent, curaxins. Curaxins is a class of small molecule drugs with broad anticancer activity. It unfolds nucleosomes and traps FACT in unfolded nucleosomes chromatin. CBL0137 is the second generation curaxins that modulates several important signaling pathways through inhibition of FACT function. Consistent with prior reports, CBL0137 decreased the protein levels of SSRP1 and SPT16 in soluble whole cell lysates in a dose-dependent manner (**Fig. 68**). In contrast, SSRP1 and SPT16 levels increased in chromatin extracts with a concurrent reduction in nuclear extracts (**Fig. 69 & 70**). This is the chromatin trapping effect induced by CBL0137. We found inhibition of FACT with CBL0137 decreased AcAPE1 and FACT colocalization (**Fig. 71**). These data indicate that inhibition of FACT with curaxins reduced APE1-binding to the damage sites and its subsequent acetylation, thus potentially may interfere the damage repair in BER pathway.

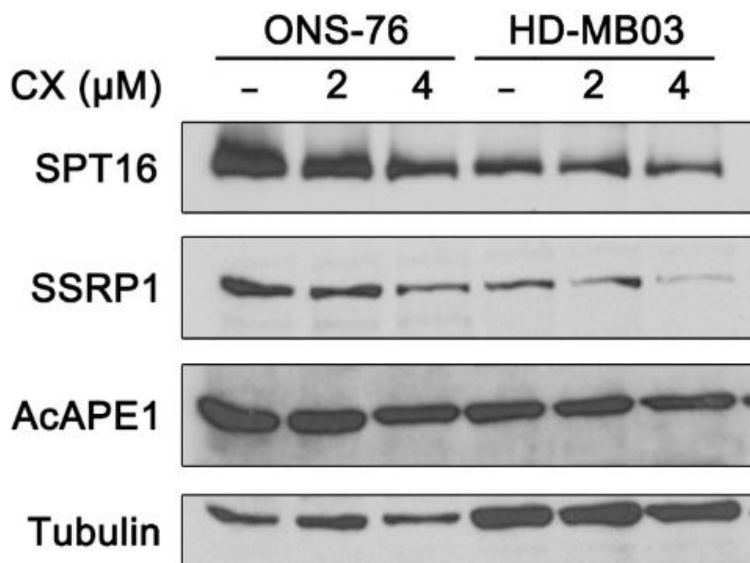


Figure 68. CBL0137 decreases the expression of AcAPE1 and FACT complex in whole cell extracts of MB cells.

To investigate the effect of CBL0137 on the expression of interested proteins, cells were treated with indicated doses of curaxins/CBL0137 (CX). Whole cell extract was used for Western blotting to examine the expression levels of SPT16, SSRP1 and AcAPE1. We found that CBL0137 decreased the level of AcAPE1 in a dose-dependent manner in HD-MB03 and ONS-76 cells. Such effect could also be observed on SSRP1 and SPT16 levels. Three biological replicates were analyzed. Representative images were shown.

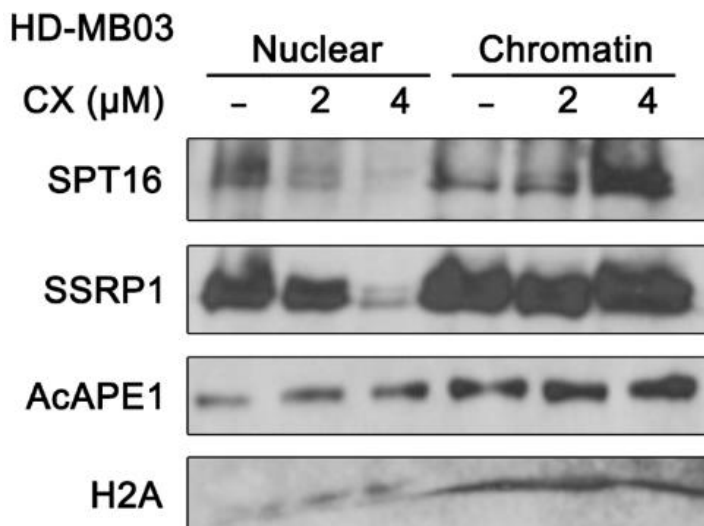


Figure 69. CBL0137 causes chromatin trapping effect on FACT complex and decreases the expression of AcAPE1 in HD-MD03 cells.

Here, we performed Western blot analysis of SPT16, SSRP1 and AcAPE1 in soluble nuclear fraction and chromatin extracts in HD-MB03 cells after treatment with CBL0137. H2A was used as internal control. We found that similar to our previous finding, chromatin trapping effect was present in HD-MB03 cells, as demonstrated by decreasing level of FACT complex in nuclear extract but increasing level in chromatin extract. Three biological replicates were analyzed. Representative images were shown.

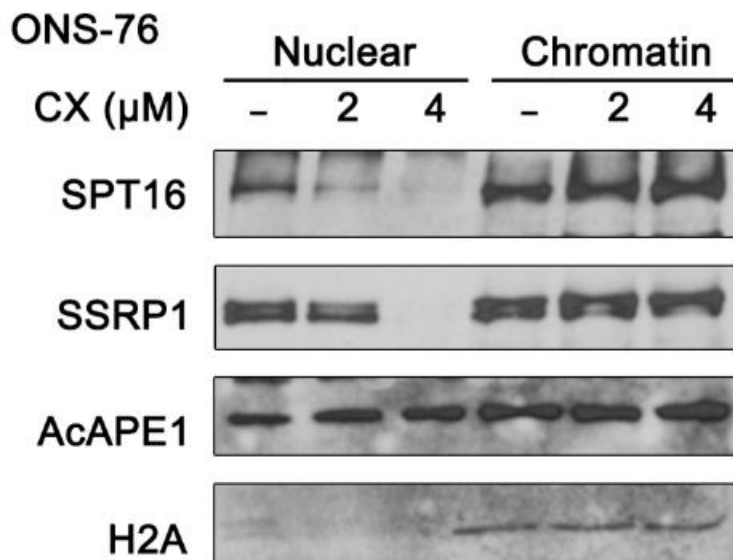


Figure 70. CBL0137 causes chromatin trapping effect on FACT complex and decreases the expression of AcAPE1 in ONS-76 cells.

Following the prior experiment, we sought to confirm the chromatin trapping effect of CBL0137 in ONS-76 cells. ONS-76 cells were treated with CX. Nuclear and chromatin extracts were used to examine the expression levels of SPT16, SSRP1 and AcAPE1. H2A was used as internal control. We found that CBL0137 treated cells had dose-dependent decrease of FACT complex in nuclear extract and dose-dependent increase in chromatin extract, consistent with chromatin trapping effect. Three biological replicates were analyzed. Representative images were shown.

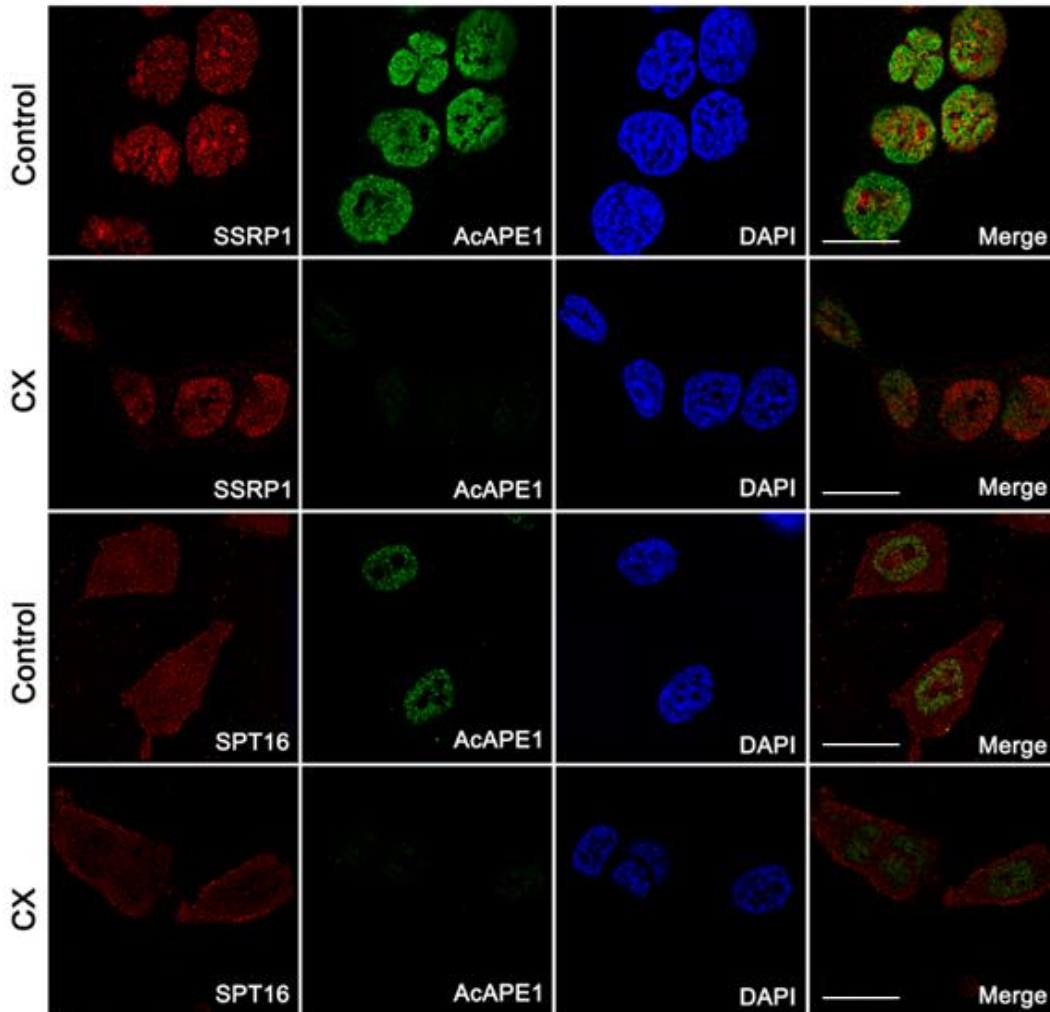


Figure 71. CX decreases the expression of AcAPE1 and its colocalization with FACT complex.

To visualize the effect of CX on the expression and its interaction with FACT complex, cells were treated with CX and submitted for immunofluorescence staining. As demonstrated by confocal microscopy, CX treatment decreased the expression of AcAPE1 and the colocalization with FACT complex in HD-MB03 cells. Multiple cells in three biological replicates were analyzed. Representative images were shown. Bar = 25 μ M.

Inhibition of FACT function with Curaxin/CBL0137 delayed radiation and cisplatin-induced DNA damage repair.

As FACT promotes binding and subsequent acetylation of APE1, we deduced that cells would accumulate SSBs or DSBs in the genome in the presence of FACT inhibitor. To provide evidence for the role of FACT in facilitating the radiation induced DNA damage repair in cells, we used single cell alkaline comet assay which detects both SSBs and DSBs damages in the genome in cells after curaxin treatment (**Fig. 72 & 73**). Cells exhibited tails indicative of DNA damages after radiation exposure or cisplatin treatment and started to recover in 24-36 hours. However, curaxin-treated cells retained significantly more tails in 24 hours. These suggest that in the presence of curaxin cells fail to efficiently repair radiation and cisplatin-induced DNA damages.

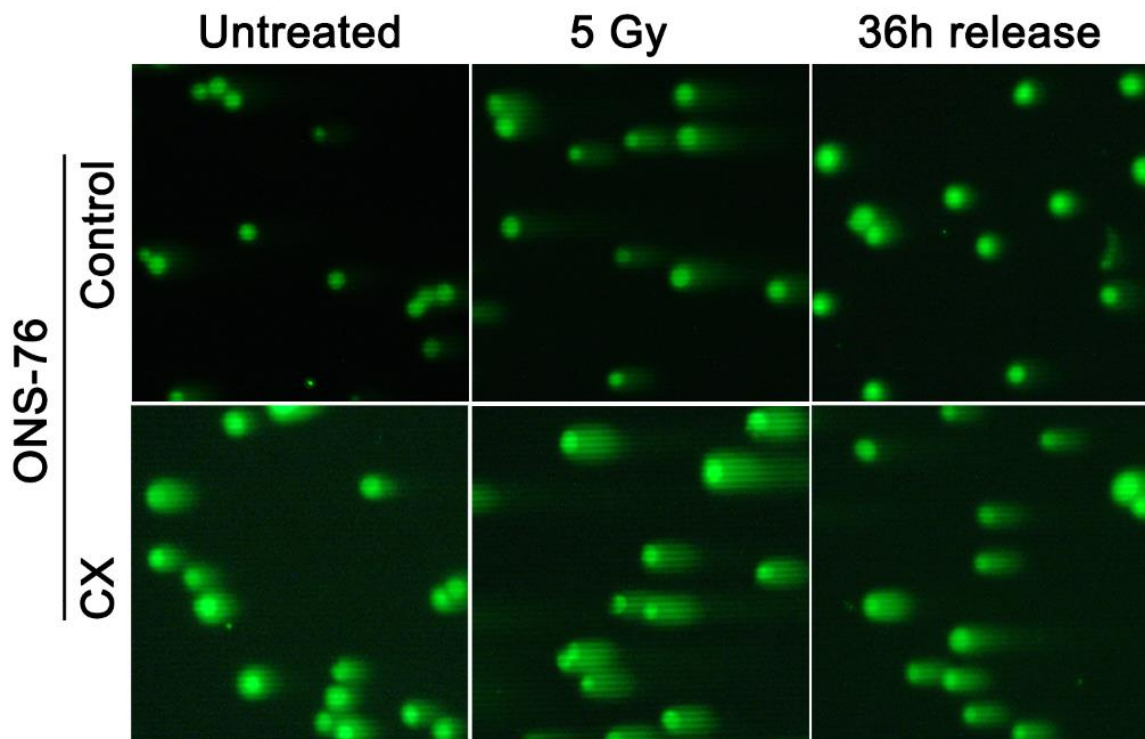


Figure 72. CX impaired DNA damage repair after irradiation.

To examine the effect of CX on the DNA repair activity, cells were irradiated with and without CX pretreatment. Neutral comet assay was used to detect DNA damage. 36-hour release was given to allow for DNA repair. We quantified the result with tail moment and presented in next figure.

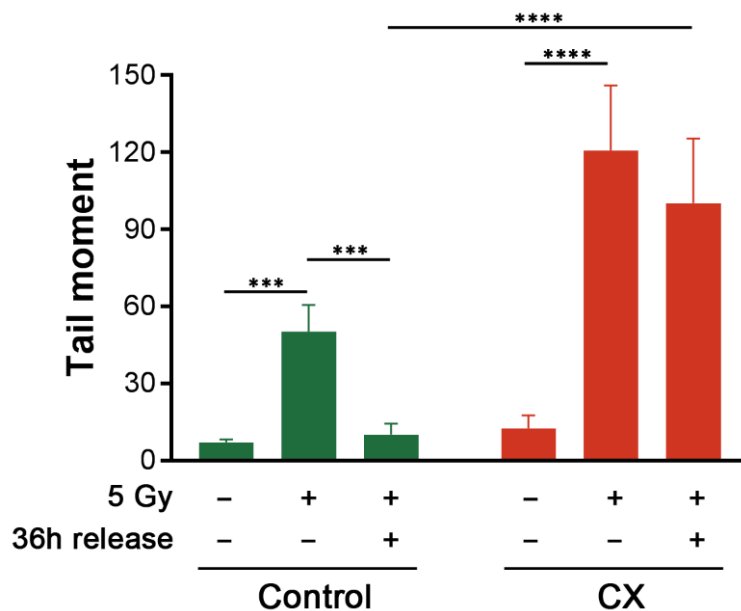


Figure 73. CX-treated cells fail to repair irradiation induced damages after 36-hour release.

Average Tail moment of 50 cells was examined in each treatment group and mean \pm SEM was shown in the bar graph. We found that 5 Gy induced DNA damages as evident by significant rise of tail moment in both groups. However, CX-treated cells were unable to repair the damages after 36-hour release, indicating the inhibitory effect of CX on DNA repair activity. Three biological replicates were analyzed. One-way ANOVA with Tukey's HSD test, *** $p < 0.001$, **** $p < 0.0001$.

Curaxin/CBL0137 treatment sensitizes MB cell lines to cisplatin and irradiation in vitro

Since our studies and others show that FACT is involved in SSBs or crosslinks damages repair in cells, we examined whether targeting FACT with CBL0137 enhanced the efficacy of radiation and cisplatin in MB cells in vitro. To eliminate the possibility that CBL0137 show cytotoxic effect per se by inducing DNA damages, cells were treated with different doses of CBL0137 alone. We found 4 μM CBL0137 alone had a minimal effect (20% cell death) on cell viability and colony formation (**Fig. 74 & 75**). However, combination of 4 μM CBL0137 with 5 Gy radiation significantly enhanced the sensitivity of HD-MB03 and ONS-76 cells to radiation and cisplatin (**Fig. 76 & 77**), suggesting that targeting FACT complex with curaxins could be a promising strategy to sensitizes these MB cells in vivo. The IC₅₀ of cisplatin on HD-MB03 cells dropped from 3.8 μM to 0.47 μM , and the IC₅₀ of cisplatin on ONS76 cells dropped from 1.2 μM to 0.67 μM , demonstrating a synergistic effect. In addition, we performed colony formation to examine the effect of CBL0137 (**Figure 78 & 79**). CBL0137 increased the sensitivity of cisplatin (noticeable at lowest dose of 0.5 μM) and irradiation (noticeable at lowest dose of 2 Gy). Together these data suggest that CX causes impaired DNA repair, exhibiting synergistic effect with cisplatin and sensitizes irradiation.

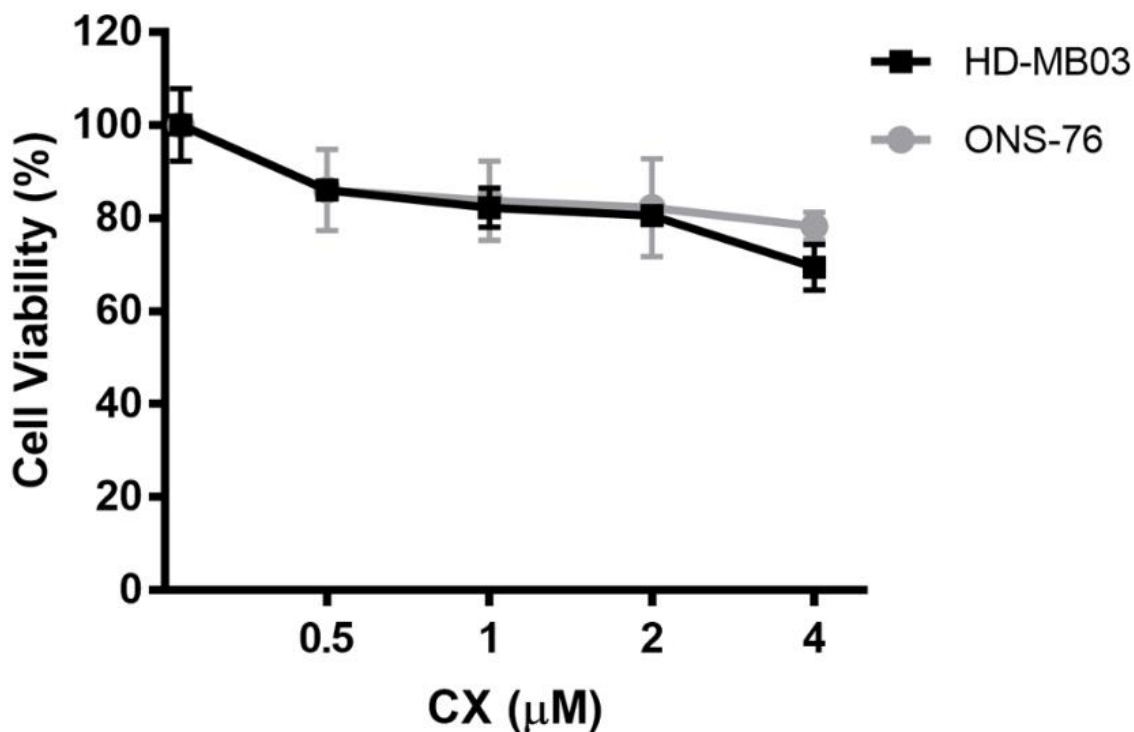


Figure 74. CX alone has minimal effect on cell viability.

To eliminate the possibility that CX affects cell viability per se, HD-MB03 and ONS-76 cells were treated with CX alone at indicated doses and MTT assay was performed to investigate the cytotoxicity of CX. We found that CX treatment had minimal effect on cell viability, suggesting its minimal toxicity when administered alone to cells. Three biological replicates were analyzed. Results are shown as the mean \pm SEM.

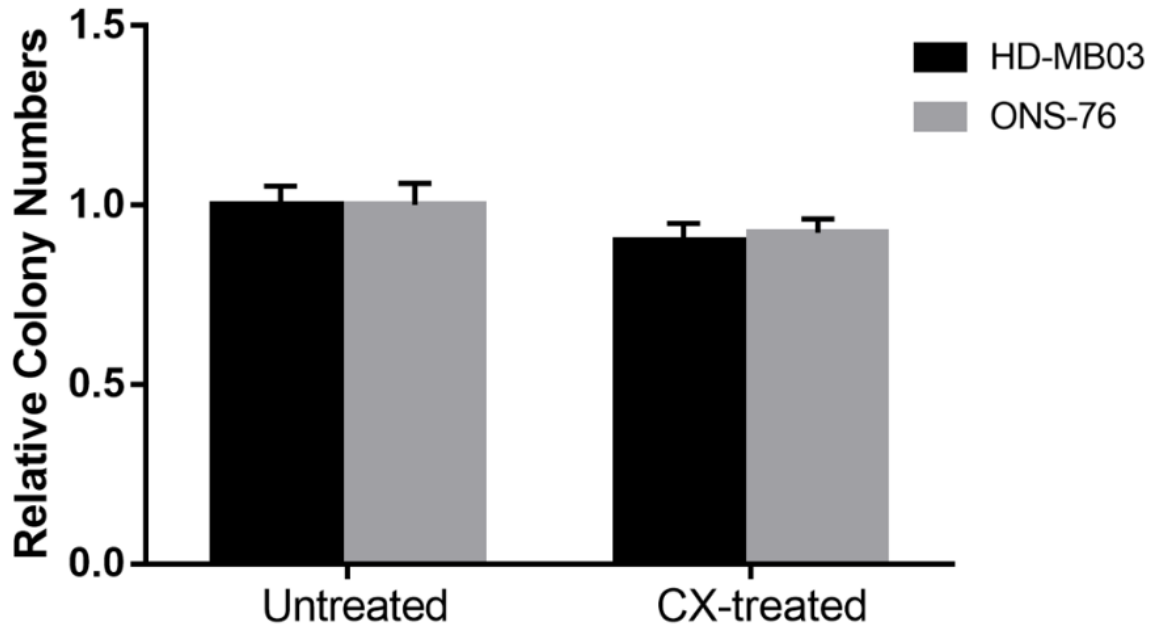


Figure 75. CX alone has minimal inhibitory effect on colony formation assay.

To provide further evidence of the minimal anti-proliferative effect of CX, HD-MB03 and ONS-76 cells were treated with CX alone and colony formation assay was performed. As demonstrated by the bar graph, we did not find significant effect of CX on colony formation assay. Three biological replicates were analyzed. Results are shown as the mean \pm SEM.

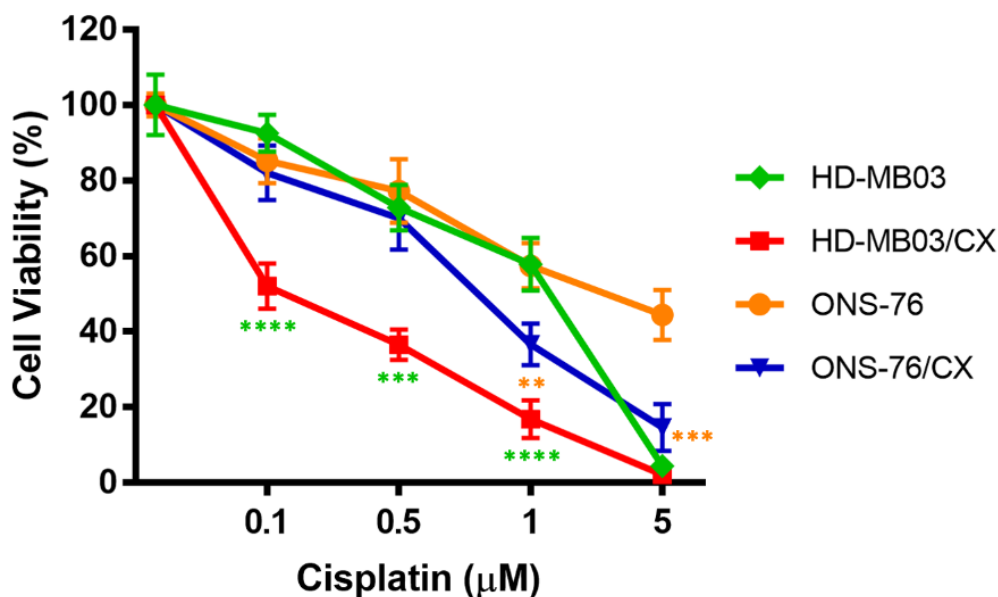


Figure 76. CX sensitizes HD-MB03 and ONS-76 cells to cisplatin.

To investigate whether CX could be used as a chemosensitizing agent for MB therapy, we pretreat cells with CX and then exposed cells to indicated doses of cisplatin. MTT assay was used to examine the cell viability. Two cell lines including HD-MB03 and ONS-76 were used. We found that CX improved the treatment efficacy of cisplatin at a dose as low as 0.1 µM for HD-MB03 cells, and 1 µM for ONS-76 cells. We also found synergistic effect when combining cisplatin and CX, suggesting that the combination treatment may be a promising strategy to achieve similar treatment outcome with lower drug dose. Green asterisks mark the comparison between HD-MB03 control and CX-treated cells, and orange asterisks mark the comparison between ONS-76 control and CX treated cells. Six technical repeats were performed per sample and three biological replicates were analyzed. Results are shown as the mean \pm SEM. One-way ANOVA with Dunnett's post-hoc test, ** $p < 0.01$, *** $p < 0.001$, **** $p < 0.0001$.

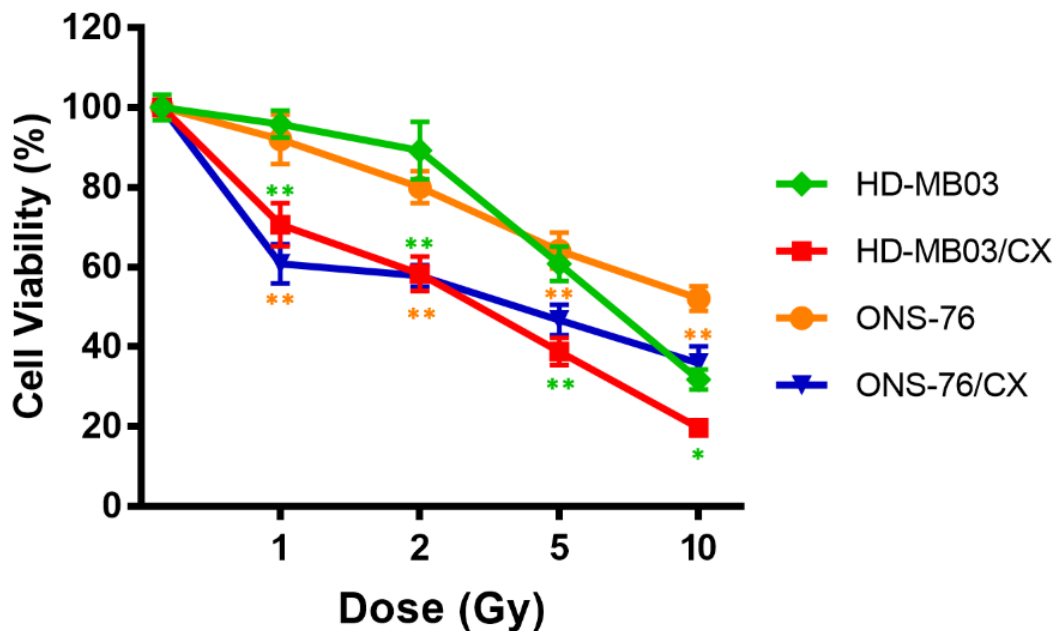


Figure 77. CX significantly decreases cell viability in radiation treatment.

To test if CX could be used to sensitize MB cells to radiation, MTT assay was used to examine the effect of CX combined with various doses of irradiation. Two cell lines including HD-MB03 and ONS-76 were used. We found that combination of CX with radiation demonstrated improved inhibitory effect on cell viability in both cell lines at dose as low as 1 Gy. Green asterisks mark the comparison between HD-MB03 control and CX-treated cells, and orange asterisks mark the comparison between ONS-76 control and CX treated cells. Six technical repeats were performed per sample and three biological replicates were analyzed. Results are shown as the mean \pm SEM. One-way ANOVA with Dunnett's post-hoc test, * $p < 0.05$, ** $p < 0.01$.

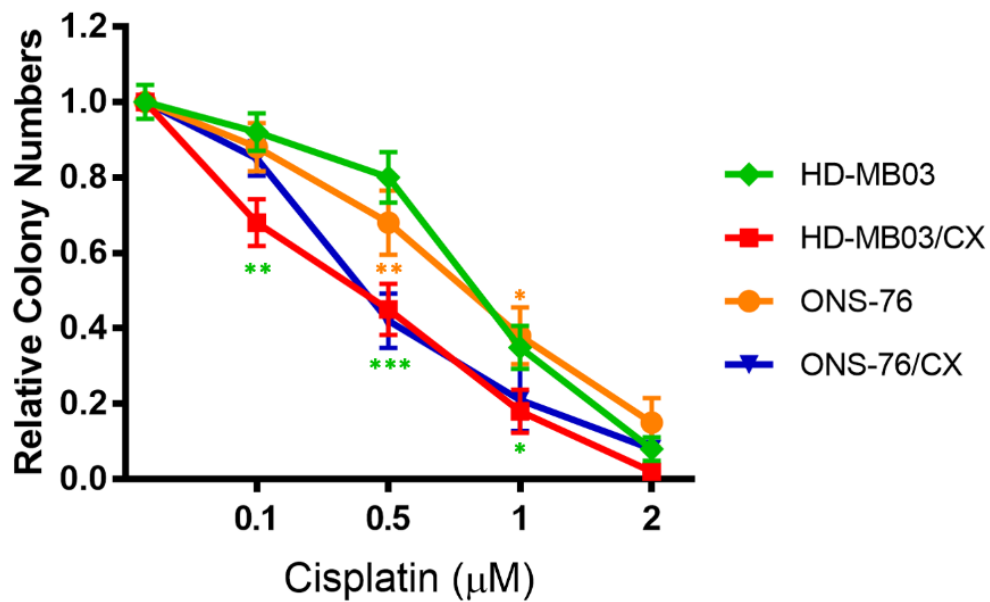
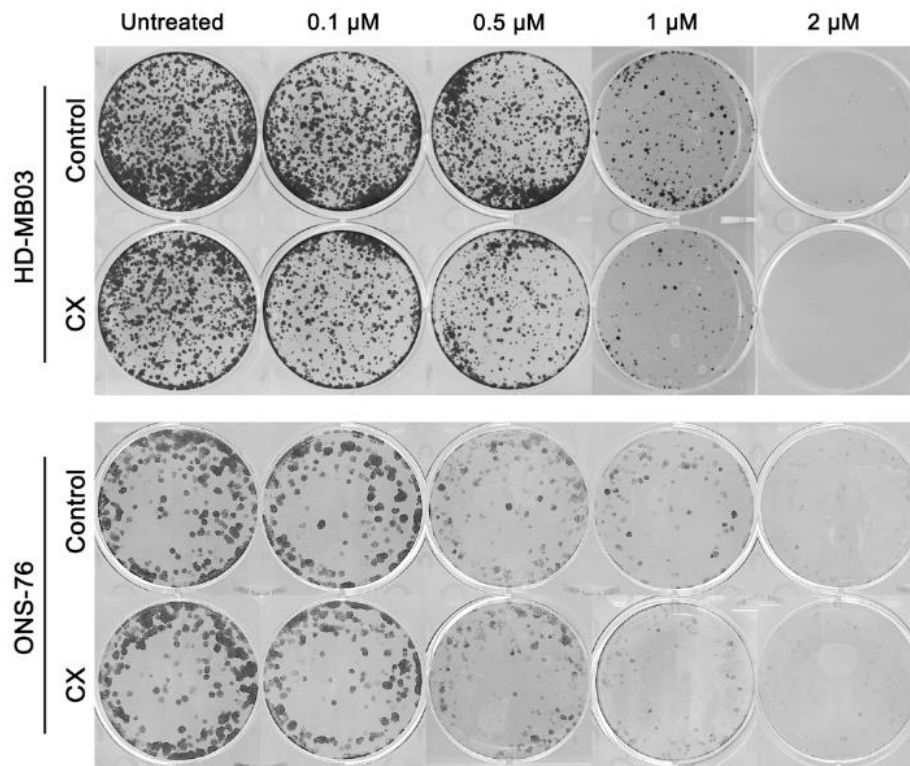
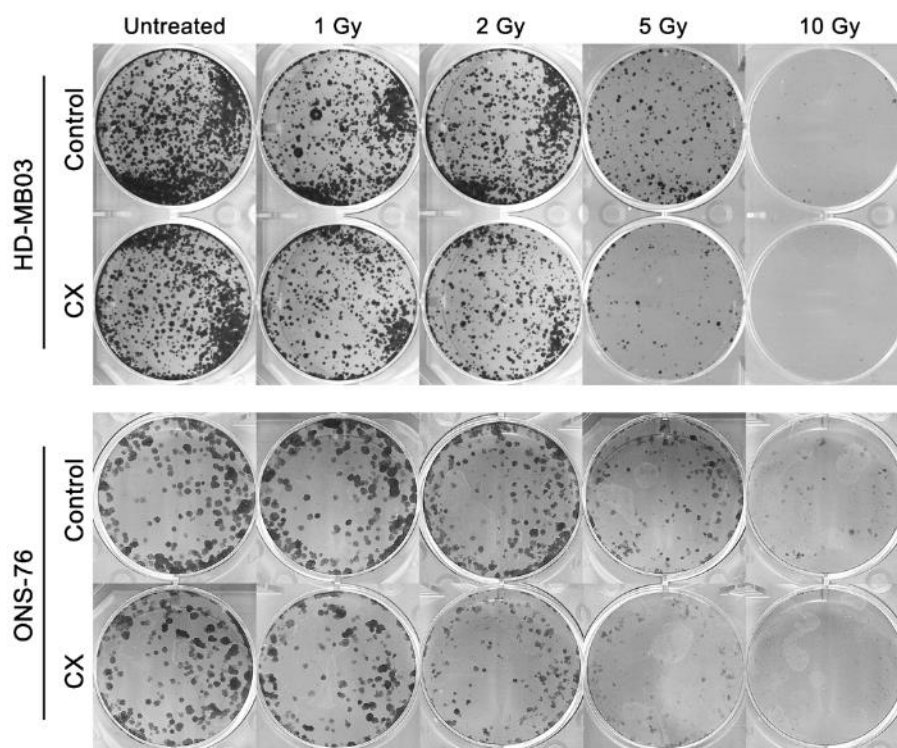


Figure 78. Combination therapy with cisplatin plus CX results in significant inhibition on colony formation in MB cells.

To examine whether addition of CX provides anti-proliferation effect of MB cells, cells were treated with CX and various doses of cisplatin. The effect of treatment was examined using

colony formation. Representative images of colonies were shown. Quantification of colony numbers in each group were plotted. Three technical repeats were performed per sample and three biological replicates were analyzed. Results are shown as the mean \pm SEM. We found that the CX sensitized HD-MB03 cells to cisplatin as evident by significantly less colony number at a dose as low as 0.1 μ M. The effect could also be observed in ONS-76 cells, however, only evident in doses of 0.5 and 1 μ M cisplatin, indicating a relatively narrow therapeutic window to gain benefit by adding CX. An alternative interpretation of this result is that similar inhibitory effect could be achieved by combining CX and 5-FU at a lower dose. This is of importance in order to lower the toxicity of cisplatin. Green asterisks mark the comparison between HD-MB03 control and CX-treated cells, and orange asterisks mark the comparison between ONS-76 control and CX treated cells. One-way ANOVA with Dunnett's post-hoc test, * $p < 0.05$, ** $p < 0.01$, *** $p < 0.001$.



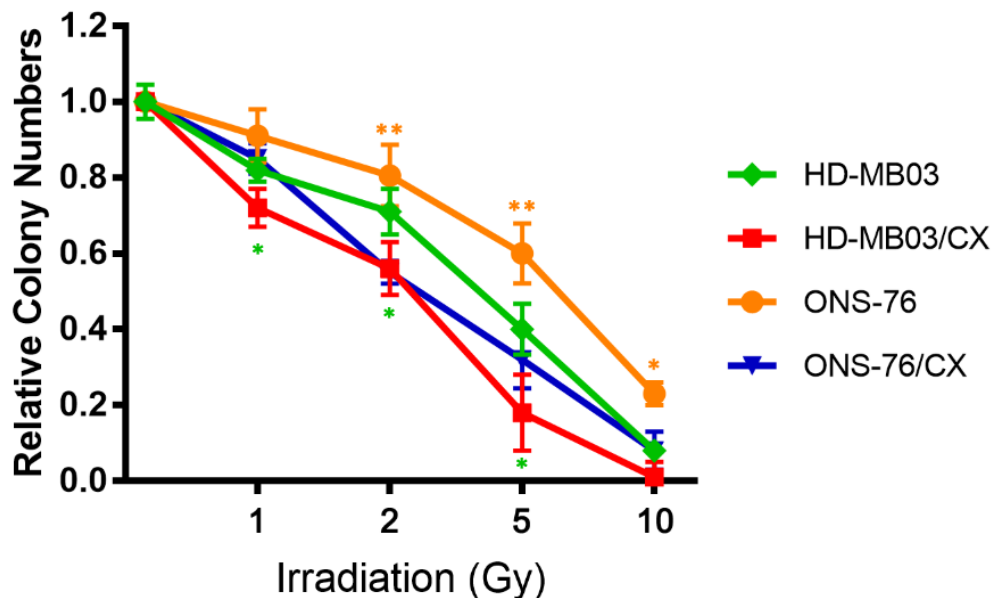


Figure 79. Combination therapy with radiation plus CX results in significant inhibition on colony formation in MB cells.

To examine whether addition of CX provides superior effect on anti-proliferation of MB cells upon irradiation, cells were treated with CX and various doses of irradiation. The effect of treatment was examined using colony formation. Representative images of colonies were shown. Quantification of colony numbers in each group were plotted. Six technical repeats were performed per sample and three biological replicates were analyzed. Results are shown as the mean \pm SEM. We found that CX sensitized MB cells to radiation treatment, as demonstrated by significant inhibition of colony formation at a dose as low as 1 Gy and 2 Gy in HD-MB03 and ONS-76 cells, respectively. Green asterisks mark the comparison between HD-MB03 control and CX-treated cells, and orange asterisks mark the comparison between ONS-76 control and CX treated cells. One-way ANOVA with Dunnett's post-hoc test, * $p < 0.05$, ** $p < 0.01$.

Combination of CX and cisplatin inhibits xenograft MB tumor growth in vivo

To examine whether inhibition of FACT with curaxins sensitizes MB cells to cisplatin and inhibits tumor growth in vivo, we utilized tumor xenograft models. We established xenograft models by subcutaneous inoculation of HD-MB03 cells with Matrigel. At two weeks after inoculation, tumors became visible and palpable. Mice were then randomly divided into 4 groups. The effects of CBL0137 and cisplatin were tested alone and in combination. Tumor growth curve showed that single agent treatment with CBL0137 alone had very little or moderate effect on tumor growth compared to vehicle group (**Fig. 80**), while combination of cisplatin and CBL0137 significantly inhibited tumor growth, demonstrating a synergistic effect. The combination of cisplatin with CBL0137 was well tolerated at the scheduled doses and there was no significant weight loss observed (**Fig. 81**). There was no major histological abnormality identified in vital organs including lung, liver and kidney (**Fig. 82**). Further analysis showed that combination group suppressed the proliferation and increased apoptosis, evident by decreased Ki-67 staining and increased TUNEL staining significantly in combination group (**Fig. 83 & 84**). This was further confirmed by IHC staining of caspase-3 and its cleavage target, PARP-1 (**Fig. 85**). In consistent with in vitro result, CX treatment decreased the staining intensity of SSRP1 and AcAPE1 in these tumor sections (**Fig. 86**). Together these data suggest that CX augments cisplatin treatment in vivo, and the combination decreases cellular proliferation and causes apoptosis.

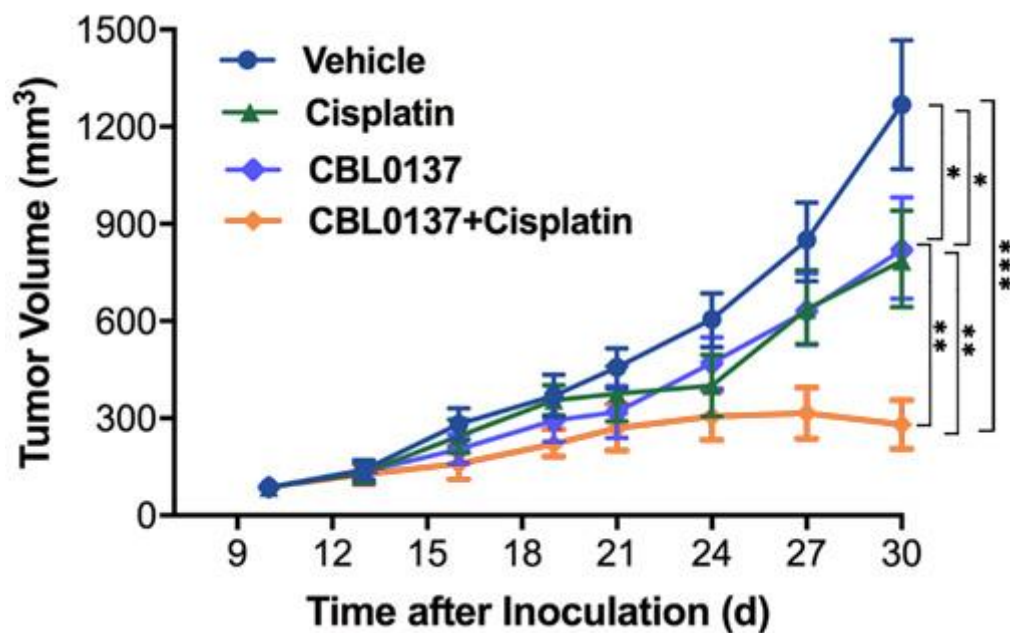


Figure 80. Combination of cisplatin plus CX inhibits HD-MB03 xenograft growth with synergistic effect.

To test whether combination therapy affect MB growth in vivo, we used xenograft model by implanting HD-MB03 cells (1×10^6 in $100 \mu\text{l}$ medium) subcutaneously over the left and right flanks in athymic nude mice ($n=5$). When tumor volume reached 100 mm^3 , mice were

randomly divided into four groups. Vehicle (100 μ L PBS), cisplatin, CBL0137 and combination of cisplatin and CBL0137 were administered to mice intraperitoneally every other day for 3 weeks. (Top) Resected xenograft tumor after completion of treatment were shown. (Bottom) Tumor volume was measured at indicated days and tumor growth curve was plotted. We calculated the average of two xenograft tumors in each mouse, and then calculated the SEM of each treatment group. Caution should be taken as $n=5$ which would make it difficult to detect difference among groups and may lead to statistical error. Future studies should use larger number of mice in each group to verify the findings we reported here. We found that monotherapy with cisplatin or CX caused mild inhibitory effect on tumor growth, while combination therapy demonstrated markedly inhibition on xenograft volume with synergistic effect. This indicates that the combination treatment may serve as a new treatment strategy to sensitize MB to cisplatin. Kruskal-Wallis test with Games-Howell post-hoc test, * $p<0.05$, ** $p<0.01$, *** $p<0.001$.

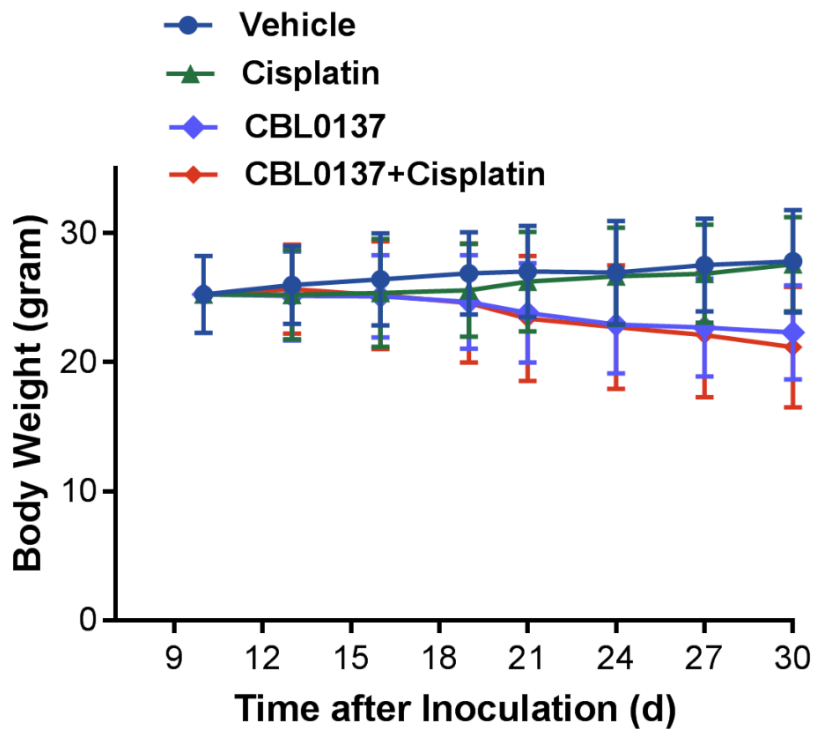


Figure 81. No significant weight change of mice was observed throughout treatment period.

Weight loss or cachectic appearance is an indicator of treatment toxicity. We measured the weight of each mouse each time before the treatment and until the completion of the treatment. There was no significant change in weight in each group (n=5), suggesting well tolerance of the treatment regimen. Results are shown as the mean \pm SEM.

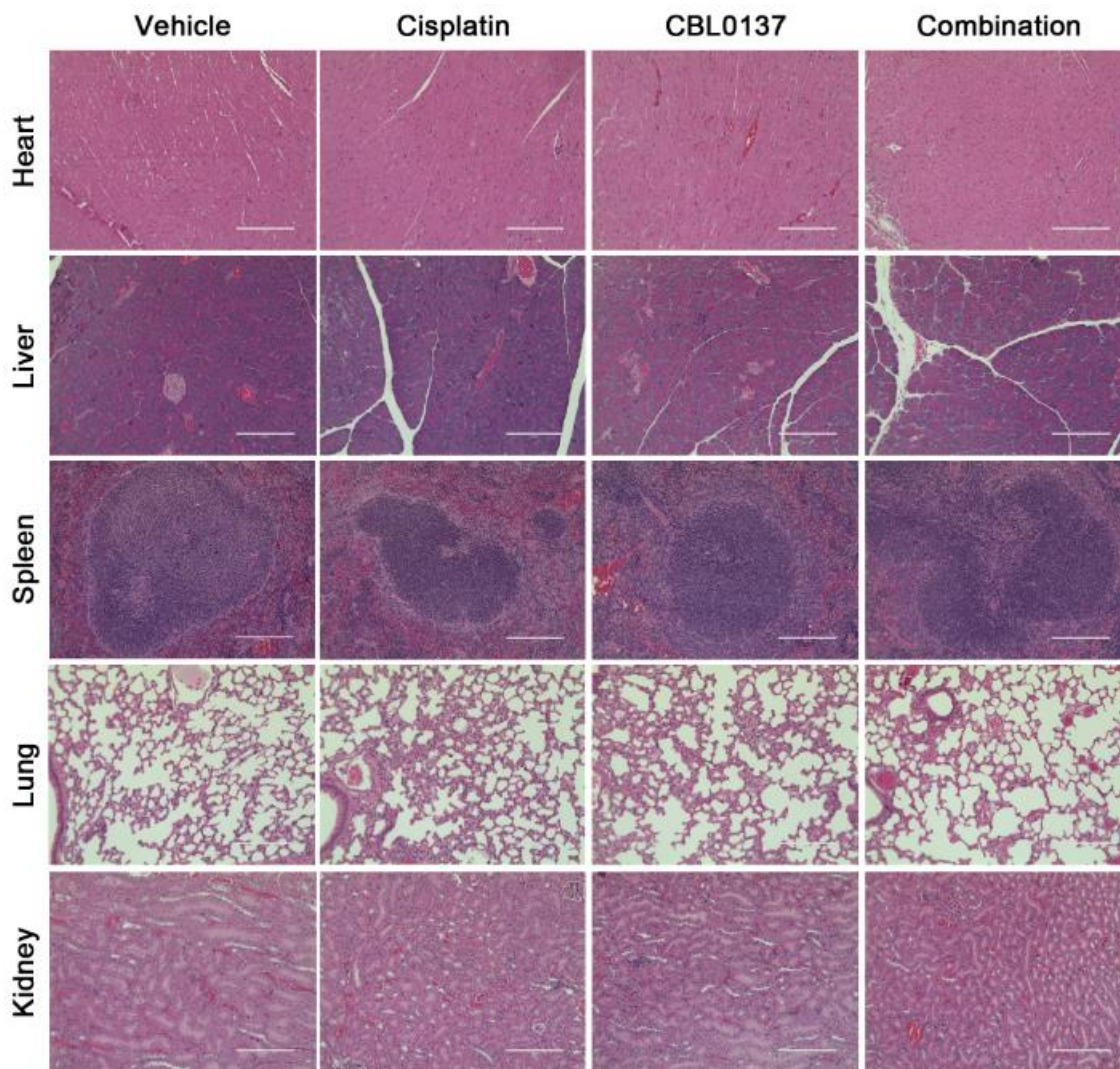


Figure 82. H & E staining demonstrates no major toxicity in major organs after treatment.

To provide further evidence that the treatment is well tolerated, we performed histology examination of major organs including heart, liver, spleen, lung and kidney in mice of all treatment group. There is no histological change among treatment groups in major organs. Organs from three independent mice from each group were analyzed. Representative images were shown.

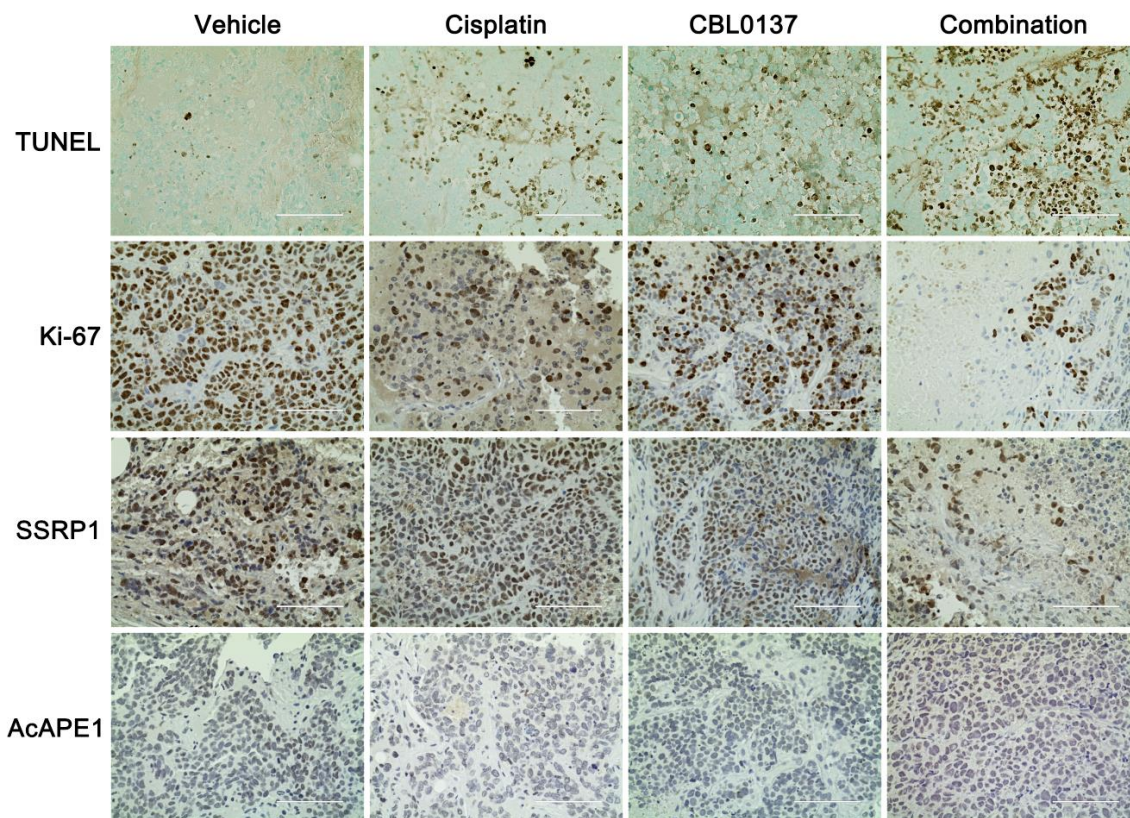


Figure 83. IHC staining of xenograft tumor demonstrates anti-proliferative and pro-apoptotic effect of combination therapy.

To understand the underlying mechanism of the inhibitory effect on tumor growth from combination therapy, we used various markers and performed IHC on xenograft tumor sections. Representative images in each group were shown. Quantification of each markers were presented in the following figures.

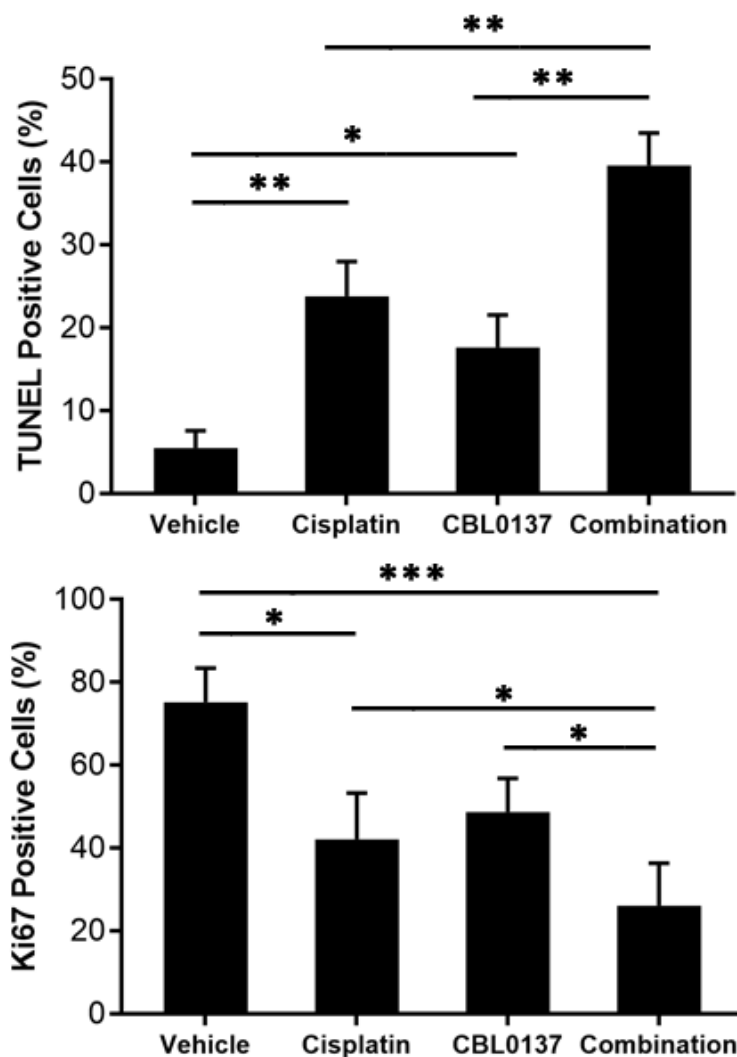


Figure 84. Combination therapy exhibits anti-proliferative and pro-apoptotic effects on MB xenograft tumors.

Bar graph depicting the percentage of positive staining cells for TUNEL (Top) and Ki-67 (Bottom). In each group, xenograft section from three independent mice were chosen and images from 10 random high power fields in were used for quantification. We found that combination therapy exhibits anti-proliferative and pro-apoptotic effects on MB xenograft tumors. The effects were significant when compared with monotherapy either by cisplatin or CBL0137 alone. One-way ANOVA with Tukey's HSD test, * $p < 0.05$, ** $p < 0.01$, *** $p < 0.001$.

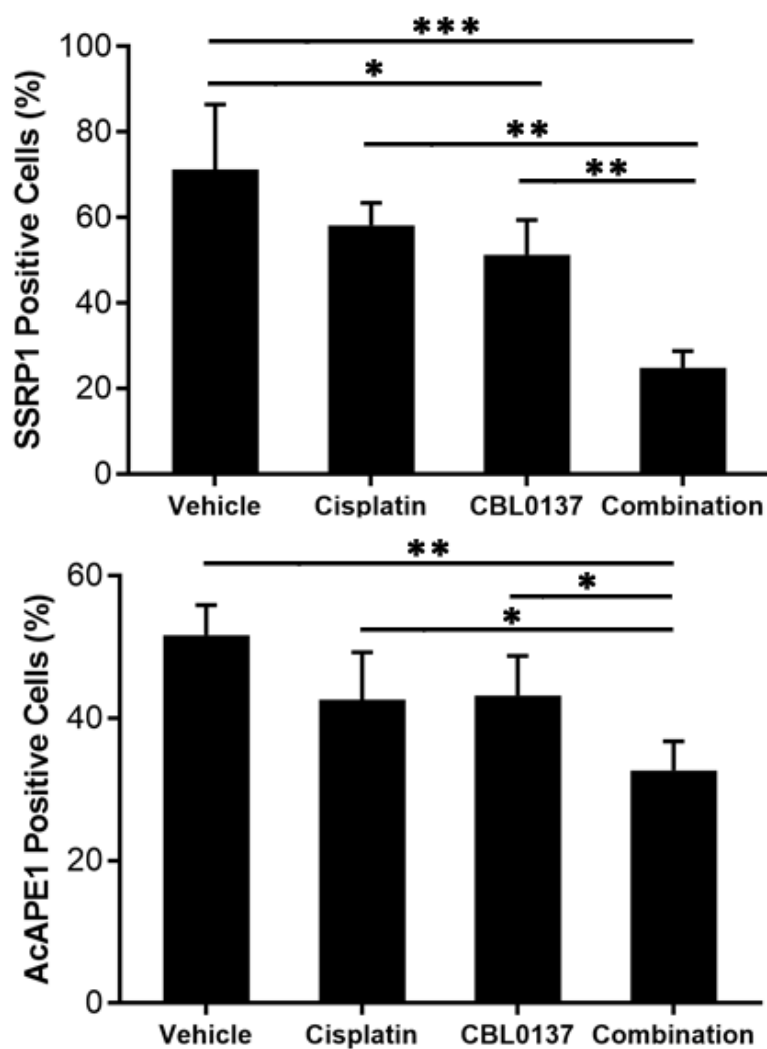


Figure 85. Combination therapy decreases the expression of AcAPE1 and SSRP1 in MB xenograft tumors.

We have shown that levels of AcAPE1 and SSRP1 were elevated in MB cell line. Here, we sought to determine the effect of combination therapy on the expression of both proteins. In each group, xenograft section from three independent mice were chosen and images from 10 random high power fields in were used for quantification. Bar graph depicting the mean \pm SEM of positive staining cells for SSRP1 (Top) and AcAPE1 (Bottom). We found that CBL0137 alone resulted in decreased level of SSRP1. Combining cisplatin

and CBL0137 lead to significantly reduction of SSRP1 when compared to CBL0137 or control group. In regard to AcAPE1, cisplatin treatment decreased the expression of AcAPE1, and combination treatment further caused suppression of AcAPE1 level. Together these data suggest that combination therapy results in significant reduction of AcAPE1 and SSRP1 level, which is superior to monotherapy. One-way ANOVA with Tukey's HSD test, * $p < 0.05$, ** $p < 0.01$, *** $p < 0.001$.

Discussion

Radiation and platinum-based chemotherapy is effective against a variety of pediatric cancer including MB. Unfortunately, the use of high dose cisplatin and radiation leads to neurotoxicity and progressive or permanent hearing loss which can affect the quality of life of childhood cancer survivor, highlighting the need for novel therapeutic targets to increase efficacy of chemoradiation therapy. In this study, we have identified FACT complex as a novel target to sensitize MB cells to cisplatin and radiation both in vitro and in vivo. Furthermore, we show that FACT complex functionally interacts with APE1 and promotes radiation and cisplatin resistance. FACT facilitates the recruitment and acetylation of APE1 at damage sites and promoting radiation and chemo-induced DNA damages repair. FACT inhibitor CBL0137/curaxin effectively inhibits DNA damage repair. We have provided multiple lines of evidence to demonstrate that targeting FACT complex with curaxins significantly improves the efficacy of chemotherapy and radiation in vitro and in vivo preclinical mouse model. Our study demonstrates that targeting FACT with curaxins is a promising strategy to sensitize MB cells to radiation and cisplatin and could be used as an adjuvant therapy to lower the side effects in MB patients.

Our data show that MB patients' tissues have elevated levels of both FACT and APE1 levels and FACT physically and functionally interact with APE1 in MB cells. Overexpression of APE1 in MB and its association with radiation and chemotherapy resistance as well as poor prognosis are well documented. APE1 primarily repairs AP sites or SSB, common intermediates in the BER pathway that are generated after radiation and many chemotherapeutic drugs, including cisplatin (2). The repair of AP sites or SSBs by APE1 on naked DNA or nucleosomal DNA substrate has been extensively investigated in vitro (115). However, DNA in the eukaryotic cell is packaged into nucleosome in chromatin. Thus, cells must repair DNA lesions including AP sites within the context of nucleosome

chromatin. Nucleosome, composed of a 147-bp segment of DNA helix wrapped around a histone protein octamer, serves as the basic unit of chromatin. However, to date, how APE1 repairs AP sites in the context of the nucleosome in chromatin remains largely unknown. Here, we show that APE1 interacts with nucleosome remodeling histone chaperone FACT complex. We found that FACT is required for recruitment and binding of APE1 to damage sites in chromatin. Histone chaperone is a group of proteins that bind histones and regulate nucleosome assembly and disruption. FACT complex as a histone chaperone possess versatile functions in vivo (154). FACT complex interacts with RNA polymerases (155,156) and facilitates transcription by disrupting nucleosomes in their path and by aiding in the redeposition of histones post-transcription (60,157). Moreover, increasing evidence suggests that FACT is involved in multiple DNA damage repair pathways. It has been shown that H2A and H2B are evicted and replaced at an accelerated pace at sites of UV-induced DNA damage by SPT16 subunit, and FACT is present in active transcription-coupled NER (TC-NER) repair complexes (64). SPT16 interacts with UV-Stimulated Scaffold Protein A (UVSSA) which is mediated by the DUF2043 domain and stimulates TC-NER-mediated repair (158). Additionally, FACT has been shown to act in concert with RSC to facilitate excision of DNA lesions during the initial step of BER (159). This is consistent with the various function of FACT complex, given its ability to modulate nucleosome. Notably, we show that downregulation of FACT complex inhibits DNA damage repair and sensitizes tumor cells to many chemotherapeutic agents. Thus our study provides the first evidence of involvement of histone chaperone complex in regulating damage repair in chromatin in cells and identifies FACT complex as a novel target for sensitization of tumor cells to chemotherapeutic drugs. As APE1 and FACT complex are both upregulated in MB, it is possible that both proteins are implicated in the treatment response and prognosis. Indeed, as shown in our results, APE1 and FACT overexpression is associated with poor survival. While APE1 can be targeted, FACT

complex is a more appealing target for the following reasons. First, FACT complex is involved in multiple DNA repair pathways, and share a common role in nucleosome modulation. Second, reports have shown that FACT complex is undetectable in normal cells of adult mammalian tissues, except for undifferentiated and stem-like cells. It is upregulated during in vitro transformation and promotes survival and growth of established tumor cells (97). Such differential expression among normal and tumor tissues is advantageous in lowering side effects when it comes to treatment. Third, there is no available molecule that target APE1 DNA repair function with high efficacy in vivo (160), but there is readily available anticancer small molecule curaxin which effectively inhibits FACT functions in cells and is under clinical trial for other solid tumors.

Curaxins is a group of small molecules that were identified in a phenotype-based screening for the ability to simultaneously activate p53 and inhibit NF- κ B without causing detectable genotoxicity (66). Curaxins have caught increasing attentions since the initiation of clinical trial. The first clinical phase I trial was launched in July 2013 to determine the maximally tolerated dose and recommended phase II dose of CBL0137 when administered intravenously (IV) to patients with metastatic or unresectable advanced solid malignancies (NCT01905228). Since then, two clinical trials with broader application were started for those with hematological malignancies, metastatic extremity melanoma or sarcoma (NCT02931110 and NCT03727789). In search for its mechanism of action, it was discovered that curaxins bind DNA without causing detectable DNA damages (67) and binding of curaxins leads to uncoiling or unfolding of nucleosome. Nucleosome disassembly caused by curaxins opens multiple FACT-binding sites, which are normally hidden inside the nucleosome and trap FACT in chromatin. Our data show CX inhibits FACT complex and causes impaired DNA repair, exhibiting synergistic effect with cisplatin and sensitizes irradiation. Importantly CX augments cisplatin treatment in

vivo, and the combination decreases cellular proliferation and causes apoptosis. FACT inhibitor CBL0137 has been shown to synergize with cisplatin in small cell lung cancer by increasing Notch signaling and targeting tumor initiating cells (126). Dermawan et al. reports that FACT expression was elevated in glioblastoma multiforme (GBM) tumors compared with non-neoplastic brain tissues, portended a worse prognosis, and positively correlated with glioblastoma stem cells markers and stem cell gene expression signatures. Lapatinib and CBL0137 synergistically inhibited the proliferation of patient-derived GBM cells and prolongs the survival of mice bearing orthotopic GBM (103). In addition, CBL0137 monotherapy was tested against the Pediatric Preclinical Testing Program (PPTP) in vitro cell line panel and against the PPTP in vivo solid tumor xenograft and acute lymphocytic leukemia (ALL) panels (161). Nonetheless, here we add to the current knowledge by providing compelling evidence that curaxins exhibit strong synergy with cisplatin and radiation in killing MB cells by inhibiting DNA damage repair.

In conclusion, here we report for the first time that APE1 and FACT complex overexpression in MB is associated with poor prognosis. FACT complex interacts with APE1 and facilitates the access of APE1 to damage sites which in turn promotes DNA damage repair. Targeting FACT complex with small molecules CBL0137/curaxin significantly improves the efficacy of cisplatin and radiation in vitro and in vivo in a preclinical model. The readily available FACT inhibitor, CBL0137, represents a highly translatable and targeted therapeutic approach that can be used clinically as an adjuvant therapy to sensitize MB patients to lower the side effects of current standard therapy in MB while achieving the similar or potentially superior treatment efficacy.

DISCUSSION

In the current study we provided biochemical evidence that FACT complex plays an important role in BER pathway. FACT complex interacts with APE1 and facilitates its access to chromatin and subsequent acetylation. Enhancement of their physical interactions upon DNA damage highlights the requirement of their physical interaction in response to DNA damages. Furthermore, the significance of their functional interaction is evident from the facts that FACT knockdown by siRNA complex or blocking FACT function with Curaxins significantly impairs APE1 functionality in BER pathway and leads to delayed repair of DNA damages and sensitizes cells to DNA insulting agents or radiation.

While this is a comprehensive study that provides multiple lines of evidence to understand the functional interaction of FACT complex and APE1 and the efficacy of combination therapy in cancer treatment, there are several unanswered questions remain to be addressed.

As shown in Chapter 1, both subunits of FACT complex including SPT16 and SSRP1 are identified in the immunoprecipitation using antibody directing at AcAPE1. It is unknown where the interaction occurs. We immunoprecipitated FLAG-tagged WT-APE1 and nonacetylatable K5R mutant from nuclear fractions. No significant differences were observed in the amount of SPT16 bound with WT and non-acetylatable K5R APE1 IPs, indicating that acetylation of APE1 is not essential for its interaction with FACT complex. Therefore we propose that FACT complex interacts with APE1 before acetylation. Our experiments also demonstrate that knockdown of FACT complex will not affect the expression of APE1 but instead cause decrease in AcAPE1 level. It is possible that FACT complex interacts with APE1 and brings it to the chromatin. Alternatively, FACT complex creates transiently accessible nucleosome structure to allow APE1 access to damage sites. Additionally, while SPT16 and SSRP1 both interact with APE1, it remains unclear

what domain is responsible for such interaction. All eukaryotic forms of the SPT16 protein are composed of three distinct structurally defined domains in combination with a negatively charged intrinsically disordered C-terminal domain termed here as the N-terminal domain (NTD), the dimerization domain (DD), the middle domain (MD), and C-terminal domain (CTD). Previously, genetic analysis has provided evidence for a functional relationship between the yeast Spt16 NTD and the C-terminal “docking domain” extension of H2A, whereas concurrent mutations within both domains cause lethality in yeast. On the other hand, the human SSRP1 protein contains three well defined domains designated the NTD/DD, the MD, and the HMG-1 domain. HMG domains can readily bind to nucleosomal DNA and may help FACT recognize, bind, and effectively reorganize chromatin. The question of what domain in each subunit of FACT complex interacts with APE1 remains to be investigated. To determine which domain of FACT is involved in the interaction with APE1, we will design several Flag-tagged both N- and C-terminal deletion mutants of SPT16 and SSRP1. We will overexpress these mutants one at a time in cells and isolate the chromatin extract by cell fractionation. Afterwards, we will check the interaction of these FLAG mutants with APE1 and/or AcAPE1.

While we provide evidence that targeting FACT complex can significantly impair the BER function, it is possible that FACT knockdown has effects on other DNA repair pathways and on gene expressions. FACT complex belongs to histone chaperones which is a diverse family of histone-binding proteins that shield non-nucleosomal histone-DNA interactions. Histone chaperones are involved in multiple cellular processes, including gene transcription, DNA replication, and DNA repair. Therefore knockdown of FACT complex will affect all these processes that can have different effect on cellular proliferation and growth. As we mentioned earlier, FACT complex is also involved in NER. Study has showed that the SPT16 subunit of the histone chaperone FACT interacts with

UVSSA, which is mediated by the DUF2043 domain. SPT16 is recruited to transcription-blocking DNA lesions, independently of UVSSA, to stimulate UVSSA recruitment and TC-NER-mediated repair. It is also involved in homologous recombination repair. More recently, SSRP1 has been shown to be recruited to SSB in PARP-dependent manner and retained at DNA damage sites by N-terminal interactions with the DNA repair protein XRCC1. These reports along with our data have suggested that FACT complex is involved in more than one pathway, and it has multiple effects that are not clearly delineated.

We have shown that curaxins demonstrates minimal toxicity at the doses we administered while exhibiting synergistic effects with chemotherapeutic agents and radiation. Future study should be directed at systematic pharmacologic study to understand its pharmacokinetics and toxicity. Curaxins is first identified in a phenotype-based screening for the ability to simultaneously activate p53 and inhibit NF- κ B without causing detectable genotoxicity (66). In search for its mechanism of action, it was discovered that curaxins bind DNA via intercalation of the carbazole body accompanied by the protrusion of two side chains into the major groove and a third side chain into the minor groove of DNA, inducing tight binding of FACT to chromatin that results in functional inhibition (67). Later, Safina et al reports that binding of curaxins leads to uncoiling of nucleosomal DNA, accumulation of negative supercoiling and conversion of multiple regions of genomic DNA into left-handed Z-form. Nucleosome disassembly caused by curaxins opens multiple FACT-binding sites, which are normally hidden inside the nucleosome. The isolated C-terminal intrinsically disordered domain (CID) of SSRP1, but not HMG domain, binds these alternative DNA structures and triggers p53 response (68). While it is claimed to be FACT inhibitor, curaxins causes chromatin trapping effects instead of binding directly to either subunits. The effects of curaxins on multiple gene expression can be explained by its mechanism of action as it affects FACT complex which

is essentially involved in DNA transcription and repair process. We can obtain RNA-seq of curaxins-treated cells to understand the global aspect of the effects on gene expression.

In our in vivo study to test the efficacy of combination therapy, subcutaneous xenograft models were used. Tumor xenografts are easy to use and reproducible, but they carry potential limitations that genetics and histology of the tumors are frequently not representative of the respective human tumor. Therefore, these models have not been as predictive of therapeutic success as one would like. By contrast, genetically engineered mouse model (GEMs) are histologically and genetically accurate models of human cancer as these mice develop de novo tumors in a natural immune-proficient microenvironment (162,163). GEMs are superior in mimicking the histopathological and molecular features of their human counterparts, displaying genetic heterogeneity, and are able to spontaneously progress toward metastatic disease. These have been used to validate candidate cancer genes and drug targets, assess therapy efficacy, and evaluate mechanisms of drug resistance at pre-clinical studies (163).

Msh2 gene was found to be one of the most commonly mutated MMR in CRC patients. Mutations in Msh2 cause Lynch syndromes I and II and sporadic colorectal cancers, which constitute about 15% of colon cancer. Previously three Msh2^{null} knockout mouse lines have been generated in the hope of developing mouse model for Lynch Syndrome. Homozygous mutant mice of all three Msh2^{null} knockouts, though MMR-deficient, develop lymphoma predominantly (164-166). Recently a novel conditional knockout mouse model for the tissue-specific inactivation of Msh2 (Msh2^{LoxP}) has been reported (167). In this model, MMR can be inactivated by Cre-LoxP-mediated inactivation of Msh2 in different tissues by the expression of various Cre-recombinase transgenes. The Msh2^{LoxP} allele can be combined with the Villin-Cre transgene (VCMsh2^{LoxP}) to specifically inactivate MMR in the intestinal mucosa. These mice develop exclusively

intestinal neoplasms. In future study, we can obtain conditional Msh2 knockout ($Msh2^{loxp}$) and Villin-Cre transgenic mice from Jackson lab (Stock No. # 016231 and # 021504). $Msh2^{loxp/+}$ will be crossed with Villin-Cre transgenic mice to generate $VCMsh2^{loxp/+}$. Heterozygotes will be intercrossed to generate $VCMsh2^{loxp/loxp}$. Msh2 inactivation from intestine will be confirmed by RT-qPCR analysis. $VCMsh2^{loxp/loxp}$ mice generally form intestine tumor after 7 months (167). Colonic tumor growth in these mice will be monitored on a longitudinal basis using Carl Stroz small animal endoscope in collaboration with Dr. Amar Singh. Once we have ascertained tumor growth in these mice, mice will be divided into three groups, each with 8 mice (4 male, 4 female). The first groups will receive vehicles, the second will receive IP injection with 20 mg/kg 5-FU, and the third will receive a combination of CBL0137 30 mg/kg and 20 mg/kg 5-FU every other day for three weeks. Tumor growth will be monitored using the colonoscope, which will also help determine the appropriate timing for sacrificing these mice. Post-sacrifice, mice will be examined for the tumor multiplicity and tumor volume. We will quantitate colonic apoptosis using TUNEL assay and proliferating cells with Ki67 staining in these tissue sections.

Similarly, we can obtain GEMs or orthotopic tumor model of medulloblastoma and tested the efficacy of CBL0137. Another problem we may encounter is the ability to cross blood brain barrier (BBB). This is a practical question as any medication that targets medulloblastoma needs to cross BBB in order to reach target. This also reflects the importance of using GEMs instead of subcutaneous xenograft model in future study to validate the efficacy of curaxins. Barone et al. implanted the glioblastoma cells orthotopically in nude mice and administered CBL0137 in various dosing regimens to assess brain and tumor accumulation of CBL0137 (168). Interestingly, CBL0137 penetrated the blood-brain barrier and accumulated in orthotopic tumors significantly more than normal brain tissue. It increased apoptosis and suppressed proliferation in both

U87MG and A1207 tumors. This may be explained by another study, where FACT complex was reported to be not expressed in normal cells of adult mammalian tissues, except for undifferentiated and stem-like cells (97). In addition, FACT was found to be upregulated during in vitro transformation and to be necessary, but not sufficient, for driving transformation. FACT also promoted survival and growth of established tumor cells. This model of curaxins specifically targeting FACT complex would be able to explain the finding of Barone's study where curaxins accumulate in tumor. However, curaxins do not bind to FACT complex as later studies have suggested that curaxins bind to DNA. Therefore the curaxins binding should not be affected by the expression level of FACT complex. Another possible explanation is the increased metabolism and blood supply of tumors. Once curaxins cross the BBB, the tumor cells are able to uptake the curaxins given the abundant blood supply. Nevertheless, the ability of curaxins to cross BBB and its efficacy in GEMs remains to be further validated.

BIBLIOGRAPHY

1. Meas R, Wyrick JJ, Smerdon MJ. Nucleosomes regulate base excision repair in chromatin. *Mutation Research/Reviews in Mutation Research* **2019**;780:29-36 doi <https://doi.org/10.1016/j.mrrev.2017.10.002>.
2. Li M, Wilson DM, 3rd. Human apurinic/aprimidinic endonuclease 1. *Antioxid Redox Signal* **2014**;20(4):678-707 doi 10.1089/ars.2013.5492.
3. Kelley MR, Kelley MR, Fishel ML. DNA repair in cancer therapy : molecular targets and clinical applications. London, United Kingdom : Academic Press is an imprint of Elsevier; 2016.
4. Wallace SS. Base excision repair: a critical player in many games. *DNA Repair (Amst)* **2014**;19:14-26 doi 10.1016/j.dnarep.2014.03.030.
5. Wilson DM, 3rd, Barsky D. The major human abasic endonuclease: formation, consequences and repair of abasic lesions in DNA. *Mutat Res* **2001**;485(4):283-307 doi 10.1016/s0921-8777(01)00063-5.
6. Xanthoudakis S, Smeyne RJ, Wallace JD, Curran T. The redox/DNA repair protein, Ref-1, is essential for early embryonic development in mice. *Proc Natl Acad Sci U S A* **1996**;93(17):8919-23 doi 10.1073/pnas.93.17.8919.
7. Meira LB, Devaraj S, Kisby GE, Burns DK, Daniel RL, Hammer RE, *et al*. Heterozygosity for the mouse Apex gene results in phenotypes associated with oxidative stress. *Cancer Res* **2001**;61(14):5552-7.
8. Loeb LA, Monnat RJ, Jr. DNA polymerases and human disease. *Nat Rev Genet* **2008**;9(8):594-604 doi 10.1038/nrg2345.
9. Winters TA, Henner WD, Russell PS, McCullough A, Jorgensen TJ. Removal of 3'-phosphoglycolate from DNA strand-break damage in an oligonucleotide

- substrate by recombinant human apurinic/aprimidinic endonuclease 1. *Nucleic Acids Res* **1994**;22(10):1866-73 doi 10.1093/nar/22.10.1866.
10. Beard WA, Prasad R, Wilson SH. Activities and mechanism of DNA polymerase beta. *Methods Enzymol* **2006**;408:91-107 doi 10.1016/s0076-6879(06)08007-4.
 11. Sobol RW, Horton JK, Kuhn R, Gu H, Singhal RK, Prasad R, *et al.* Requirement of mammalian DNA polymerase-beta in base-excision repair. *Nature* **1996**;379(6561):183-6 doi 10.1038/379183a0.
 12. Tomkinson AE, Vijayakumar S, Pascal JM, Ellenberger T. DNA ligases: structure, reaction mechanism, and function. *Chem Rev* **2006**;106(2):687-99 doi 10.1021/cr040498d.
 13. Demple B, Herman T, Chen DS. Cloning and expression of APE, the cDNA encoding the major human apurinic endonuclease: definition of a family of DNA repair enzymes. *Proc Natl Acad Sci U S A* **1991**;88(24):11450-4 doi 10.1073/pnas.88.24.11450.
 14. Robson CN, Hickson ID. Isolation of cDNA clones encoding a human apurinic/aprimidinic endonuclease that corrects DNA repair and mutagenesis defects in *E. coli* xth (exonuclease III) mutants. *Nucleic Acids Res* **1991**;19(20):5519-23 doi 10.1093/nar/19.20.5519.
 15. Seki S, Hatsushika M, Watanabe S, Akiyama K, Nagao K, Tsutsui K. cDNA cloning, sequencing, expression and possible domain structure of human APEX nuclease homologous to *Escherichia coli* exonuclease III. *Biochim Biophys Acta* **1992**;1131(3):287-99 doi 10.1016/0167-4781(92)90027-w.
 16. Xanthoudakis S, Curran T. Identification and characterization of Ref-1, a nuclear protein that facilitates AP-1 DNA-binding activity. *Embo j* **1992**;11(2):653-65.

17. Burkovics P, Szukacsov V, Unk I, Haracska L. Human Ape2 protein has a 3'-5' exonuclease activity that acts preferentially on mismatched base pairs. *Nucleic acids research* **2006**;34(9):2508-15 doi 10.1093/nar/gkl259.
18. Mol CD, Izumi T, Mitra S, Tainer JA. DNA-bound structures and mutants reveal abasic DNA binding by APE1 and DNA repair coordination [corrected]. *Nature* **2000**;403(6768):451-6 doi 10.1038/35000249.
19. Chen DS, Herman T, Demple B. Two distinct human DNA diesterases that hydrolyze 3'-blocking deoxyribose fragments from oxidized DNA. *Nucleic Acids Res* **1991**;19(21):5907-14 doi 10.1093/nar/19.21.5907.
20. Izumi T, Hazra TK, Boldogh I, Tomkinson AE, Park MS, Ikeda S, *et al.* Requirement for human AP endonuclease 1 for repair of 3'-blocking damage at DNA single-strand breaks induced by reactive oxygen species. *Carcinogenesis* **2000**;21(7):1329-34.
21. Seki S, Ikeda S, Watanabe S, Hatsushika M, Tsutsui K, Akiyama K, *et al.* A mouse DNA repair enzyme (APEX nuclease) having exonuclease and apurinic/aprimidinic endonuclease activities: purification and characterization. *Biochim Biophys Acta* **1991**;1079(1):57-64 doi 10.1016/0167-4838(91)90024-t.
22. Berquist BR, McNeill DR, Wilson DM, 3rd. Characterization of abasic endonuclease activity of human Ape1 on alternative substrates, as well as effects of ATP and sequence context on AP site incision. *J Mol Biol* **2008**;379(1):17-27 doi 10.1016/j.jmb.2008.03.053.
23. Vascotto C, Fantini D, Romanello M, Cesaratto L, Deganuto M, Leonardi A, *et al.* APE1/Ref-1 interacts with NPM1 within nucleoli and plays a role in the rRNA quality control process. *Mol Cell Biol* **2009**;29(7):1834-54 doi 10.1128/mcb.01337-08.

24. Ischenko AA, Saparbaev MK. Alternative nucleotide incision repair pathway for oxidative DNA damage. *Nature* **2002**;415(6868):183-7 doi 10.1038/415183a.
25. Gros L, Ishchenko AA, Ide H, Elder RH, Saparbaev MK. The major human AP endonuclease (Ape1) is involved in the nucleotide incision repair pathway. *Nucleic acids research* **2004**;32(1):73-81 doi 10.1093/nar/gkh165.
26. Kelley MR, Georgiadis MM, Fishel ML. APE1/Ref-1 role in redox signaling: translational applications of targeting the redox function of the DNA repair/redox protein APE1/Ref-1. *Curr Mol Pharmacol* **2012**;5(1):36-53.
27. Okazaki T, Chung U, Nishishita T, Ebisu S, Usuda S, Mishiro S, *et al.* A redox factor protein, ref1, is involved in negative gene regulation by extracellular calcium. *J Biol Chem* **1994**;269(45):27855-62.
28. Chung U, Igarashi T, Nishishita T, Iwanari H, Iwamatsu A, Suwa A, *et al.* The interaction between Ku antigen and REF1 protein mediates negative gene regulation by extracellular calcium. *J Biol Chem* **1996**;271(15):8593-8 doi 10.1074/jbc.271.15.8593.
29. Bhakat KK, Izumi T, Yang SH, Hazra TK, Mitra S. Role of acetylated human AP-endonuclease (APE1/Ref-1) in regulation of the parathyroid hormone gene. *Embo j* **2003**;22(23):6299-309 doi 10.1093/emboj/cdg595.
30. Busso CS, Lake MW, Izumi T. Posttranslational modification of mammalian AP endonuclease (APE1). *Cell Mol Life Sci* **2010**;67(21):3609-20 doi 10.1007/s00018-010-0487-3.
31. Yacoub A, Kelley MR, Deutsch WA. The DNA repair activity of human redox/repair protein APE/Ref-1 is inactivated by phosphorylation. *Cancer Res* **1997**;57(24):5457-9.

32. Fritz G, Kaina B. Phosphorylation of the DNA repair protein APE/REF-1 by CKII affects redox regulation of AP-1. *Oncogene* **1999**;18(4):1033-40 doi 10.1038/sj.onc.1202394.
33. McKenzie JA, Strauss PR. A quantitative method for measuring protein phosphorylation. *Anal Biochem* **2003**;313(1):9-16 doi 10.1016/s0003-2697(02)00464-5.
34. Qu J, Liu GH, Huang B, Chen C. Nitric oxide controls nuclear export of APE1/Ref-1 through S-nitrosation of cysteines 93 and 310. *Nucleic Acids Res* **2007**;35(8):2522-32 doi 10.1093/nar/gkl1163.
35. Chattopadhyay R, Das S, Maiti AK, Boldogh I, Xie J, Hazra TK, *et al.* Regulatory role of human AP-endonuclease (APE1/Ref-1) in YB-1-mediated activation of the multidrug resistance gene MDR1. *Mol Cell Biol* **2008**;28(23):7066-80 doi 10.1128/mcb.00244-08.
36. Yamamori T, DeRicco J, Naqvi A, Hoffman TA, Mattagajasingh I, Kasuno K, *et al.* SIRT1 deacetylates APE1 and regulates cellular base excision repair. *Nucleic Acids Res* **2010**;38(3):832-45 doi 10.1093/nar/gkp1039.
37. Fantini D, Vascotto C, Marasco D, D'Ambrosio C, Romanello M, Vitagliano L, *et al.* Critical lysine residues within the overlooked N-terminal domain of human APE1 regulate its biological functions. *Nucleic Acids Res* **2010**;38(22):8239-56 doi 10.1093/nar/gkq691.
38. Roychoudhury S, Nath S, Song H, Hegde ML, Bellot LJ, Mantha AK, *et al.* Human Apurinic/Apyrimidinic Endonuclease (APE1) Is Acetylated at DNA Damage Sites in Chromatin, and Acetylation Modulates Its DNA Repair Activity. *Mol Cell Biol* **2017**;37(6) doi 10.1128/mcb.00401-16.

39. Busso CS, Iwakuma T, Izumi T. Ubiquitination of mammalian AP endonuclease (APE1) regulated by the p53-MDM2 signaling pathway. *Oncogene* **2009**;28(13):1616-25 doi 10.1038/onc.2009.5.
40. Busso CS, Wedgeworth CM, Izumi T. Ubiquitination of human AP-endonuclease 1 (APE1) enhanced by T233E substitution and by CDK5. *Nucleic acids research* **2011**;39(18):8017-28 doi 10.1093/nar/gkr401.
41. Shah F, Logsdon D, Messmann RA, Fehrenbacher JC, Fishel ML, Kelley MR. Exploiting the Ref-1-APE1 node in cancer signaling and other diseases: from bench to clinic. *npj Precision Oncology* **2017**;1(1):19 doi 10.1038/s41698-017-0023-0.
42. Kelley MR, Cheng L, Foster R, Tritt R, Jiang J, Broshears J, *et al.* Elevated and altered expression of the multifunctional DNA base excision repair and redox enzyme Ape1/ref-1 in prostate cancer. *Clin Cancer Res* **2001**;7(4):824-30.
43. Kakolyris S, Kaklamanis L, Engels K, Turley H, Hickson ID, Gatter KC, *et al.* Human apurinic endonuclease 1 expression in a colorectal adenoma-carcinoma sequence. *Cancer Res* **1997**;57(9):1794-7.
44. Sengupta S, Mantha AK, Song H, Roychoudhury S, Nath S, Ray S, *et al.* Elevated level of acetylation of APE1 in tumor cells modulates DNA damage repair. *Oncotarget* **2016**;7(46):75197-209 doi 10.18632/oncotarget.12113.
45. Abbotts R, Madhusudan S. Human AP endonuclease 1 (APE1): from mechanistic insights to druggable target in cancer. *Cancer Treat Rev* **2010**;36(5):425-35 doi 10.1016/j.ctrv.2009.12.006.
46. Xiang DB, Chen ZT, Wang D, Li MX, Xie JY, Zhang YS, *et al.* Chimeric adenoviral vector Ad5/F35-mediated APE1 siRNA enhances sensitivity of human colorectal cancer cells to radiotherapy in vitro and in vivo. *Cancer Gene Ther* **2008**;15(10):625-35 doi 10.1038/cgt.2008.30.

47. Fishel ML, Jiang Y, Rajeshkumar NV, Scandura G, Sinn AL, He Y, *et al.* Impact of APE1/Ref-1 redox inhibition on pancreatic tumor growth. *Mol Cancer Ther* **2011**;10(9):1698-708 doi 10.1158/1535-7163.Mct-11-0107.
48. Cardoso AA, Jiang Y, Luo M, Reed AM, Shahda S, He Y, *et al.* APE1/Ref-1 regulates STAT3 transcriptional activity and APE1/Ref-1-STAT3 dual-targeting effectively inhibits pancreatic cancer cell survival. *PLoS One* **2012**;7(10):e47462 doi 10.1371/journal.pone.0047462.
49. Sawides P, Xu Y, Liu L, Bokar JA, Silverman P, Dowlati A, *et al.* Pharmacokinetic profile of the base-excision repair inhibitor methoxyamine-HCl (TRC102; MX) given as an one-hour intravenous infusion with temozolomide (TMZ) in the first-in-human phase I clinical trial. *Journal of Clinical Oncology* **2010**;28(15_suppl):e13662-e doi 10.1200/jco.2010.28.15_suppl.e13662.
50. Talpaert-Borle M, Liuzzi M. Reaction of apurinic/aprimidinic sites with [14C]methoxyamine. A method for the quantitative assay of AP sites in DNA. *Biochim Biophys Acta* **1983**;740(4):410-6 doi 10.1016/0167-4781(83)90089-1.
51. Caimi PF, Cooper BW, William BM, Dowlati A, Barr PM, Fu P, *et al.* Phase I clinical trial of the base excision repair inhibitor methoxyamine in combination with fludarabine for patients with advanced hematologic malignancies. *Oncotarget* **2017**;8(45):79864-75 doi 10.18632/oncotarget.20094.
52. Meehan RS, Chen AP, O'Sullivan Coyne GH, Collins JM, Kummar S, Anderson L, *et al.* A phase 1 trial of TRC102 (methoxyamine HCl) with temozolomide (TMZ) in patients with solid tumors and lymphomas. *Journal of Clinical Oncology* **2016**;34(15_suppl):2556- doi 10.1200/JCO.2016.34.15_suppl.2556.
53. Eads JR, Krishnamurthi SS, Saltzman JN, Meropol NJ, Bokar JA, Gibbons J, *et al.* Phase I clinical trial of temozolomide and methoxyamine (TRC-102) in

- patients with advanced solid tumors. *Journal of Clinical Oncology* **2015**;33(15_suppl):2558- doi 10.1200/jco.2015.33.15_suppl.2558.
54. Hiramoto M, Shimizu N, Sugimoto K, Tang J, Kawakami Y, Ito M, *et al.* Nuclear targeted suppression of NF-kappa B activity by the novel quinone derivative E3330. *J Immunol* **1998**;160(2):810-9.
 55. Shimizu N, Sugimoto K, Tang J, Nishi T, Sato I, Hiramoto M, *et al.* High-performance affinity beads for identifying drug receptors. *Nat Biotechnol* **2000**;18(8):877-81 doi 10.1038/78496.
 56. Saitou Y, Shiraki K, Yamanaka T, Miyashita K, Inoue T, Yamanaka Y, *et al.* Augmentation of tumor necrosis factor family-induced apoptosis by E3330 in human hepatocellular carcinoma cell lines via inhibition of NF kappa B. *World J Gastroenterol* **2005**;11(40):6258-61 doi 10.3748/wjg.v11.i40.6258.
 57. Ransom M, Dennehey BK, Tyler JK. Chaperoning histones during DNA replication and repair. *Cell* **2010**;140(2):183-95 doi 10.1016/j.cell.2010.01.004.
 58. Orphanides G, LeRoy G, Chang CH, Luse DS, Reinberg D. FACT, a factor that facilitates transcript elongation through nucleosomes. *Cell* **1998**;92(1):105-16 doi 10.1016/s0092-8674(00)80903-4.
 59. Orphanides G, Reinberg D. RNA polymerase II elongation through chromatin. *Nature* **2000**;407(6803):471-5 doi 10.1038/35035000.
 60. Belotserkovskaya R, Oh S, Bondarenko VA, Orphanides G, Studitsky VM, Reinberg D. FACT Facilitates Transcription-Dependent Nucleosome Alteration. *Science* **2003**;301(5636):1090 doi 10.1126/science.1085703.
 61. Heo K, Kim H, Choi SH, Choi J, Kim K, Gu J, *et al.* FACT-mediated exchange of histone variant H2AX regulated by phosphorylation of H2AX and ADP-ribosylation of Spt16. *Mol Cell* **2008**;30(1):86-97 doi 10.1016/j.molcel.2008.02.029.

62. Keller DM, Lu H. p53 serine 392 phosphorylation increases after UV through induction of the assembly of the CK2.hSPT16.SSRP1 complex. *J Biol Chem* **2002**;277(51):50206-13 doi 10.1074/jbc.M209820200.
63. Winkler DD, Luger K. The histone chaperone FACT: structural insights and mechanisms for nucleosome reorganization. *J Biol Chem* **2011**;286(21):18369-74 doi 10.1074/jbc.R110.180778.
64. Dinant C, Ampatzidis-Michailidis G, Lans H, Tresini M, Lagarou A, Grosbart M, *et al.* Enhanced Chromatin Dynamics by FACT Promotes Transcriptional Restart after UV-Induced DNA Damage. *Molecular Cell* **2013**;51(4):469-79 doi <https://doi.org/10.1016/j.molcel.2013.08.007>.
65. Oliveira DV, Kato A, Nakamura K, Ikura T, Okada M, Kobayashi J, *et al.* Histone chaperone FACT regulates homologous recombination by chromatin remodeling through interaction with RNF20. *Journal of Cell Science* **2014**;127(4):763 doi 10.1242/jcs.135855.
66. Gurova KV, Hill JE, Guo C, Prokvolit A, Burdelya LG, Samoylova E, *et al.* Small molecules that reactivate p53 in renal cell carcinoma reveal a NF- κ B-dependent mechanism of p53 suppression in tumors. *Proceedings of the National Academy of Sciences of the United States of America* **2005**;102(48):17448 doi 10.1073/pnas.0508888102.
67. Gasparian AV, Burkhart CA, Purmal AA, Brodsky L, Pal M, Saranadasa M, *et al.* Curaxins: anticancer compounds that simultaneously suppress NF- κ B and activate p53 by targeting FACT. *Sci Transl Med* **2011**;3(95):95ra74-95ra74 doi 10.1126/scitranslmed.3002530.
68. Safina A, Cheney P, Pal M, Brodsky L, Ivanov A, Kirsanov K, *et al.* FACT is a sensor of DNA torsional stress in eukaryotic cells. *Nucleic Acids Res* **2017**;45(4):1925-45 doi 10.1093/nar/gkw1366.

69. Andre T, Boni C, Mounedji-Boudiaf L, Navarro M, Taberero J, Hickish T, *et al.* Oxaliplatin, fluorouracil, and leucovorin as adjuvant treatment for colon cancer. *N Engl J Med* **2004**;350(23):2343-51 doi 10.1056/NEJMoa032709.
70. Ribic CM, Sargent DJ, Moore MJ, Thibodeau SN, French AJ, Goldberg RM, *et al.* Tumor microsatellite-instability status as a predictor of benefit from fluorouracil-based adjuvant chemotherapy for colon cancer. *N Engl J Med* **2003**;349(3):247-57 doi 10.1056/NEJMoa022289.
71. Carethers JM, Smith EJ, Behling CA, Nguyen L, Tajima A, Doctolero RT, *et al.* Use of 5-fluorouracil and survival in patients with microsatellite-unstable colorectal cancer. *Gastroenterology* **2004**;126(2):394-401.
72. Sinicrope FA, Mahoney MR, Smyrk TC, Thibodeau SN, Warren RS, Bertagnolli MM, *et al.* Prognostic impact of deficient DNA mismatch repair in patients with stage III colon cancer from a randomized trial of FOLFOX-based adjuvant chemotherapy. *J Clin Oncol* **2013**;31(29):3664-72 doi 10.1200/JCO.2013.48.9591.
73. Bracht K, Nicholls AM, Liu Y, Bodmer WF. 5-Fluorouracil response in a large panel of colorectal cancer cell lines is associated with mismatch repair deficiency. *Br J Cancer* **2010**;103(3):340-6 doi 10.1038/sj.bjc.6605780.
74. Longley DB, Harkin DP, Johnston PG. 5-fluorouracil: mechanisms of action and clinical strategies. *Nat Rev Cancer* **2003**;3(5):330-8 doi 10.1038/nrc1074.
75. Sawyer RC, Stolfi RL, Martin DS, Spiegelman S. Incorporation of 5-fluorouracil into murine bone marrow DNA in vivo. *Cancer Res* **1984**;44(5):1847-51.
76. Kunz C, Focke F, Saito Y, Schuermann D, Lettieri T, Selfridge J, *et al.* Base excision by thymine DNA glycosylase mediates DNA-directed cytotoxicity of 5-fluorouracil. *PLoS Biol* **2009**;7(4):e91 doi 10.1371/journal.pbio.1000091.

77. Fischer F, Baerenfaller K, Jiricny J. 5-Fluorouracil is efficiently removed from DNA by the base excision and mismatch repair systems. *Gastroenterology* **2007**;133(6):1858-68 doi 10.1053/j.gastro.2007.09.003.
78. Tajima A, Hess MT, Cabrera BL, Kolodner RD, Carethers JM. The mismatch repair complex hMutS alpha recognizes 5-fluorouracil-modified DNA: implications for chemosensitivity and resistance. *Gastroenterology* **2004**;127(6):1678-84.
79. Meyers M, Wagner MW, Hwang H-S, Kinsella TJ, Boothman DA. Role of the hMLH1 DNA Mismatch Repair Protein in Fluoropyrimidine-mediated Cell Death and Cell Cycle Responses. *Cancer Research* **2001**;61(13):5193.
80. Mauro DJ, De Riel JK, Tallarida RJ, Sirover MA. Mechanisms of excision of 5-fluorouracil by uracil DNA glycosylase in normal human cells. *Mol Pharmacol* **1993**;43(6):854-7.
81. Nath S, Roychoudhury S, Kling MJ, Song H, Biswas P, Shukla A, *et al.* The extracellular role of DNA damage repair protein APE1 in regulation of IL-6 expression. *Cell Signal* **2017**;39:18-31 doi 10.1016/j.cellsig.2017.07.019.
82. Mitra S, Izumi T, Boldogh I, Bhakat KK, Hill JW, Hazra TK. Choreography of oxidative damage repair in mammalian genomes. *Free Radic Biol Med* **2002**;33(1):15-28.
83. Roychoudhury S, Pramanik S, Harris HL, Bhakat KK. Biochemical and Cellular Assays to Assess the Effects of Acetylation on Base Excision Repair Enzymes. *Methods Mol Biol* **2019**;1983:191-206 doi 10.1007/978-1-4939-9434-2_11.
84. Sengupta S, Mantha AK, Mitra S, Bhakat KK. Human AP endonuclease (APE1/Ref-1) and its acetylation regulate YB-1-p300 recruitment and RNA polymerase II loading in the drug-induced activation of multidrug resistance gene MDR1. *Oncogene* **2011**;30(4):482-93 doi 10.1038/onc.2010.435.

85. Kim SH, Chang HJ, Kim DY, Park JW, Baek JY, Kim SY, *et al.* What Is the Ideal Tumor Regression Grading System in Rectal Cancer Patients after Preoperative Chemoradiotherapy? *Cancer Res Treat* **2016**;48(3):998-1009 doi 10.4143/crt.2015.254.
86. Jackson EB, Theriot CA, Chattopadhyay R, Mitra S, Izumi T. Analysis of nuclear transport signals in the human apurinic/apyrimidinic endonuclease (APE1/Ref1). *Nucleic Acids Res* **2005**;33(10):3303-12.
87. Hoogstraten D, Nigg AL, Heath H, Mullenders LH, van Driel R, Hoeijmakers JH, *et al.* Rapid switching of TFIIH between RNA polymerase I and II transcription and DNA repair in vivo. *Mol Cell* **2002**;10(5):1163-74.
88. Schuffler PJ, Fuchs TJ, Ong CS, Wild PJ, Rupp NJ, Buhmann JM. TMARKER: A free software toolkit for histopathological cell counting and staining estimation. *J Pathol Inform* **2013**;4(Suppl):S2 doi 10.4103/2153-3539.109804.
89. Ianevski A, He L, Aittokallio T, Tang J. SynergyFinder: a web application for analyzing drug combination dose-response matrix data. *Bioinformatics* **2017**;33(15):2413-5 doi 10.1093/bioinformatics/btx162.
90. Gordon MS, Rosen LS, Mendelson D, Ramanathan RK, Goldman J, Liu L, *et al.* A phase 1 study of TRC102, an inhibitor of base excision repair, and pemetrexed in patients with advanced solid tumors. *Invest New Drugs* **2013**;31(3):714-23 doi 10.1007/s10637-012-9876-9.
91. Dinant C, Ampatzidis-Michailidis G, Lans H, Tresini M, Lagarou A, Grosbart M, *et al.* Enhanced chromatin dynamics by FACT promotes transcriptional restart after UV-induced DNA damage. *Mol Cell* **2013**;51(4):469-79 doi 10.1016/j.molcel.2013.08.007.
92. Gao Y, Li C, Wei L, Teng Y, Nakajima S, Chen X, *et al.* SSRP1 Cooperates with PARP and XRCC1 to Facilitate Single-Strand DNA Break Repair by Chromatin

- Priming. *Cancer Res* **2017**;77(10):2674-85 doi 10.1158/0008-5472.CAN-16-3128.
93. Belotserkovskaya R, Oh S, Bondarenko VA, Orphanides G, Studitsky VM, Reinberg D. FACT facilitates transcription-dependent nucleosome alteration. *Science* **2003**;301(5636):1090-3 doi 10.1126/science.1085703.
94. Wyatt MD, Pittman DL. Methylating agents and DNA repair responses: Methylated bases and sources of strand breaks. *Chem Res Toxicol* **2006**;19(12):1580-94 doi 10.1021/tx060164e.
95. Sengupta S, Mitra S, Bhakat KK. Dual regulatory roles of human AP-endonuclease (APE1/Ref-1) in CDKN1A/p21 expression. *PLoS One* **2013**;8(7):e68467 doi 10.1371/journal.pone.0068467.
96. Dunn KW, Kamocka MM, McDonald JH. A practical guide to evaluating colocalization in biological microscopy. *Am J Physiol Cell Physiol* **2011**;300(4):C723-C42 doi 10.1152/ajpcell.00462.2010.
97. Garcia H, Miecznikowski JC, Safina A, Commane M, Ruusulehto A, Kilpinen S, *et al.* Facilitates chromatin transcription complex is an "accelerator" of tumor transformation and potential marker and target of aggressive cancers. *Cell Rep* **2013**;4(1):159-73 doi 10.1016/j.celrep.2013.06.013.
98. Reits EA, Neefjes JJ. From fixed to FRAP: measuring protein mobility and activity in living cells. *Nat Cell Biol* **2001**;3(6):E145-7 doi 10.1038/35078615.
99. Sustr D, Hlaváček A, Duschl C, Volodkin D. Multi-Fractional Analysis of Molecular Diffusion in Polymer Multilayers by FRAP: A New Simulation-Based Approach. *The Journal of Physical Chemistry B* **2018**;122(3):1323-33 doi 10.1021/acs.jpcc.7b11051.

100. Beranek DT. Distribution of methyl and ethyl adducts following alkylation with monofunctional alkylating agents. *Mutat Res* **1990**;231(1):11-30 doi 10.1016/0027-5107(90)90173-2.
101. Pu X, Wang Z, Klaunig JE. Alkaline Comet Assay for Assessing DNA Damage in Individual Cells. *Curr Protoc Toxicol* **2015**;65:3.12.1-1 doi 10.1002/0471140856.tx0312s65.
102. Neshar E, Safina A, Aljahdali I, Portwood S, Wang ES, Koman I, *et al.* Role of chromatin damage and chromatin trapping of FACT in mediating the anticancer cytotoxicity of DNA-binding small molecule drugs. *Cancer Res* **2018** doi 10.1158/0008-5472.CAN-17-2690.
103. Dermawan JK, Hitomi M, Silver DJ, Wu Q, Sandlesh P, Sloan AE, *et al.* Pharmacological Targeting of the Histone Chaperone Complex FACT Preferentially Eliminates Glioblastoma Stem Cells and Prolongs Survival in Preclinical Models. *Cancer Res* **2016**;76(8):2432-42 doi 10.1158/0008-5472.Can-15-2162.
104. Koman IE, Commane M, Paszkiewicz G, Hoonjan B, Pal S, Safina A, *et al.* Targeting FACT complex suppresses mammary tumorigenesis in Her2/neu transgenic mice. *Cancer Prev Res (Phila)* **2012**;5(8):1025-35 doi 10.1158/1940-6207.CAPR-11-0529.
105. Dermawan JK, Gurova K, Pink J, Dowlati A, De S, Narla G, *et al.* Quinacrine overcomes resistance to erlotinib by inhibiting FACT, NF-kappaB, and cell-cycle progression in non-small cell lung cancer. *Mol Cancer Ther* **2014**;13(9):2203-14 doi 10.1158/1535-7163.mct-14-0013.
106. Gasparian AV, Burkhart CA, Purmal AA, Brodsky L, Pal M, Saranadasa M, *et al.* Curaxins: anticancer compounds that simultaneously suppress NF-kappaB and

- activate p53 by targeting FACT. *Sci Transl Med* **2011**;3(95):95ra74 doi 10.1126/scitranslmed.3002530.
107. Fedchenko N, Reifenrath J. Different approaches for interpretation and reporting of immunohistochemistry analysis results in the bone tissue - a review. *Diagn Pathol* **2014**;9:221- doi 10.1186/s13000-014-0221-9.
108. Bhakat KK, Sengupta S, Adeniyi VF, Roychoudhury S, Nath S, Bellot LJ, *et al.* Regulation of limited N-terminal proteolysis of APE1 in tumor via acetylation and its role in cell proliferation. *Oncotarget* **2016**;7(16):22590-604 doi 10.18632/oncotarget.8026.
109. Walther A, Johnstone E, Swanton C, Midgley R, Tomlinson I, Kerr D. Genetic prognostic and predictive markers in colorectal cancer. *Nature Reviews Cancer* **2009**;9:489 doi 10.1038/nrc2645.
110. van Triest B, Pinedo HM, van Hensbergen Y, Smid K, Telleman F, Schoenmakers PS, *et al.* Thymidylate synthase level as the main predictive parameter for sensitivity to 5-fluorouracil, but not for folate-based thymidylate synthase inhibitors, in 13 nonselected colon cancer cell lines. *Clin Cancer Res* **1999**;5(3):643-54.
111. Sinicrope FA, Rego RL, Halling KC, Foster NR, Sargent DJ, La Plant B, *et al.* Thymidylate synthase expression in colon carcinomas with microsatellite instability. *Clin Cancer Res* **2006**;12(9):2738-44 doi 10.1158/1078-0432.ccr-06-0178.
112. Benatti P, Gafà R, Barana D, Marino M, Scarselli A, Pedroni M, *et al.* Microsatellite Instability and Colorectal Cancer Prognosis. *Clinical Cancer Research* **2005**;11(23):8332.

113. Vilar E, Gruber SB. Microsatellite instability in colorectal cancer—the stable evidence. *Nature Reviews Clinical Oncology* **2010**;7:153 doi 10.1038/nrclinonc.2009.237.
114. Bapat A, Fishel ML, Kelley MR. Going ape as an approach to cancer therapeutics. *Antioxid Redox Signal* **2009**;11(3):651-68.
115. Li M, Volker J, Breslauer KJ, Wilson DM, 3rd. APE1 incision activity at abasic sites in tandem repeat sequences. *J Mol Biol* **2014**;426(11):2183-98 doi 10.1016/j.jmb.2014.03.014.
116. Hinz JM. Impact of abasic site orientation within nucleosomes on human APE1 endonuclease activity. *Mutat Res* **2014**;766-767:19-24 doi 10.1016/j.mrfmmm.2014.05.008.
117. Lirussi L, Antoniali G, Vascotto C, D'Ambrosio C, Poletto M, Romanello M, *et al.* Nucleolar accumulation of APE1 depends on charged lysine residues that undergo acetylation upon genotoxic stress and modulate its BER activity in cells. *Mol Biol Cell* **2012**;23(20):4079-96 doi 10.1091/mbc.E12-04-0299.
118. Bhakat KK, Mantha AK, Mitra S. Transcriptional regulatory functions of mammalian AP-endonuclease (APE1/Ref-1), an essential multifunctional protein. *Antioxid Redox Signal* **2009**;11(3):621-38.
119. Formosa T. The role of FACT in making and breaking nucleosomes. *Biochimica et biophysica acta* **2012**;1819(3-4):247-55 doi 10.1016/j.bbagr.2011.07.009.
120. Charles Richard JL, Shukla MS, Menoni H, Ouararhni K, Lone IN, Roulland Y, *et al.* FACT Assists Base Excision Repair by Boosting the Remodeling Activity of RSC. *PLoS Genet* **2016**;12(7):e1006221 doi 10.1371/journal.pgen.1006221.
121. Andersen S, Heine T, Sneve R, Konig I, Krokan HE, Epe B, *et al.* Incorporation of dUMP into DNA is a major source of spontaneous DNA damage, while excision

- of uracil is not required for cytotoxicity of fluoropyrimidines in mouse embryonic fibroblasts. *Carcinogenesis* **2005**;26(3):547-55 doi 10.1093/carcin/bgh347.
122. Carter DR, Murray J, Cheung BB, Gamble L, Koach J, Tsang J, *et al.* Therapeutic targeting of the MYC signal by inhibition of histone chaperone FACT in neuroblastoma. *Sci Transl Med* **2015**;7(312):312ra176 doi 10.1126/scitranslmed.aab1803.
123. Lock R, Carol H, Maris JM, Kolb EA, Gorlick R, Reynolds CP, *et al.* Initial testing (stage 1) of the curaxin CBL0137 by the pediatric preclinical testing program. *Pediatr Blood Cancer* **2017**;64(4) doi 10.1002/pbc.26263.
124. Burkhart C, Fleishman D, Kohn R, Commane M, Garrigan J, Kurbatov V, *et al.* Curaxin CBL0137 eradicates drug resistant cancer stem cells and potentiates efficacy of gemcitabine in preclinical models of pancreatic cancer. *Oncotarget* **2014**;5(22):11038-53 doi 10.18632/oncotarget.2701.
125. Safina A, Garcia H, Commane M, Guryanova O, Degan S, Kolesnikova K, *et al.* Complex mutual regulation of facilitates chromatin transcription (FACT) subunits on both mRNA and protein levels in human cells. *Cell Cycle* **2013**;12(15):2423-34 doi 10.4161/cc.25452.
126. De S, Lindner DJ, Coleman CJ, Wildey G, Dowlati A, Stark GR. The FACT inhibitor CBL0137 Synergizes with Cisplatin in Small-Cell Lung Cancer by Increasing NOTCH1 Expression and Targeting Tumor-Initiating Cells. *Cancer Res* **2018**;78(9):2396-406 doi 10.1158/0008-5472.can-17-1920.
127. McNeil DE, Cote TR, Clegg L, Rorke LB. Incidence and trends in pediatric malignancies medulloblastoma/primitive neuroectodermal tumor: a SEER update. *Surveillance Epidemiology and End Results. Med Pediatr Oncol* **2002**;39(3):190-4 doi 10.1002/mpo.10121.

128. Smoll NR, Drummond KJ. The incidence of medulloblastomas and primitive neuroectodermal tumours in adults and children. *J Clin Neurosci* **2012**;19(11):1541-4 doi 10.1016/j.jocn.2012.04.009.
129. Lastowska M, Trubicka J, Niemira M, Paczkowska-Abdulsalam M, Karkucinska-Wieckowska A, Kaleta M, *et al.* Medulloblastoma with transitional features between Group 3 and Group 4 is associated with good prognosis. *J Neurooncol* **2018**;138(2):231-40 doi 10.1007/s11060-018-2797-5.
130. Taylor MD, Northcott PA, Korshunov A, Remke M, Cho Y-J, Clifford SC, *et al.* Molecular subgroups of medulloblastoma: the current consensus. *Acta Neuropathol* **2012**;123(4):465-72 doi 10.1007/s00401-011-0922-z.
131. Tait DM, Thornton-Jones H, Bloom HJ, Lemerle J, Morris-Jones P. Adjuvant chemotherapy for medulloblastoma: the first multi-centre control trial of the International Society of Paediatric Oncology (SIOP I). *Eur J Cancer* **1990**;26(4):464-9.
132. Kortmann RD, Kuhl J, Timmermann B, Mittler U, Urban C, Budach V, *et al.* Postoperative neoadjuvant chemotherapy before radiotherapy as compared to immediate radiotherapy followed by maintenance chemotherapy in the treatment of medulloblastoma in childhood: results of the German prospective randomized trial HIT '91. *Int J Radiat Oncol Biol Phys* **2000**;46(2):269-79 doi 10.1016/s0360-3016(99)00369-7.
133. Packer RJ, Gajjar A, Vezina G, Rorke-Adams L, Burger PC, Robertson PL, *et al.* Phase III study of craniospinal radiation therapy followed by adjuvant chemotherapy for newly diagnosed average-risk medulloblastoma. *J Clin Oncol* **2006**;24(25):4202-8 doi 10.1200/jco.2006.06.4980.
134. Taylor RE, Bailey CC, Robinson K, Weston CL, Ellison D, Ironside J, *et al.* Results of a randomized study of preradiation chemotherapy versus radiotherapy

- alone for nonmetastatic medulloblastoma: The International Society of Paediatric Oncology/United Kingdom Children's Cancer Study Group PNET-3 Study. *J Clin Oncol* **2003**;21(8):1581-91 doi 10.1200/jco.2003.05.116.
135. King AA, Seidel K, Di C, Leisenring WM, Perkins SM, Krull KR, *et al.* Long-term neurologic health and psychosocial function of adult survivors of childhood medulloblastoma/PNET: a report from the Childhood Cancer Survivor Study. *Neuro Oncol* **2017**;19(5):689-98 doi 10.1093/neuonc/now242.
136. Fouladi M, Gilger E, Kocak M, Wallace D, Buchanan G, Reeves C, *et al.* Intellectual and functional outcome of children 3 years old or younger who have CNS malignancies. *J Clin Oncol* **2005**;23(28):7152-60 doi 10.1200/jco.2005.01.214.
137. Mulhern RK, Palmer SL, Merchant TE, Wallace D, Kocak M, Brouwers P, *et al.* Neurocognitive consequences of risk-adapted therapy for childhood medulloblastoma. *J Clin Oncol* **2005**;23(24):5511-9 doi 10.1200/jco.2005.00.703.
138. Mulhern RK, Kepner JL, Thomas PR, Armstrong FD, Friedman HS, Kun LE. Neuropsychologic functioning of survivors of childhood medulloblastoma randomized to receive conventional or reduced-dose craniospinal irradiation: a Pediatric Oncology Group study. *J Clin Oncol* **1998**;16(5):1723-8 doi 10.1200/jco.1998.16.5.1723.
139. Packer RJ, Vezina G. Management of and Prognosis With Medulloblastoma: Therapy at a Crossroads. *JAMA Neurology* **2008**;65(11):1419-24 doi 10.1001/archneur.65.11.1419.
140. Boiteux S, Guillet M. Abasic sites in DNA: repair and biological consequences in *Saccharomyces cerevisiae*. *DNA Repair (Amst)* **2004**;3(1):1-12.
141. Jung Y, Lippard SJ. Direct Cellular Responses to Platinum-Induced DNA Damage. *Chemical Reviews* **2007**;107(5):1387-407 doi 10.1021/cr068207j.

142. Basu A, Krishnamurthy S. Cellular Responses to Cisplatin-Induced DNA Damage. *Journal of Nucleic Acids* **2010**;2010:16 doi 10.4061/2010/201367.
143. Lomax ME, Folkes LK, O'Neill P. Biological Consequences of Radiation-induced DNA Damage: Relevance to Radiotherapy. *Clinical Oncology* **2013**;25(10):578-85 doi <https://doi.org/10.1016/j.clon.2013.06.007>.
144. Vignard J, Mirey G, Salles B. Ionizing-radiation induced DNA double-strand breaks: A direct and indirect lighting up. *Radiotherapy and Oncology* **2013**;108(3):362-9 doi <https://doi.org/10.1016/j.radonc.2013.06.013>.
145. Izumi T, Brown DB, Naidu CV, Bhakat KK, Macinnes MA, Saito H, *et al.* Two essential but distinct functions of the mammalian abasic endonuclease. *Proc Natl Acad Sci U S A* **2005**;102(16):5739-43 doi 10.1073/pnas.0500986102.
146. Kothandapani A, Dangeti VS, Brown AR, Banze LA, Wang XH, Sobol RW, *et al.* Novel role of base excision repair in mediating cisplatin cytotoxicity. *The Journal of biological chemistry* **2011**;286(16):14564-74 doi 10.1074/jbc.M111.225375.
147. Sawant A, Floyd AM, Dangeti M, Lei W, Sobol RW, Patrick SM. Differential role of base excision repair proteins in mediating cisplatin cytotoxicity. *DNA Repair (Amst)* **2017**;51:46-59 doi 10.1016/j.dnarep.2017.01.002.
148. Wilson DM, 3rd, Seidman MM. A novel link to base excision repair? *Trends Biochem Sci* **2010**;35(5):247-52 doi 10.1016/j.tibs.2010.01.003.
149. Wang D, Xiang DB, Yang XQ, Chen LS, Li MX, Zhong ZY, *et al.* APE1 overexpression is associated with cisplatin resistance in non-small cell lung cancer and targeted inhibition of APE1 enhances the activity of cisplatin in A549 cells. *Lung cancer (Amsterdam, Netherlands)* **2009**;66(3):298-304 doi 10.1016/j.lungcan.2009.02.019.
150. Ray S, Coulter DW, Gray SD, Sughrue JA, Roychoudhury S, McIntyre EM, *et al.* Suppression of STAT3 NH2 -terminal domain chemosensitizes

- medulloblastoma cells by activation of protein inhibitor of activated STAT3 via de-repression by microRNA-21. *Mol Carcinog* **2018**;57(4):536-48 doi 10.1002/mc.22778.
151. Yarnell AT, Oh S, Reinberg D, Lippard SJ. Interaction of FACT, SSRP1, and the high mobility group (HMG) domain of SSRP1 with DNA damaged by the anticancer drug cisplatin. *The Journal of biological chemistry* **2001**;276(28):25736-41 doi 10.1074/jbc.M101208200.
152. Gao Y, Li C, Wei L, Teng Y, Nakajima S, Chen X, *et al.* SSRP1 Cooperates with PARP and XRCC1 to Facilitate Single-Strand DNA Break Repair by Chromatin Priming. *Cancer Res* **2017**;77(10):2674-85 doi 10.1158/0008-5472.CAN-16-3128.
153. Koster J, Molenaar JJ, Versteeg R. Abstract A2-45: R2: Accessible web-based genomics analysis and visualization platform for biomedical researchers. *Cancer Research* **2015**;75(22 Supplement 1):A2-45 doi 10.1158/1538-7445.TRANSCAGEN-A2-45.
154. Winkler DD, Luger K. The histone chaperone FACT: structural insights and mechanisms for nucleosome reorganization. *The Journal of biological chemistry* **2011**;286(21):18369-74 doi 10.1074/jbc.R110.180778.
155. Birch JL, Tan BC, Panov KI, Panova TB, Andersen JS, Owen-Hughes TA, *et al.* FACT facilitates chromatin transcription by RNA polymerases I and III. *Embo j* **2009**;28(7):854-65 doi 10.1038/emboj.2009.33.
156. Tessarz P, Santos-Rosa H, Robson SC, Sylvestersen KB, Nelson CJ, Nielsen ML, *et al.* Glutamine methylation in histone H2A is an RNA-polymerase-I-dedicated modification. *Nature* **2013**;505:564 doi 10.1038/nature12819

<https://www.nature.com/articles/nature12819#supplementary-information>.

157. Formosa T, Ruone S, Adams MD, Olsen AE, Eriksson P, Yu Y, *et al.* Defects in SPT16 or POB3 (yFACT) in Saccharomyces cerevisiae; Cause Dependence on the Hir/Hpc Pathway: Polymerase Passage May Degrade Chromatin Structure. *Genetics* **2002**;162(4):1557.
158. Wienholz F, Zhou D, Turkyilmaz Y, Schwertman P, Tresini M, Pines A, *et al.* FACT subunit Spt16 controls UVSSA recruitment to lesion-stalled RNA Pol II and stimulates TC-NER. *Nucleic Acids Res* **2019**;47(8):4011-25 doi 10.1093/nar/gkz055.
159. Charles Richard JL, Shukla MS, Menoni H, Ouararhni K, Lone IN, Roulland Y, *et al.* FACT Assists Base Excision Repair by Boosting the Remodeling Activity of RSC. *PLOS Genetics* **2016**;12(7):e1006221 doi 10.1371/journal.pgen.1006221.
160. Kelley MR, Luo M, Reed A, Su D, Delaplane S, Borch RF, *et al.* Functional analysis of novel analogues of E3330 that block the redox signaling activity of the multifunctional AP endonuclease/redox signaling enzyme APE1/Ref-1. *Antioxid Redox Signal* **2011**;14(8):1387-401 doi 10.1089/ars.2010.3410.
161. Lock R, Carol H, Maris JM, Kolb EA, Gorlick R, Reynolds CP, *et al.* Initial testing (stage 1) of the curaxin CBL0137 by the pediatric preclinical testing program. *Pediatr Blood Cancer* **2017**;64(4):10.1002/pbc.26263 doi 10.1002/pbc.26263.
162. Becher OJ, Holland EC. Genetically engineered models have advantages over xenografts for preclinical studies. *Cancer Res* **2006**;66(7):3355-8, discussion 8-9 doi 10.1158/0008-5472.Can-05-3827.
163. Kersten K, de Visser KE, van Miltenburg MH, Jonkers J. Genetically engineered mouse models in oncology research and cancer medicine. *EMBO Mol Med* **2017**;9(2):137-53 doi 10.15252/emmm.201606857.

164. de Wind N, Dekker M, Berns A, Radman M, te Riele H. Inactivation of the mouse Msh2 gene results in mismatch repair deficiency, methylation tolerance, hyperrecombination, and predisposition to cancer. *Cell* **1995**;82(2):321-30 doi 10.1016/0092-8674(95)90319-4.
165. Reitmair AH, Schmits R, Ewel A, Bapat B, Redston M, Mitri A, *et al.* MSH2 deficient mice are viable and susceptible to lymphoid tumours. *Nat Genet* **1995**;11(1):64-70 doi 10.1038/ng0995-64.
166. Smits R, Hofland N, Edelmann W, Geugien M, Jagmohan-Changur S, Albuquerque C, *et al.* Somatic Apc mutations are selected upon their capacity to inactivate the beta-catenin downregulating activity. *Genes Chromosomes Cancer* **2000**;29(3):229-39.
167. Kucherlapati MH, Lee K, Nguyen AA, Clark AB, Hou H, Jr., Rosulek A, *et al.* An Msh2 conditional knockout mouse for studying intestinal cancer and testing anticancer agents. *Gastroenterology* **2010**;138(3):993-1002.e1 doi 10.1053/j.gastro.2009.11.009.
168. Barone TA, Burkhart CA, Safina A, Haderski G, Gurova KV, Purmal AA, *et al.* Anticancer drug candidate CBL0137, which inhibits histone chaperone FACT, is efficacious in preclinical orthotopic models of temozolomide-responsive and -resistant glioblastoma. *Neuro Oncol* **2017**;19(2):186-96 doi 10.1093/neuonc/now141.